The Solution of Time-Domain Electric Field Integral Equations via Problem-Independent Inversion of the Laplace Transform

by

Glenn Iwasa

A Thesis Submitted to the
University of Ottawa
in partial fulfillment of the requirements for the degree of

Master of Applied Science
in Electrical & Computer Engineering

Ottawa-Carleton Institute for Electrical and Computer Engineering
School of Electrical Engineering and Computer Science
Faculty of Engineering
University of Ottawa

Abstract

This thesis derives and validates a new computational electromagnetic formulation via the re-initialized numerical inverse of the Laplace transform (NILT*n*) for solutions of two-dimensional and three-dimensional time-domain electrical-field integral equations (TD-EFIE) via the Method of Moments (MoM). The TD solution is found with a high degree of temporal accuracy and ensuring mathematical stability (L-stable), while taking relatively large time-steps. As a bonus, this formulation can accurately determine the frequency-domain (FD) solution of the EFIE via a fast-Fourier-transform of the interpolated TD solution. The interpolated TD solution is found using the information available via the NILT*n* to interpolate the non-interpolated TD waveform with minimal computational cost. The use of the re-initialized NILT*n* to solve the TD-EFIE was inspired by its application in TD lumped circuit analysis. The results are proven via various 2D and 3D examples and comparing both the TD and FD results to well-known computational electromagnetic methods.

Acknowledgements

I am extremely indebted to the University of Ottawa for giving me the opportunity to complete my graduate studies in Electrical Engineering.

Words cannot express my gratitude to my supervisors Dr. Emad Gad and Dr. Derek McNamara for their wisdom and guidance. Both of you are amazing role models not only in my academic endeavors, but in life as well.

I would also like thank my supervisors for permission granted me to use selected parts of their notes and publications in some of the background section in Chapter 2.

Finally, many thanks to my friends and family. Your support means the world to me, and completing this thesis would have been impossible without it.

Table of Symbols, Acronyms & Technical Terms

Acronym/Word/Symbol	Description/Meaning
c	$1/\sqrt{\mu_o \varepsilon_o}$
CEM	computational electromagnetics
CFIE	combined field integral equation
EFIE	electric field integral equation
explicit	"stated in detail, leaving nothing merely implied"
FD	Frequency-domain
implicit	"implied though not plainly expressed" (in mathematical context, some quantity is not expressed directly in terms of independent variables)
IDFT	inverse discrete Fourier transform
IE	integral equation
LM	light-metre
MNA	modified nodal analysis
MoM	method of moments
MOT	marching-on-in-time
m	metre
MFIE	magnetic field integral equation
NILT	numeric inverse of the Laplace transform
NILT*n*	modified numeric inverse of the Laplace transform
ns	nano-second
PEC	perfect electrically conducting
s	complex frequency $s = \mathrm{Re}(s) + j\,\mathrm{Im}(s) = \mathrm{Re}(s) + j\omega$
spatial	"denoting space"
temporal	"denoting time"
TD	time-domain

Table of Contents

List of Figures

List of Tables

CHAPTER 1 - Introduction

"The shortest path between two truths in the real domain passes through the complex domain".

Attributed to mathematician Jacques Hadamard
in *The Mathematical Intelligencer*, Vol.13, 1991

1.1 TIME- AND FREQUENCY-DOMAIN SOLUTIONS OF INTEGRAL EQUATION MODELS IN COMPUTATIONAL ELECTROMAGNETICS

The use of the method of moments (MoM) to find numerical solutions of frequency-domain (time-harmonic) integral equations for scattering from perfectly electrically conducting (PEC) objects is well-established in electromagnetic engineering practice [PETE 97] [VOLA 12]. There has nevertheless been sustained interest [REN 23] in techniques to determine the time-domain solution[1] of such problems directly, as opposed to inverse Fourier transformation of frequency-domain solutions. This has been done using differential equation-based finite-element time-domain approaches (FETD), as well as time-domain integral equation-based moment of methods [JIN 14]. It is the latter approach, and in particular the time-domain electric field integral equation (TD-EFIE) for scattering from PEC objects, that is the focus of the research in this thesis.

Interest in direct time-domain solutions of electromagnetic problems can be attributed to several factors:

■ Wideband frequency-domain information can be extracted from a single time-domain solution that results from a pulsed excitation, using the discrete Fourier transform.

■ There are some systems (e.g. ultra-wideband antennas) for which the details of the time response are of paramount importance.

[1] By this we mean problems involving arbitrary time dependence.

■ If there are any materials present whose electromagnetic properties (*viz.* permittivity, permeability and conductivity) are non-linear or deliberately time-varying, time-domain analysis is a necessity[2].

TD-IEs are particularly suited to open systems that are able to radiate (whether this is desired or not), as the Green's function forming the kernel of the IE automatically accounting for the unbounded domain. Unlike differential equations based methods such as the time-domain finite-element method and the finite-difference time-domain method, no artificial means of truncating the solution domain (such as absorbing boundary conditions or perfectly matched layers) are needed.

All numerical solutions[3] of the TD-EFIE, even that to be developed further in this thesis, are built upon the MoM to effect the discretization of the spatial variation of the physical quantity to be found (e.g. electric current density). They differ in the precise route they follow to arrive at the time-domain solution. The most widely discussed is the so-called marching-on-in-time (MOT) approach that discretizes the time-variation of the unknown quantity directly. The solution at some time (the "now" as some authors call it) depend on the solution at earlier times, as the user solves for what is "now" step by step. Special care has to be taken to ensure the accuracy and stability of the solution, such as the need to evaluate certain terms with extreme (quasi-exact) accuracy, and the need to have a time-step that is sufficiently small for accuracy (but not too small to cause instability) in the time-stepping. A similar route that also arrives at a time-stepping formulation, but without direct discretization of the time variable (and associated difficulties) is the so-called convolution quadrature method. It obtains the MOT-like time-stepping expressions via a more circuitous route, but one that appears to be less sensitive to the preciseness which the various terms are evaluated, and to the step size. The so-called NILT*n* approach (possible in both a non-time-stepped form, and a so-called re-initialized time-stepped form), utilizes MoM solutions of the TD-EFIE in the complex frequency (Laplace transform) domain and a problem-independent inverse Laplace transform to reach time-domain solutions.

[2] Even if the impressed source is a single-frequency tone, the presence of non-linearity will cause a multiplicity of other frequencies to be excited.
[3] These will be reviewed in Chapter 2.

The re-initialized form offers very stable solutions for larger time-steps than the other methods. However, although well-established in the analysis of lumped circuits, its use in solving electromagnetic fields problems is relatively recent. In particular, an all-important re-initialized NILT*n* formulation for solution of the TD-EFIE has not been available and (as we will see) not as straightforward as that for lumped circuit analysis. The research of this thesis provides such a formulation for the first time.

1.2 THESIS CONTRIBUTIONS & OUTLINE

The research described in this thesis develops, for the first time, a means of performing re-initialization in the so-called NILT*n*/MoM solutions of a TD-EFIE. Only in this way are we able to obtain a procedure that allows the solution to progress out to as large a time value as one wishes, and yet maintain stability without a degradation in solution accuracy. This is an important achievement.

■ **Chapter 2** : This chapter assembles the key technical concepts needed to conduct the research described in the thesis, and is the foundation in which it builds upon. This includes the frequency-domain and time-domain versions of the electric field integral equation used to model electromagnetic scattering by PEC objects. The emphasis of this thesis is the attainment of time-domain solutions, and the excitation used will be a Gaussian pulse; this concept is thus discussed as well. Although time-domain solutions may be the primary objective of some analysis, very often they are also used as a means of obtaining frequency-domain solutions over a wide frequency range in a computationally efficient manner. As this thesis focuses on TD-EFIE, this chapter will also discuss various implementations of the MOT solutions for the TD-EFIE. Finally, this chapter will describe the implementation of NILT*n* in the context of mathematics, lumped circuit analysis, and its recent use in computational electromagnetics.

■ **Chapter 3** : This chapter formulates a NILT*n*/MoM solution for a two-dimensional (2D) problem of an incident plane wave scattering from a PEC cylinder of arbitrary cross-section, with the electric field of the incident plane wave parallel to the cylinder axis (a TM_z problem). The PEC cylinder may be an open or closed object. Full implementation details, that are not

available elsewhere, are provided. Numerical results are shown and explained. Such 2D problems were considered first in order to obtain both clarity and familiarity with, the intricacies of using the NILT*n* procedure for solution of the TD-EFIE. This was done because to the author's knowledge, such a procedure does not appear to have been done before. The successful implementation of the 2D problem allowed the author to proceed quite naturally to the 3D problems described in Chapter 4.

■ **Chapter 4** : We do not develop the re-initialized form of NILT*n* for the 2D case in Chapter 3. However, having successfully satisfied ourselves in that chapter on how to carefully construct the NILT*n*/MoM procedure for solution of a TD-EFIE, in this chapter we do for the 3D case what was done for the 2D situation in Chapter 3, but still, importantly, without re-initialization. Although the some of the overall details remain the same as Chapter 2, the 3D case obviously has some differences from those of the 2D case (e.g. different Green's functions; unknown exists over a surface and not a contour; more complicated expansion and testing functions, and more intricate numerical integrations to evaluate the s-domain interaction matrices; and so on).

■ **Chapter 5** : This takes the work of Chapter 4 and complements it with the crucial ability to perform re-initialization. We demonstrate through numerical experiments how important this ability is. Finally, there is a brief discussion on the computational efficiency of the re-initialized NILT*n*.

■ Finally, **Chapter 6** summarizes the contributions of the thesis, and suggests possible future work.

CHAPTER 2 - Theoretical Background

2.1 INTRODUCTION

As indicated in Chapter 1, this chapter assembles the key technical concepts and notation needed to conduct the research described in the thesis and lays the technical foundation upon which this thesis builds. It is structured as follows:

■ Section 2.2 writes down the integral expressions for the time-domain electric field due to a known electric surface current density.

■ Section 2.3 presents the frequency-domain (ω-domain), complex frequency-domain (s-domain), and time-domain (t-domain) versions of the electric field integral equation (EFIE) used to model electromagnetic scattering by perfectly electrically conducting (PEC) objects.

■ The emphasis in this thesis is the attainment of time-domain solutions, and the excitation used will be a Gaussian pulse; this concept is thus discussed in Section 2.4.

■ Although time-domain solutions may be the primary objective of some analysis, very often they are used as a means of obtaining ω-domain solutions over a wide frequency range in a computationally efficient manner, and so we review the (albeit well-known) manner of obtaining the latter from the former in Section 2.5.

■ In broad terms, we can say that three methods have been used for the numerical solution of the TD-EFIE. The method of moments (MoM) serves as the foundation for two of these methods. The methods differ in the manner in which the dependence on the time-variable is handled. These can be classified as the marching-on-in-time (MOT) approach, the convolution quadrature approach, and the NILT*n* approach. The first two methods are briefly reviewed in Section 2.6.

■ Section 2.7 gathers the essential details needed for application of the NILT*n* method to finding solutions of the TD-EFIE. Important expressions are extracted from literature and explained, because they will be used in Chapter 3, 4 and 5. The second part of Section 2.7 presents a computationally efficient way to interpolate time-domain solutions at times intermediate to those provided in fixed steps in the above-mentioned time-stepping solutions. It is efficient because it exploits time-derivative information that is provided almost as a bonus by the NILT*n* methods.

■ Section 2.8 describes the few instances where the NILT*n* approach has been used to find time-domain solutions in full-wave electromagnetics problems (as opposed to lumped circuit analysis problems).

■ Section 2.9 concludes the chapter.

2.2 ELECTRIC FIELD DUE TO AN ELECTRIC SURFACE CURRENT DENSITY

The electric field $\bar{\mathcal{E}}(\bar{r},t)$ at a point $\bar{r}$ in free space at time *t*, due to a surface electric current density $\bar{\mathcal{J}}_s(\bar{r},t)$ on a surface S is [SMIT 97][RAO 20]

$$\bar{\mathcal{E}}(\bar{r},t) = -\nabla\Phi(\bar{r},t) - \frac{\partial\bar{\mathcal{A}}(\bar{r},t)}{\partial t} \tag{2.2-1}$$

with

$$\bar{\mathcal{A}}(\bar{r},t) = \mu_o \iint_S \frac{\bar{\mathcal{J}}_s(\bar{r}',t-|\bar{r}-\bar{r}'|/c)}{4\pi|\bar{r}-\bar{r}'|}\,dS' \tag{2.2-2}$$

and

$$\Phi(\bar{r},t) = \frac{1}{\varepsilon_o}\iint_S \frac{\rho_s(\bar{r}',t-|\bar{r}-\bar{r}'|/c)}{4\pi|\bar{r}-\bar{r}'|}\,dS' \tag{2.2-3}$$

with ρ_s the electric surface charge density. Paraphrasing [SMIT 97], these expressions tell us that we must evaluate the sources at an earlier time $t-|\bar{r}-\bar{r}'|/c$, something that can be difficult to implement in calculations. We may view (2.2-2) and (2.2-3) as arising from each surface element of *S*, with an element dS' having vector potential contribution

$$\mu_o \frac{\bar{\mathcal{J}}_s(\bar{r}',t-|\bar{r}-\bar{r}'|/c)}{4\pi|\bar{r}-\bar{r}'|} \tag{2.2-4}$$

and scalar potential contribution

$$\frac{1}{\varepsilon_o}\frac{\rho_s(\bar{r}',t-|\bar{r}-\bar{r}'|/c)}{4\pi|\bar{r}-\bar{r}'|} \tag{2.2-5}$$

The term $|\bar{r}-\bar{r}'|/c$ is precisely the time needed for the field to travel from point $\bar{r}'$ to $\bar{r}$; each contribution must depart element dS' at an earlier time in order to arrive at observation point $\bar{r}$ at time *t*. It is for this reason that (2.2-2) and (2.2-3) are called retarded potentials. The presence of the retarded time-dependence in the source terms in (2.2-2) and (2.2-3) indicates that, as is essential, they satisfy causality. The field at point $\bar{r}$ at time *t* (the "here and now" as [BLUC 97] aptly puts it) depends on what the current and charge density were at point $\bar{r}'$ at time $t-|\bar{r}-\bar{r}'|/c$, in other words after a time delay $|\bar{r}-\bar{r}'|/c$. Indeed, the superposition (via the

integration process) of their contributions from all points $\bar{r}'$ over the surface occupied by the source. Using the sifting property of the delta function, namely

$$\rho_s(\bar{r}', t-|\bar{r}-\bar{r}'|/c) = \int_{-\infty}^{\infty} \rho_s(\bar{r}', t')\ \delta[t'-(t-|\bar{r}-\bar{r}'|/c)]\ dt' = \int_{-\infty}^{\infty} \rho_s(\bar{r}', t')\ \delta(t-t'-|\bar{r}-\bar{r}'|/c)\, dt' \tag{2.2-6}$$

[SMIT 97] re-writes (2.2-2) and (2.2-3) as

$$\bar{\mathcal{A}}(\bar{r}, t) = \mu_o \int_{-\infty}^{\infty} \left\{ \iint_S \bar{\mathcal{J}}_s(\bar{r}', t')\ \frac{\delta(t-t'-|\bar{r}-\bar{r}'|/c)}{4\pi|\bar{r}-\bar{r}'|} dS' \right\} dt' \tag{2.2-7}$$

and

$$\Phi(\bar{r}, t) = \frac{1}{\varepsilon_o} \int_{-\infty}^{\infty} \left\{ \iint_S \rho_s(\bar{r}', t')\ \frac{\delta(t-t'-|\bar{r}-\bar{r}'|/c)}{4\pi|\bar{r}-\bar{r}'|} dS' \right\} dt' \tag{2.2-8}$$

The above are convolution integrals in the time-domain. The common factor in the integrands is the scalar free space time-domain Green's function

$$\mathcal{G}(\bar{r}, \bar{r}', t, t') = \frac{\delta(t-t'-|\bar{r}-\bar{r}'|/c)}{4\pi|\bar{r}-\bar{r}'|} \tag{2.2-9}$$

We can therefore write

$$\bar{\mathcal{A}}(\bar{r}, t) = \mu_o \int_{-\infty}^{\infty} \left\{ \iint_S \bar{\mathcal{J}}_s(\bar{r}', t')\, \mathcal{G}(\bar{r}, \bar{r}', t, t')\, dS' \right\} dt' = \mu_o \iint_S \bar{\mathcal{J}}_s(\bar{r}', t') * \mathcal{G}(\bar{r}, \bar{r}', t, t')\, dS' \tag{2.2-10}$$

and

$$\Phi(\bar{r}, t) = \frac{1}{\varepsilon_o} \int_{-\infty}^{\infty} \left\{ \iint_S \rho_s(\bar{r}', t')\ \mathcal{G}(\bar{r}, \bar{r}', t, t')\, dS' \right\} dt' = \frac{1}{\varepsilon_o} \iint_S \rho_s(\bar{r}', t') * \mathcal{G}(\bar{r}, \bar{r}', t, t')\, dS' \tag{2.2-11}$$

where symbol $*$ denotes convolution with respect to the time variable.

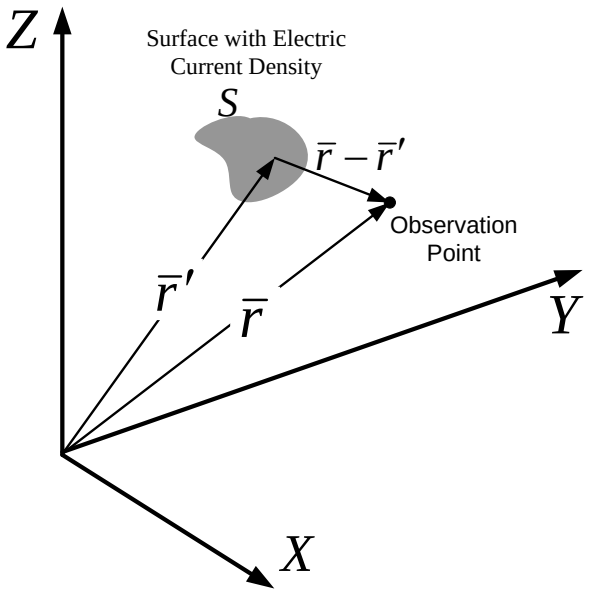

Fig. 2.2-1: Depiction of the spatial coordinate system.

The charge conservation principle relates the electric charge and current density through

$$\nabla \cdot \bar{\mathscr{J}}_s(\bar{r},t) = -\frac{\partial}{\partial t}\{\rho_s(\bar{r},t)\} \tag{2.2-12}$$

and so

$$\rho_s(\bar{r},t) = -\int_{-\infty}^{t} \nabla \cdot \bar{\mathscr{J}}_s(\bar{r},\gamma)\, d\gamma \tag{2.2-13}$$

we consider only systems for which the excitation, and hence due to the causality requirement, the response, is zero for $t < 0$, hence we can write (2.2-13) as

$$\rho_s(\bar{r},t) = -\int_{0}^{t} \nabla \cdot \bar{\mathscr{J}}_s(\bar{r},\gamma)\, d\gamma \tag{2.2-14}$$

and

$$\rho_s(\bar{r},t-R/c) = -\int_{0}^{t-R/c} \nabla \cdot \bar{\mathscr{J}}_s(\bar{r},\gamma)\, d\gamma \tag{2.2-15}$$

with $R = |\bar{r}-\bar{r}'|$ used for convenience, and γ as merely a dummy variable.

Substitution of (2.2-14) into (2.2-11) then yields

$$\Phi(\bar{r},t)=\frac{1}{\varepsilon_o}\int_0^t\left\{\iint_S \nabla'\cdot\bar{\mathscr{J}}_s(\bar{r}',\gamma)*\mathcal{G}(\bar{r},\bar{r}',\gamma,t')\,dS'\right\}d\gamma \tag{2.2-16}$$

whereas its substitution into (2.2-8) yields

$$\Phi(\bar{r},t)=\frac{1}{\varepsilon_o}\int_0^t\left(\int_{-\infty}^{\infty}\left\{\iint_{S_c}\nabla'\cdot\bar{\mathscr{J}}_s(\bar{r}',t')\,\frac{\delta(\gamma-t'-|\bar{r}-\bar{r}'|/c)}{|\bar{r}-\bar{r}'|}dS'\right\}dt'\right)d\gamma \tag{2.2-17}$$

2.3 ELECTRIC FIELD INTEGRAL EQUATIONS FOR A PEC OBJECT

2.3.1 Initial Remarks

The work of this thesis concerns the determination of the time-domain electric current density $\bar{\mathscr{J}}_s(\bar{r},t)$ induced at points $\bar{r}$ on the surface of a PEC object when a prescribed incident field (due to some impressed source) impinges on the object, using integral equation (IE) models. In particular, we will deal only with the time-domain electric field integral equation (TD-EFIE), and so this is discussed next.

2.3.2 General Forms of the Time-Domain Electric Field Integral Equation (TD-EFIE)

The most widely discussed integral equation in computational electromagnetics is the electric-field integral equation (EFIE) that models scattering from a PEC object. An arbitrarily shaped PEC scatterer, shown in Fig. 2.3-1, is considered to be situated in an otherwise unbounded homogeneous medium of permittivity ε, permeability μ, and zero conductivity. The surface of the PEC object is denoted by S. In the absence of the PEC object, specified impressed sources generate a known incident field $\bar{\mathscr{E}}^{inc}(\bar{r},t)$. The surface equivalence principle [PETE 97] permits us to replace the original physical problem by an electric surface current density $\bar{\mathscr{J}}_s$ on S, but with the PEC object absent, and which thus radiates in the homogeneous medium. This $\bar{\mathscr{J}}_s$ gives rise to a scattered field $\bar{\mathscr{E}}^{scat}\left\{\bar{r},t,\bar{\mathscr{J}}_s(\bar{r},t)\right\}$, thus, the total field at any observation point $\bar{r}$ then being the sum of the incident and scattered fields, namely $\bar{\mathscr{E}}(\bar{r},t)=\bar{\mathscr{E}}^{inc}(\bar{r},t)+\bar{\mathscr{E}}^{scat}(\bar{r},t)$. The scattered field, which we denote by $\bar{\mathscr{E}}^{scat}\left\{\bar{r},t,\bar{\mathscr{J}}_s(\bar{r},t)\right\}$ to show its dependence on $\bar{\mathscr{J}}_s$, can be written as the spatio-temporal convolution[4] between the time-domain Green's function for the unbounded background medium and surface current density $\bar{\mathscr{J}}_s$. The physical boundary condition on the PEC object requires that $\hat{n}(\bar{r})\times\bar{\mathscr{E}}(\bar{r},t)=0$ at points $\bar{r}\in S'$. It's enforcement, along with (2.2-1), results in the TD-EFIE

[4] By using (2.2-1), (2.2-10) and (2.2-11).

$$\hat{n}(\bar{r})\times\bar{\mathscr{E}}^{scat}\left\{\bar{r},t,\bar{\mathscr{J}}_s(\bar{r},t)\right\}=-\hat{n}(\bar{r})\times\bar{\mathscr{E}}^{inc}(\bar{r},t)\qquad \bar{r}\in S' \tag{2.3-1}$$

with the unknown $\bar{\mathscr{J}}_s$ located within integrals in (2.2-1). This is referred to as the *undifferentiated* form of the TD-EFIE, the reason being that (for purposes that will become apparent in Section 2.3.3) we can differentiate both sides of (2.3-1) with respect to time to obtain its so-called *differentiated* form

$$\hat{n}(\bar{r})\times\frac{\partial}{\partial t}\bar{\mathscr{E}}^{scat}\left\{\bar{r},t,\bar{\mathscr{J}}_s(\bar{r},t)\right\}=-\hat{n}(\bar{r})\times\frac{\partial}{\partial t}\bar{\mathscr{E}}^{inc}(\bar{r},t)\qquad \bar{r}\in S' \tag{2.3-2}$$

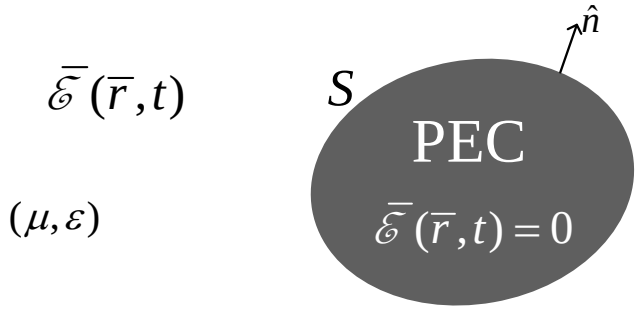

Fig. 2.3-1: Representation of original physical problem

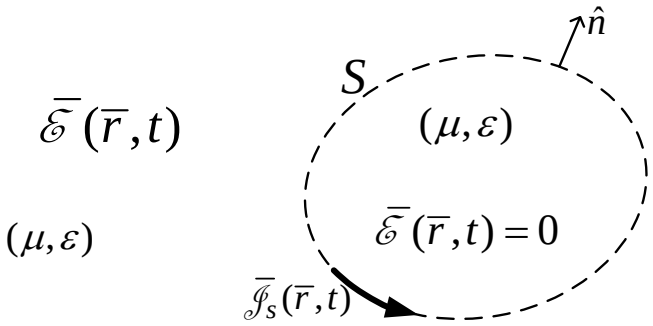

Fig. 2.3-2: Problem equivalent to the original physical problem in the region external to the conducting object

2.3.3 Detailed Forms of the Time-Domain Electric Field Integral Equation

A. Detailed Form of the Undifferentiated TD-EFIE

If we use (2.2-1), (2.2-7), and (2.2-17) in (2.3-1) we can write the TD-EFIE as

$$\frac{\mu}{4\pi}\hat{n}(\bar{r})\times\frac{\partial}{\partial t}\left(\iint_S \bar{\mathscr{J}}_s(\bar{r}',t')*\mathcal{G}(\bar{r},\bar{r}',t,t')\,dS'\right)$$
$$-\frac{1}{4\pi\varepsilon_o}\hat{n}(\bar{r})\times\nabla\int_0^t\left(\iint_S \nabla'\cdot\bar{\mathscr{J}}_s(\bar{r}',\gamma)*\mathcal{G}(\bar{r},\bar{r}',\gamma,t')\,dS'\right)d\gamma = \hat{n}(\bar{r})\times\bar{\mathscr{E}}^{inc}(\bar{r},t) \qquad \bar{r}\in S \tag{2.3-3}$$

If we instead use (2.2-1), (2.2-10), and (2.2-17) in (2.3-1) we obtain the identical (just more explicitly written) form

$$\frac{\mu}{4\pi}\hat{n}(\bar{r})\times\frac{\partial}{\partial t}\left(\int_{-\infty}^{\infty}\left\{\iint_S \bar{\mathscr{J}}_s(\bar{r}',t')\,\frac{\delta(t-t'-|\bar{r}-\bar{r}'|/c)}{|\bar{r}-\bar{r}'|}\,dS'\right\}dt'\right)$$
$$-\frac{1}{4\pi\varepsilon_o}\hat{n}(\bar{r})\times\nabla\int_0^t\left(\int_{-\infty}^{\infty}\left\{\iint_{S_c} \nabla'\cdot\bar{\mathscr{J}}_s(\bar{r}',t')\,\frac{\delta(\gamma-t'-|\bar{r}-\bar{r}'|/c)}{|\bar{r}-\bar{r}'|}\,dS'\right\}dt'\right)d\gamma = \hat{n}(\bar{r})\times\bar{\mathscr{E}}^{inc}(\bar{r},t) \qquad \bar{r}\in S \tag{2.3-4}$$

B. Detailed Forms of the Differentiated TD-EFIE

Inspection of (2.3-3) and (2.3-4) shows that the 2nd term contains a time integral of the divergence of the current density, originating of course from the replacement of the electric charge density by a surface current density term using the continuity equation (2.2-12). It can be removed by differentiating both sides of (2.3-3) or (2.3-4) with respect to time to obtain the differentiated forms of the TD-EFIE

$$\frac{\mu}{4\pi}\hat{n}(\bar{r})\times\frac{\partial^2}{\partial t^2}\left(\iint_S \bar{\mathscr{J}}_s(\bar{r}',t')*\mathcal{G}(\bar{r},\bar{r}',t,t')\,dS'\right)$$
$$-\frac{1}{4\pi\varepsilon_o}\hat{n}(\bar{r})\times\nabla\left(\iint_S \nabla'\cdot\bar{\mathscr{J}}_s(\bar{r}',t')*\mathcal{G}(\bar{r},\bar{r}',t,t')\,dS'\right)=\hat{n}(\bar{r})\times\frac{\partial}{\partial t}\bar{\mathscr{E}}^{inc}(\bar{r},t)\qquad \bar{r}\in S \tag{2.3-5}$$

or

$$\frac{\mu}{4\pi}\hat{n}(\bar{r})\times\frac{\partial^2}{\partial t^2}\left(\int_{-\infty}^{\infty}\left\{\iint_S \bar{\mathscr{J}}_s(\bar{r}',t')\,\frac{\delta(t-t'-|\bar{r}-\bar{r}'|/c)}{|\bar{r}-\bar{r}'|}\,dS'\right\}dt'\right)$$
$$-\frac{1}{4\pi\varepsilon_o}\hat{n}(\bar{r})\times\nabla\left(\int_{-\infty}^{\infty}\left\{\iint_{S_c} \nabla'\cdot\bar{\mathscr{J}}_s(\bar{r}',t')\,\frac{\delta(t-t'-|\bar{r}-\bar{r}'|/c)}{|\bar{r}-\bar{r}'|}\,dS'\right\}dt'\right)=\hat{n}(\bar{r})\times\frac{\partial}{\partial t}\bar{\mathscr{E}}^{inc}(\bar{r},t)\qquad \bar{r}\in S \tag{2.3-6}$$

The TD-EFIE expression (2.3-6) is the form that will be the springboard for the derivation of the re-initialized NILT*n* approach in Chapter 5.

2.3.4 Complex Frequency-Domain (s-Domain) Electric Field Integral Equation

A. Complex Frequency Domain Form of the Undifferentiated TD-EFIE

In order to obtain the complex frequency-domain EFIE we take the Laplace transform of both sides of the TD-EFIE in (2.3-5). Noting that the definition of convolution is used in place of the aforementioned TD convolution symbol $*$, the transform of the first term on the left-hand side of (2.3-5) is

$$\mathcal{L}\left[\frac{\partial}{\partial t}\left(\int_{-\infty}^{\infty}\left\{\iint_S \bar{\mathcal{J}}_s(\bar{r}',t')\,\frac{\delta(t-t'-|\bar{r}-\bar{r}'|/c)}{|\bar{r}-\bar{r}'|}\,dS'\right\}\,dt'\right)\right]$$

$$=\mathcal{L}\left[\frac{\partial}{\partial t}\left(\iint_S \frac{\bar{\mathcal{J}}_s(\bar{r}',t-|\bar{r}-\bar{r}'|/c)}{|\bar{r}-\bar{r}'|}\,dS'\right)\right]$$

$$=s\mathcal{L}\left(\iint_S \frac{\bar{\mathcal{J}}_s(\bar{r}',t-|\bar{r}-\bar{r}'|/c)}{|\bar{r}-\bar{r}'|}\,dS'\right)-\left(\iint_S \frac{\bar{\mathcal{J}}_s(\bar{r}',t-|\bar{r}-\bar{r}'|/c)}{|\bar{r}-\bar{r}'|}\,dS'\right)_{t=0}$$

(2.3-7)

In order to have a causal system, we assume that $\bar{\mathcal{J}}_s(\bar{r},t)=0$ for $t<0$. Due to this initial condition, the last terms on the right-hand side of (2.3.7) are zero, and (2.3-7) simplifies to

$$\mathcal{L}\left[\frac{\partial}{\partial t}\left(\int_{-\infty}^{\infty}\left\{\iint_S \bar{\mathcal{J}}_s(\bar{r}',t')\,\frac{\delta(t-t'-|\bar{r}-\bar{r}'|/c)}{|\bar{r}-\bar{r}'|}\,dS'\right\}\,dt'\right)\right]=s\iint_S \frac{\bar{J}_s(\bar{r},s)e^{-s|\bar{r}-\bar{r}'|/c}}{|\bar{r}-\bar{r}'|}\,dS' \qquad (2.3\text{-}8)$$

The transform of the second term on the left-hand side of (2.3-5) is

$$\mathcal{L}\left[\nabla\int_0^t\left(\int_{-\infty}^{\infty}\left\{\iint_{S_c}\nabla'\cdot\bar{\mathcal{J}}_s(\bar{r}',t')\,\frac{\delta(\gamma-t'-|\bar{r}-\bar{r}'|/c)}{|\bar{r}-\bar{r}'|}\,dS'\right\}\,dt'\right)d\gamma\right]$$

$$=\mathcal{L}\left[\nabla\int_0^t\left(\iint_S \frac{\bar{\mathcal{J}}_s(\bar{r}',t-|\bar{r}-\bar{r}'|/c)}{|\bar{r}-\bar{r}'|}\,dS'\right)d\gamma\right]$$

$$=\frac{1}{s}\nabla\mathcal{L}\left(\iint_S \frac{\bar{\mathcal{J}}_s(\bar{r}',t-|\bar{r}-\bar{r}'|/c)}{|\bar{r}-\bar{r}'|}\,dS'\right)+\frac{1}{s}\int_0^0\left(\iint_S \frac{\bar{\mathcal{J}}_s(\bar{r}',\gamma-|\bar{r}-\bar{r}'|/c)}{|\bar{r}-\bar{r}'|}\,dS'\right)d\gamma$$

(2.3-9)

The second term on the left-hand side of (2.3-9) again due to causality is identically zero, and so we have

$$\mathcal{L}\left[\nabla \int_0^t \left(\int_{-\infty}^{\infty} \left\{ \iint_{S_c} \nabla' \cdot \bar{\mathcal{J}}_s(\bar{r}', t') \frac{\delta(\gamma - t' - |\bar{r} - \bar{r}'|/c)}{|\bar{r} - \bar{r}'|} dS' \right\} dt' \right) d\gamma \right] = \frac{1}{s} \nabla \left(\iint_S \frac{\bar{J}_s(\bar{r}, s) e^{-s|\bar{r} - \bar{r}'|/c}}{|\bar{r} - \bar{r}'|} dS' \right)$$

(2.3-10)

Finally, taking the Laplace transform of the excitation term on the right-hand side of (2.3-5) gives

$$\mathcal{L}\left\{\hat{n}(\bar{r}) \times \bar{\mathcal{E}}^{inc}(\bar{r}, t)\right\} = \hat{n}(\bar{r}) \times \bar{E}^{inc}(\bar{r}, s) \tag{2.3-11}$$

where

$$\bar{E}^{inc}(\bar{r}, s) = \mathcal{L}\left(\bar{\mathcal{E}}^{inc}(\bar{r}, t)\right) \tag{2.3-12}$$

Thus, the s-domain form of the undifferentiated TD-EFIE is

$$\frac{\mu_0}{4\pi} \hat{n}(\bar{r}) \times s \iint_S \frac{\bar{J}_s(\bar{r}, s) e^{-s|\bar{r} - \bar{r}'|/c}}{|\bar{r} - \bar{r}'|} dS' - \frac{1}{4\pi\varepsilon_o} \hat{n}(\bar{r}) \times \frac{1}{s} \nabla \left(\iint_S \frac{\bar{J}_s(\bar{r}, s) e^{-s|\bar{r} - \bar{r}'|/c}}{|\bar{r} - \bar{r}'|} dS' \right) = \hat{n}(\bar{r}) \times \bar{E}^{inc}(\bar{r}, s)$$

(2.3-13)

B. Complex Frequency Domain Form of the Differentiated TD-EFIE

We take the Laplace transform of both sides of the differentiated TD-EFIE in (2.3-6). The transform of the first term on the left-hand side of (2.3-6) is

$$\mathcal{L}\left[\frac{\partial^2}{\partial t^2}\left(\int_{-\infty}^{\infty}\left\{\iint_S \bar{\mathscr{J}}_s(\bar{r}',t')\,\frac{\delta(t-t'-|\bar{r}-\bar{r}'|/c)}{|\bar{r}-\bar{r}'|}\,dS'\right\}dt'\right)\right]$$

$$=\mathcal{L}\left[\frac{\partial^2}{\partial t^2}\left(\iint_S \frac{\bar{\mathscr{J}}_s(\bar{r}',t-|\bar{r}-\bar{r}'|/c)}{|\bar{r}-\bar{r}'|}\,dS'\right)\right]$$

$$=s^2\mathcal{L}\left(\iint_S \frac{\bar{\mathscr{J}}_s(\bar{r}',t-|\bar{r}-\bar{r}'|/c)}{|\bar{r}-\bar{r}'|}\,dS'\right)$$

$$-s\left(\iint_S \frac{\bar{\mathscr{J}}_s(\bar{r}',t-|\bar{r}-\bar{r}'|/c)}{|\bar{r}-\bar{r}'|}\,dS'\right)_{t=0}-\left(\frac{\partial}{\partial t}\iint_S \frac{\bar{\mathscr{J}}_s(\bar{r}',t-|\bar{r}-\bar{r}'|/c)}{|\bar{r}-\bar{r}'|}\,dS'\right)_{t=0}$$

(2.3-14)

As stated in Part A of the section, in order to have a causal system we assume that $\bar{\mathscr{J}}_s(\bar{r},t)=0$ for $t<0$. In addition, we will always specify the incident field[5] that $\partial\bar{\mathscr{J}}_s(\bar{r},t)/\partial t=0$ for $t<0$ as well. Because of these initial conditions the final two terms on the right-hand side of (2.3-14) are zero, and we have

$$\mathcal{L}\left[\frac{\partial^2}{\partial t^2}\left(\int_{-\infty}^{\infty}\left\{\iint_S \bar{\mathscr{J}}_s(\bar{r}',t')\,\frac{\delta(t-t'-|\bar{r}-\bar{r}'|/c)}{|\bar{r}-\bar{r}'|}\,dS'\right\}dt'\right)\right]=s^2\iint_S \frac{\bar{J}_s(\bar{r}',s)\,e^{-s|\bar{r}-\bar{r}'|/c}}{|\bar{r}-\bar{r}'|}\,dS' \qquad (2.3\text{-}15)$$

The transform of the second term on the left-hand side of (2.3-6) is

[5] As will be explained in Section 2.4, the incident field or impressed voltage used in this thesis always has a Gaussian pulse shape in the time-domain. We will always shift the peak of the Gaussian pulse sufficiently forward along the time axis so that these two conditions are met for all practical purposes.

$$\mathcal{L}\left[\nabla\left(\int_{-\infty}^{\infty}\left\{\iint_S \nabla'\cdot\bar{\mathscr{J}}_s(\bar{r}',t')\,\frac{\delta(t-t'-|\bar{r}-\bar{r}'|/c)}{|\bar{r}-\bar{r}'|}dS'\right\}dt'\right)\right]$$
$$=\mathcal{L}\left[\nabla\left(\iint_S \frac{\nabla'\cdot\bar{\mathscr{J}}_s(\bar{r}',t-|\bar{r}-\bar{r}'|/c)}{|\bar{r}-\bar{r}'|}dS'\right)\right]$$
$$=\nabla\left[\mathcal{L}\left(\iint_S \frac{\nabla'\cdot\bar{\mathscr{J}}_s(\bar{r}',t-|\bar{r}-\bar{r}'|/c)}{|\bar{r}-\bar{r}'|}dS'\right)\right]$$
$$=\nabla\left(\iint_S \frac{\nabla'\cdot\bar{J}_s(\bar{r}',s)\,e^{-s|\bar{r}-\bar{r}'|/c}}{|\bar{r}-\bar{r}'|}dS'\right) \tag{2.3-16}$$

Finally, taking the Laplace transform of the excitation term on the right-hand side of (2.3-6) gives

$$\mathcal{L}\left(\hat{n}(\bar{r})\times\frac{\partial}{\partial t}\bar{\mathscr{E}}^{inc}(\bar{r},t)\right)$$
$$=\hat{n}(\bar{r})\times\mathcal{L}\left(\frac{\partial}{\partial t}\bar{\mathscr{E}}^{inc}(\bar{r},t)\right) \tag{2.3-17}$$
$$=\hat{n}(\bar{r})\times\left\{s\,\bar{E}^{inc}(\bar{r},s)-\bar{\mathscr{E}}^{inc}(\bar{r},0)\right\}$$

The assumed initial conditions mean that $\bar{\mathscr{E}}^{inc}(\bar{r},0)=0$, and so

$$\mathcal{L}\left(\hat{n}(\bar{r})\times\frac{\partial}{\partial t}\bar{\mathscr{E}}^{inc}(\bar{r},t)\right)=s\,\hat{n}(\bar{r})\times\bar{E}^{inc}(\bar{r},s) \tag{2.3-18}$$

where $\bar{E}^{inc}(\bar{r},s)=\mathcal{L}\left(\bar{\mathscr{E}}^{inc}(\bar{r},t)\right)$. Thus, the s-domain form of the differentiated TD-EFIE is

$$\frac{\mu}{4\pi}\hat{n}(\bar{r})\times s^2\iint_S \frac{\bar{J}_s(\bar{r}',s)\,e^{-s|\bar{r}-\bar{r}'|/c}}{|\bar{r}-\bar{r}'|}dS'$$
$$-\frac{1}{4\pi\varepsilon_o}\hat{n}(\bar{r})\times\nabla\left(\iint_S \frac{\nabla'\cdot\bar{J}_s(\bar{r}',s)\,e^{-s|\bar{r}-\bar{r}'|/c}}{|\bar{r}-\bar{r}'|}dS'\right)=s\,\hat{n}(\bar{r})\times\bar{E}^{inc}(\bar{r},s) \tag{2.3-19}$$

2.3.5 Frequency-Domain Electric Field Integral Equation

The frequency-domain EFIE for the 3D problem is well-documented [PETE 97]. It can in fact be obtained from the complex frequency-domain form[6] by replacing s by $j\omega$ in (2.3-13), to obtain

$$\frac{j\omega\mu}{4\pi}\hat{n}(\bar{r})\times\iint_S \frac{\bar{J}_s(\bar{r},\omega)e^{-j\omega|\bar{r}-\bar{r}'|/c}}{|\bar{r}-\bar{r}'|}dS' - \frac{1}{j4\pi\omega\varepsilon}\hat{n}(\bar{r})\times\nabla\left(\iint_S \frac{\bar{J}_s(\bar{r},\omega)e^{-j\omega|\bar{r}-\bar{r}'|/c}}{|\bar{r}-\bar{r}'|}dS'\right) = \hat{n}(\bar{r})\times\bar{E}^{inc}(\bar{r},\omega) \tag{2.3-20}$$

2.3.6 Other Time-Domain Integral Equations

The magnetic field integral equation (MFIE) and combined field integral equation (CFIE) for scattering form PEC objects can be derived in the frequency-domain [PETE 97], complex frequency-domain [DÉLY 23], and time-domain [BEGH 13]. However, these can only be used for closed PEC objects. We therefore in this thesis only consider the EFIE, which is applicable to both open and closed PEC objects.

[6] We do this using the s-domain form of the undifferentiated TD-EFIE only. It is what is usually meant by the frequency-domain EFIE for scattering from a PEC object.

2.4 GAUSSIAN PULSE IMPRESSED PORT VOLTAGES & INCIDENT PLANE WAVE FIELDS

2.4.1 Gaussian Pulse Impressed Voltage Excitation (Antenna Excitation)

In the case of an antenna problem such as that in Fig. 2.4-1, we will consider application of an impressed voltage $v_{in}(t)$ at the input terminals of the antenna, given by [JIN 14, Sect.12.1.2]

$$v_{in}(t) = V_o\, e^{-\frac{1}{2}\left(\frac{t-t_o}{\tau_w}\right)^2} \tag{2.4-1}$$

and graphed in Fig. 2.4-2. It has its maximum value of V_o at time $t = t_o$, with t_o referred to as the delay. The value of $v_{in}(t)$ is $0.02V_o$ (that is, down to 2% of its maximum value) approximately at times $t = t_o \pm 2\sqrt{2}\tau_{\rm w}$, and so we could refer to $T_{\rm w} = 2(2\sqrt{2}\tau_{\rm w}) = 4\sqrt{2}\tau_{\rm w}$ as the pulse-width[7]. Substitution of this relation between $T_{\rm w}$ and $\tau_{\rm w}$ into (2.4-1) allows the latter to be written as [RAO 99]

$$v_{in}(t) = V_0\, e^{-\left(\frac{4}{T_{\rm w}}(t-t_o)\right)^2} \tag{2.4-2}$$

In order to ensure[8] that $v_{in}(t)$ is negligible for $t < 0$, some authors recommend that $t_o \geq 10\tau_{\rm w}$ (in other words $t_o \geq 1.77T_{\rm w}$) although others have used $t_o \geq 8.5\tau_{\rm w}$ ($t_o \geq 1.50T_{\rm w}$).

The spectrum of (2.4-1) is given by the Fourier transform [JIN 14]

$$V_{in}(\omega) = \mathcal{F}\{v_{in}(t)\} = \sqrt{2\pi}\,V_o\; e^{-\frac{1}{2}(\omega\tau_{\rm w})^2}\, e^{-j\omega t_o} \tag{2.4-3}$$

Fig. 2.4-2 shows a plot of (2.4-3). If we take the upper frequency as $\omega_u = 3/\tau_{\rm w}$, then $f_u = \omega_u / 2\pi = 3/2\pi\tau_{\rm w}$, which in terms of $T_{\rm w}$ reads[9]

[7] Some authors prefer to use $T_{\rm d} = 4\tau_{\rm w}$ as the pulse-width, albeit not usually in the computational electromagnetics literature concerning applications in the frequency range below 300 GHz.
[8] Some authors say this is to ensure a quasi-quiescent state for $t < 0$.

$$f_u = \frac{6\sqrt{2}}{\pi T_{\mathrm{w}}} \tag{2.4-4}$$

the smaller T_{w} is, the more frequency harmonics are included. Later in the thesis we will also require the Laplace transform of $v_{in}(t)$, and so write it here as

$$V_{in}(s) = \frac{V_0 T_w \sqrt{\pi}}{8} e^{-(4t_o/T_w)^2} \mathrm{erfcx}\left(\frac{sT_w}{8} - \frac{4t_0}{T_w} \right) \tag{2.4-5}$$

with erfcx the so-called scaled complex complementary error function or Faddeeva function [WEID 94], defined by

$$\mathrm{erfcx}(z) = e^{z^2} \mathrm{erfc}(z) \tag{2.4-6}$$

and $\mathrm{erfc}(...)$ is the usual complementary error function.

[9] If we express T_{w} in ns, then (2.4-4) gives f_u in GHz.

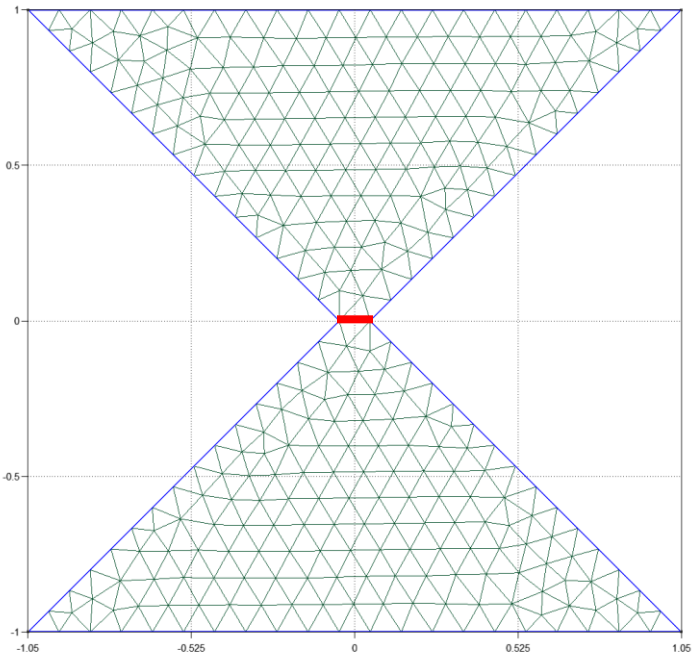

Fig. 2.4-1: Antenna problem : Gaussian excitation (impressed) voltage at the antenna port (—).

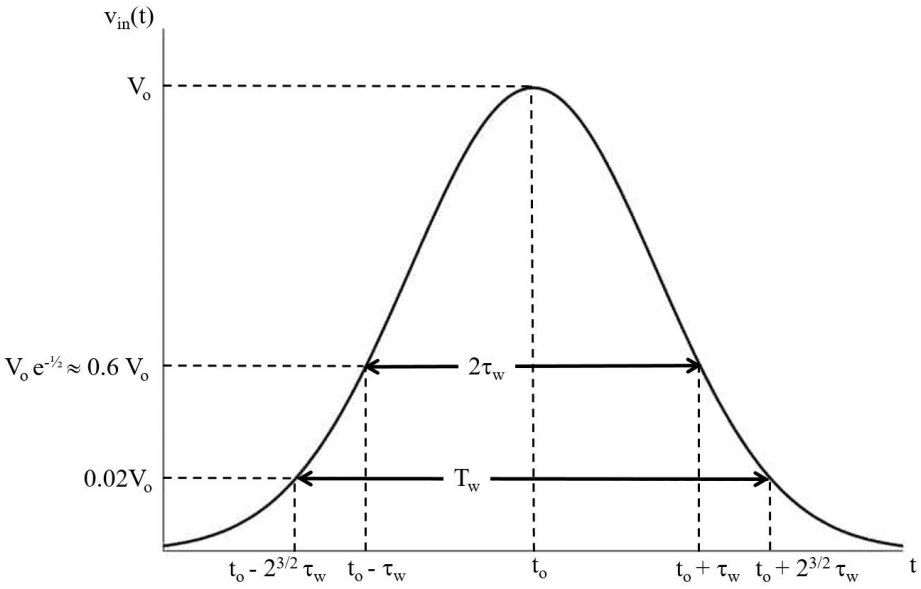

Fig. 2.4-2: Graph of Gaussian pulse function. Not drawn to scale.

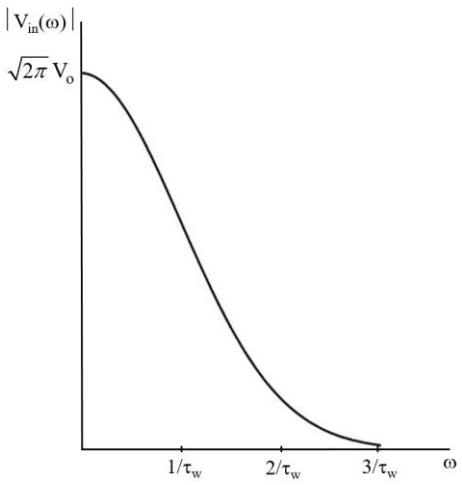

Fig. 2.4-3: Frequency spectrum of the Gaussian pulse function. Not drawn to scale.

2.4.2 Gaussian Plane Wave Field Excitation

An incident Gaussian pulse plane wave can be expressed as

$$\bar{\mathcal{E}}^{inc}(\bar{r},t) = \hat{u}^{inc}\, E_o \exp\left(-\frac{\left\{ t - t_o - (\bar{r}\cdot\hat{k}^{inc}/c) \right\}^2}{\left\{ T_w/4 \right\}^2} \right) \tag{2.4-6}$$

where $\hat{u}^{inc}$ is the polarization vector of the incident field, and $\hat{k}^{inc}$ its propagation direction. The Laplace transform of this $\bar{\mathcal{E}}^{inc}(\bar{r},t)$ is

$$\bar{E}^{inc}(\bar{r},s) = \hat{u}^{inc}\, \frac{E_0 T_w \sqrt{\pi}}{8} \exp\left(-\frac{\left\{ t_o + (\bar{r}\cdot\hat{k}^{inc}/c) \right\}^2}{\left\{ T_w/4 \right\}^2} \right) \operatorname{erfcx}\left(\frac{sT_w}{8} - \frac{t_0 + \left(\bar{r}\cdot\hat{k}^{inc}\right)/c}{T_w/4} \right) \tag{2.4-7}$$

If the incident plane wave is incoming on the PEC object from direction $(\theta^{inc}, \phi^{inc})$ then its direction of travel is described by unit vector

$$\hat{k}^{inc} = \hat{x}\sin\theta^{inc}\cos\phi^{inc} + \hat{y}\sin\theta^{inc}\sin\phi^{inc} + \hat{z}\cos\theta^{inc} \tag{2.4-8}$$

and so

$$\bar{r}\cdot\hat{k}^{inc} = x\sin\theta^{inc}\cos\phi^{inc} + y\sin\theta^{inc}\sin\phi^{inc} + z\cos\theta^{inc} \tag{2.4-9}$$

therefore, substituting (2.4-9) into (2.4-7) yields

$$\bar{E}^{inc}(x,y,z,s) = \hat{u}^{inc}\,\frac{E_0 T_w \sqrt{\pi}}{8}\,exp\left(- \frac{\left\{ t_0 + \dfrac{x\sin\theta^{inc}\cos\phi^{inc} + y\sin\theta^{inc}\sin\phi^{inc} + z\cos\theta^{inc}}{c} \right\}^2}{\left\{ T_w / 4 \right\}^2} \right)$$

$$\times \quad \text{erfcx}\left(\frac{sT_w}{8} - \frac{\left\{ t_0 + \dfrac{x\sin\theta^{inc}\cos\phi^{inc} + y\sin\theta^{inc}\sin\phi^{inc} + z\cos\theta^{inc}}{c} \right\}}{\left\{ T_w / 4 \right\}} \right)$$

(2.4-10)

2.5 EXTRACTING WIDEBAND FREQUENCY INFORMATION FROM TIME-DOMAIN SOLUTIONS

An electric current density $\bar{\mathscr{J}}_s(\bar{r},t)$ due to an incident field $\mathscr{E}^{inc}(\bar{r},t)$ can have an arbitrary time-variation. The frequency response $\bar{J}_s(\bar{r},\omega)$ can be obtained [BENN 70] as the Fourier transform of $\bar{\mathscr{J}}_s(\bar{r},t)$, being due to an incident field $\bar{E}^{inc}(\bar{r},\omega)$ that is the Fourier transform of $\bar{\mathscr{E}}^{inc}(\bar{r},t)$. Similar comments can be made in the case of antenna excitation by a voltage pulse at the antenna terminal.

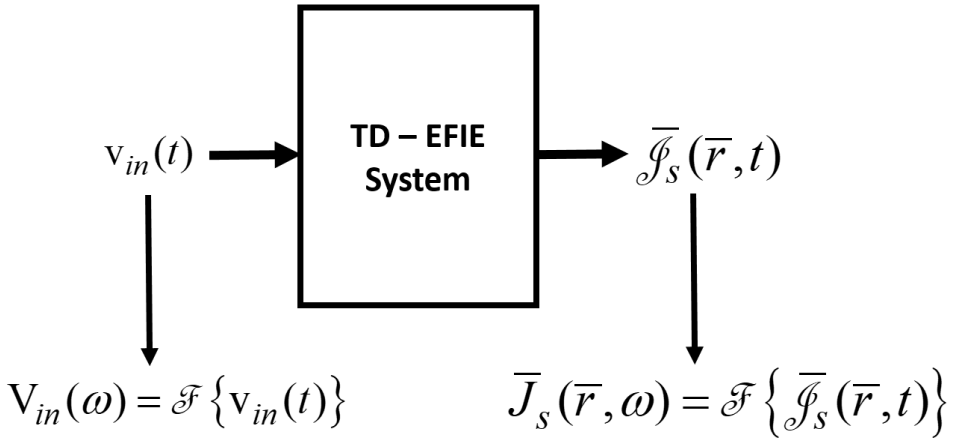

Fig. 2.5-1: Transformation from time-domain quantities to frequency-domain quantities.

2.6 MOMENT METHOD MARCHING-ON-IN-TIME (MOT) SOLUTION OF THE TD-EFIE

2.6.1 Initial Remarks

In order to properly place the work of the present thesis into context, the widely explored MOT method of moments approach for the numerical solution of TD-IEs will be reviewed, albeit not at all exhaustively. Only a selected number of more recent key references are provided, remembering that these themselves cite many more that allowed the progress in the MOT solutions of TD-IEs since the 1970's to be followed.

2.6.2 Direct Time-Discretization Enabled Marching-on-in-Time (MOT) Method

In order to formulate the MOT/MoM solution of the TD-EFIE (of which there are the differentiated and undifferentiated forms), and other TD-IEs, for PEC objects, the current density is approximated using spatial and temporal expansion functions. These are usually N_s sub-domain Rao-Wilton-Glisson (RWG) functions or its higher-order versions [GRAG 15] over a triangular mesh, and N_t sub-domain piecewise Lagrange interpolators up to the 2nd order, [GERA 09] time-shifted by an amount Δt, respectively. There is a temporal expansion function for each point in time at which the solution will be sampled. The spatial testing functions are normally RWG functions, in other words a Galerkin MoM in space. Collocation is typically used for testing in time at equidistant time steps, effectively using Dirac-delta functions for such testing, although there have been some exceptions [BEGH 13]. This space-time discretization results in an implicit MOT formulation. If we adopt the concise notation from Section 10.6.2 of [JIN 10], where further details can be found for all the terms mentioned below, the MOT procedure can arranged to read

$$[\mathcal{Z}^{(0)}][I]^{(k)} = [\mathcal{V}]^{(k)} - \sum_{p=1}^{k-1} [\mathcal{Z}^{(k-p)}][I]^{(p)} \qquad k = 1, 2, 3, ... \tag{2.6-1}$$

integer k identifies the particular point in time, $[I]^{(k)}$ the column vector of coefficients of the spatial expansion functions for that k (point in time), $[\mathcal{Z}^{(k-p)}]$ is the MoM square matrix[10], and $\{\mathcal{V}\}^{(k)}$ is a vector related to the incident field. The appropriateness of the terminology "time-marching" is easily appreciated by increasing the value of k in steps starting from $k=1$ to see that the above represents successive matrix equations

$$[\mathcal{Z}^{(0)}][I]^{(1)} = [\mathcal{V}]^{(1)} \tag{2.6-2}$$

$$[\mathcal{Z}^{(0)}][I]^{(2)} = [\mathcal{V}]^{(2)} - [\mathcal{Z}^{(1)}][I]^{(1)} \tag{2.6-3}$$

$$[\mathcal{Z}^{(0)}][I]^{(3)} = [\mathcal{V}]^{(3)} - [\mathcal{Z}^{(2)}][I]^{(1)} - [\mathcal{Z}^{(1)}][I]^{(2)} \tag{2.6-4}$$

and so forth. A matrix equation must be solved for each new value of k (it is an implicit scheme), determining the right-hand side of the said matrix equation (that depends on the solution at the previous step) being the most time-consuming part, since $[\mathcal{Z}^{(0)}]$ turns out to be sparse.

The elements of the N_t interaction matrices $[\mathcal{Z}^{(q)}]$ each of size $N_s \times N_s$ are functions of the step size but not of time. However, some involve complicated space-time integration over sub-regions of the triangles, different in detail from their frequency-domain counterparts, explicit expressions being available in [JIN 14]. It is apparent that at each point in time the above time-stepping matrix equation involves an updating of the known right-hand side using the current vectors at previous times. This updating (involving matrix-vector products) is the most time-consuming part of the process. The temporal discretization has converted the continuous convolution in time into a sequence of discrete convolutions.

Early MOT solutions of TD-IEs were plagued by what researchers have classified as late-time instabilities, low-frequency breakdown instabilities, and DC instabilities (static loop modes)

[10] Usually simply called interaction matrices. They do not have the dimensions of impedance, and so should not be called impedance matrices as would be done in solutions of the frequency-domain EFIE.

[FURS 00][RYNN 90]. Although general stability proofs that provide criteria to make the formulations unconditionally stable do not yet appear to be available, many strategies have since been devised to keep these at bay, and verified through extensive numerical experiments. Solutions for the current density that exhibit spurious fluctuations that grow in amplitude are called late-time instabilities. In [SHI 11], numerical experiments revealed that the use of semi-analytical so-called quasi-exact integration in the determination of the elements of $\left[\mathcal{Z}^{(q)}\right]$ enables excellent late-time stability properties in the TD-EFIE even for small time-steps (and hence accurate solutions), for temporal expansion functions up to the 2nd order. This approach was extended to the TD-MFIE and TD-CFIE in [WANG 21], revealing the same ability to obtain accurate solutions through appropriate adjustment of the spatial and temporal discretization rates. MOT solutions of the TD-EFIE are also troubled by spurious static currents (DC instability). The solutions contain spurious static loop currents constant in the case of the undifferentiated TD-EFIE and linearly increasing for the differentiated one, which can limit late-time accuracy. These would not be present in an exact solution, but emerge due to the discretization and unavoidable finite accuracy of the numerical computations. An altered TD-EFIE, based on the incorporation of quasi-Helmhotz projectors and rescaling has been shown in [BEGH 15] to be capable of solution using the MOT process without the occurrence of DC instabilities, and free of the ill-conditioning that results for large time-steps. The later situation arises when the PEC object is electrically small relative to the shortest wavelength in the excitation (and is analogous to the "low-frequency problem" in frequency-domain solutions, caused by the separation of electric and magnetic effects of charges and currents at these frequencies), the mesh density being governed by the need to resolve the geometrical features of the object. In most cases though, the mesh density will be driven by the need to resolve the shortest wavelength in the excitation. We do not expect interior cavity modes of closed PEC objects to be excited when such objects are externally-excited. Theoretically, under zero initial conditions, TD-IEs for closed PEC objects should not admit such spurious modes as part of their solution either. However, the process of discretization and numerical errors these are observed in MOT solutions, and although not leading to late-time instabilities, may corrupt the solutions of the TD-EFIE and TD-MFIE, even with quasi-exact integration. They do not appear in solutions of the TD-CFIE [SHAN 00][WANG 21] or for the TD-EFIE with open PEC objects.

2.6.3 Convolution Quadrature Enabled Marching-on-in-Time (MOT) Method

The above space-time MOT procedure results when the time variable in the TD-EFIE is discretized directly. The convolution-quadrature method [WANG 11][DÉLY 20][DÉLY 23] achieves temporal discretization via an indirect route. The formulation and implementation of the method is technically complex, composed of many steps, and with several parameters needing to be appropriately chosen, but a very detailed discussion on its successful implementation is conveniently outlined in [DÉLY 23]. A qualitative appreciation of its essence can be had by considering that the TD-EFIE is Laplace-transformed to the complex frequency-domain and spatially discretized (via the MoM procedure) into a matrix equation $[Z(s)][I(s)]=[V(s)]$. The expressions for the terms of the matrix $[Z(s)]$ being very similar to that obtained in the frequency-domain MoM solutions of the EFIE. We also recall that an inverse Z-transform, which is the discrete equivalent of the inverse Laplace transform, transforms a continuous function into a discrete sequence of sampled function values [MCCL 16]. Furthermore, recognizing that multiplication by the complex frequency *s* corresponds to differentiation with respect to time, implicit Runge-Kutta (IRK) methods are used to express *s* as a function of the Z-domain[11] variable z, which upon substitution into $[Z(s)][I(s)]=[V(s)]$ converts the matrix equation into the Z-domain form. Use of the above-mentioned inverse Z-transform (that can be accomplished using the discrete Fourier transform [WANG 11] or trapezoidal rule [DÉLY 20]), then converts the Z-domain matrix equation into a sequence of discrete convolutions that can be rewritten in a form similar to that quoted for the MOT procedure discussed earlier. The *s*-domain matrix equation is not actually solved for $[I(s)]$, as will be done in the so-called NILT approach described below (albeit for the purpose of circuit analysis). Researchers have noted that this convolution-quadrature route can in practice offer up to fifth order accuracy in time, and is late-time stable independent of the choice of temporal step-size. A decided advantage is the determination of the interaction matrix terms is grounded in well-tested frequency-domain MoM implementations, and so the stability of such methods are apparently less dependent on the precision of the integration formulas. [DÉLY 23] observes that "the main disadvantage of

[11] We do not mean an "impedance domain" here of course.

convolution quadrature schemes, based as they are on time stepping schemes for the solution of ordinary differential equations, can introduce dispersion errors that increase for broadband inputs".

2.7 FOUNDATIONS OF THE NUMERICAL INVERSION OF THE LAPLACE TRANSFORM (NILT) TECHNIQUE IN LINEAR CIRCUIT ANALYSIS

2.7.1 Preliminary Remarks and Goals

A technique for numerical inversion of the Laplace transform (NILT), perhaps not as widely familiar in the field of computational electromagnetics, relies on known pre-determined coefficients that are entirely problem-independent and effectively permit high-order representation with respect to the time variable. It was originally developed for time-domain circuit analysis [VLAC 83], where the coupled differential equations are expressed in matrix equation form, with the unknown currents occupying a column vector.

The NILT approach is not inherently a time-stepped one, because it does not discretize time directly. The solution for the time-domain current density at the current time (the "now") does not explicitly depend on the previous solution at an earlier time. As will be shown later, the solution at each different point in time uses a set of complex frequency-domain solutions of the EFIE at (different) prescribed values of the complex frequency s. The NILT solution becomes less accurate (but never unstable) as the value of t moves further away from zero. The accuracy of the solution further out in time can be improved using easily accessible derivative (up to order n, say) information on the Laplace domain solutions $[I(s)]$, resulting in so-called NILTn methods [TAO 21][GAD 22]. A significant advantage of the NILT approach when used in (non-field) differential equation-based circuit analysis has been, if a process called re-initialization is employed, the NILTn approach is converted into a pseudo time-stepping procedure that provides accurate and stable results even further out in time.

As stated, a key advantage of the NILT approach in circuit analysis has been its ability to move forward in time using relatively large time steps while, maintaining accuracy and being free of stability problems. However, users are often interested, not only in the value of the waveform at particular points in time, but also in the temporal shape of the underlying waveform in between those time points. This demand constitutes a challenge for both the initial-value and re-initialized value of the NILTn as it fundamentally challenges what is so advantageous of the method (the ability to determine the time-domain waveform accurately and stably through sparsely spaced time points). In [GAD 22], the use of explicit Hermite interpolation using cycle

index polynomials was recommended. The interpolation method is based on constructing a polynomial that satisfies a set of values of the quantity in question, along with the first few time-derivatives of the quantity at a set of pre-specified points. It was shown in [GAD 22] that both the initial value mode and the re-initialized mode of the NILT*n* can be slightly altered to compute the necessary time-derivatives[12] to be used for the Hermite interpolation.

The goal of this section is to introduce to the reader the concept of the NILT. This thesis will apply the NILT*n*, in both its initial value mode of operation (not a time-stepped method) and re-initialized mode (a time-stepped method). However, we will make use of all previously completed work regarding the NILT without re-deriving[13] it, and thus only a summary of pertinent expressions is provided. Readers that are interested in the full derivation of the existing NILT formulations can find this in [VLAC 83], [TAO 21], [GAD 22], and [BARD 22]. In addition, an interpolation method based on Hermite interpolation [GAD 22] is introduced and an explanation is given of the concept.

2.7.2 Mathematical Foundations of the NILT

A. Notation

In Section 2.7, the following mathematical notation will be used. Let $\mathbb{N}$, to define the set of non-negative integer number, $n \in \mathbb{N}$ will denote a non-negative integer, $n = 0,1,2,\ldots$. Let $\mathbb{C}$ define the sets of complex numbers. The required notation will require the use of a multi-index. A multi-index in the context of this section defines a vector in $\mathbb{N}^M$, i.e., a vector whose M components are non-negative integers. A bold font lowercase letter, e.g. $\boldsymbol{l}$, will be used to denote a given multi-index, while its individual components will be denoted by a subscripted italic (non-bold) lowercase of the same letter, i.e., $l_i, i = 1,2,\ldots,M$, where $l_i \in \mathbb{N}$.

[12] Without any need for numerical differentiation.
[13] What does not exist will of course will be derived *ab initio*.

A set of multi-indices, Λ_p^M , is a set defined by

$$\Lambda_p^M := \left\{ \boldsymbol{l} \in \mathbb{N}^M : \sum_{i=1}^{M} l_i = p \right\} \tag{2.7-1}$$

the factorial of a multi-index will be defined as the product of the factorials of its components,

$$\boldsymbol{l}! := \prod_{i=1}^{M} l_i! \tag{2.7-2}$$

finally, a multi-index, $\boldsymbol{l}$,when used as the power of another complex vector $\boldsymbol{d} \in \mathbb{C}^M$ defines the operation

$$\boldsymbol{d}^{\boldsymbol{l}} := \prod_{i=1}^{M} d_i^{l_i} \tag{2.7-2}$$

Furthermore, $\tilde{x}^{[n]}(t)$ will be used to denote the NILT*n* approximation to $x(t)$ at arbitrary time t, remarking that $\tilde{x}^{[0]}(t)$ is the same value obtained by the classical NILT, i.e, NILT0

B. Foundations of the NILT

NILT is essentially a time-domain approach that is grounded in the complex frequency-domain. In addition, the advantage of NILT compared to conventional transient time-domain simulators stems from several factors. First, it enables approximating waveforms with high-degree polynomials, a fact that allows the step taken in marching through time to be larger than the step afforded by conventional simulators, which relies on low-order approximating polynomials to maintain the numerical stability. NILT on the other hand, is structurally stable regardless of the degree of thee underlying approximating polynomial. The stability is mathematically recognized as the L-stable is another factor that adds the NILT robustness.

The basic idea of the NILT is to recover the time-domain waveform using its Laplace-domain representation. The NILT approach begins from the classical definition of determining the time-

domain function $x(t)$ from the inverse Laplace transform of the Laplace domain function $X(s)$. It is assumed that $x(t)$ is stable, and therefore, $X(s)$ will have no singularities in the right-half plane

$$x(t) = \mathcal{L}^{-1}\{X(s)\} = \frac{1}{2\pi j}\int_{\alpha - j\infty}^{\alpha + j\infty} X(s)e^{st}ds \tag{2.7-3}$$

where $j = \sqrt{-1}$, $\mathcal{L}$ denotes the Laplace transformation, and α is a constant chosen such that all singularities in $X(s)$ lie on the left of the vertical line $\Re(s) = \alpha$. It then proceeds by substituting st with z, and representing e^z by its [*N/M*] Padé approximation $\xi_{N,M}(z)$ given by [BAKE 95]

$$\xi_{N,M}(z) = \frac{P_N(z)}{Q_M(z)} = \frac{\sum_{i=1}^{N}\alpha_{i,M,N}z^i}{\sum_{i=1}^{M}(-1)^i\alpha_{i,N,M}z^i} \tag{2.7-4}$$

where $\alpha_{i,M,N}$ is

$$\alpha_{i,M,N} = \frac{(M+N-i)!}{(M+N)!}\binom{M}{i} \tag{2.7-5}$$

It can be shown that $\xi_{N,M}(z)$ can be represented as a form of the pole-residue partial fraction

$$\xi_{N,M}(z) = \sum_{i=1}^{M}\frac{k_i}{z - z_i} \tag{2.7-6}$$

where the poles and residues, respectively, z_i and k_i, are obtained from the roots of the polynomial $Q_M(z)$ in (2.7-4). Although these values can be found mathematically, some of the possible values of z_i and k_i for a given *M* and *N* are shown in Fig. 2.7-1

Table 10.1.2. A Selection of Poles z_i and Residues K_i' for Various N, M.

		$N = M - 3$		$N = M - 2$		$N = M - 1$	
M	i	$\mathrm{Re}(z_i)$ $\mathrm{Im}(z_i)$	$\mathrm{Re}(K_i')$ $\mathrm{Im}(K_i')$	$\mathrm{Re}(z_i)$ $\mathrm{Im}(z_i)$	$\mathrm{Re}(K_i')$ $\mathrm{Im}(K_i')$	$\mathrm{Re}(z_i)$ $\mathrm{Im}(z_i)$	$\mathrm{Re}(K_i')$ $\mathrm{Im}(K_i')$
2	1			1.000000000000000 1.000000000000000	0.000000000000000 −2.000000000000000	2.000000000000000 1.414213562373095	2.000000000000000 −7.071067811865476
4	1	2.764346415715100 1.162323629283275	−1.486485011597801 −12.10916705674577	3.779019967010193 1.380176524272843	2.256958744418140 −39.63308700050173	4.787193103128467 1.567476416895208	26.60307999194297 −120.1434654740949
	2	1.235653584284900 3.437652493671051	1.486485011597801 3.433270826956831	2.220980032989807 4.160391445506932	−2.256958744418140 11.10883163787590	3.212806896871534 4.773087433276643	−22.60307999194297 24.94335170050046
10	1	10.82098193052256 1.517953393700372	2186.697231341063 −48581.24805840772	11.83009373916819 1.593753005885813	16286.62368050479 −139074.7115516051	12.83767707781087 1.666062584162301	73804.09376005109 −393980.9270580073
	2	10.21449035429789 4.562479433009242	−3989.181746394491 27449.17684030028	11.22085377939519 4.792964167565670	−28178.11171305163 74357.58237274176	12.22613148416215 5.012719263676865	−122553.9994117030 190817.1978146481
	3	8.932235514658323 7.637703369344925	2320.955454239880 −8164.422991702790	9.933383722175002 8.033106334266296	14629.74025233142 −19181.80818501836	10.93430343060001 8.409672996003091	57833.14454064847 −36338.37020019288
	4	6.786787372173086 10.78715258382734	−556.8837335166699 1044.522752571332	7.781146264464616 11.36889164904993	−2870.418161032078 −1674.109484084304	8.776434640082610 11.92185389830121	−9310.721692796347 3.803546061166028
	5	3.245504828348141 14.14179989064435	38.41279433021752 −29.05774606159169	4.234522494797000 14.95704378128156	132.1659412474876 17.47674798877164	5.225453367344362 15.72952904563926	237.4828037997930 282.6073846434469

Fig. 2.7-1: Table (extracted from [VLAC 83]) showing a selection of poles z_i and residuals K_i' for various *N* and *M* combinations. Note that the framed entry should be 1674.109484084304 and not the negative value shown.

The NILT approximations of $x(t)$ are obtained through applying the Cauchy theorem of residues on the line integrals in (2.7-3) with the finite summation of the residues of $X\left(\frac{z}{t}\right)\xi_{N,M}(z)$ at the poles of $\xi_{N,M}(z)$. Those poles are known to lie in the right-half plane of the complex domain $\Re(s) > 0$ [BAKE 95]. Those steps, combined, results in obtaining an approximation $\tilde{x}(t) \approx x(t)$, and is for an even *M* given by,

$$\tilde{x}^{[0]}(t) = -\frac{2}{t}\sum_{i=1}^{M/2} \mathcal{R}e\left\{k_i X\left(\frac{z_i}{t}\right)\right\} \tag{2.7-7}$$

or for an odd *M*,

$$\tilde{x}^{[0]}(t) = -\frac{2}{t}\sum_{i=1}^{(M-1)/2} \mathcal{R}e\left\{k_i X\left(\frac{z_i}{t}\right)\right\} - \frac{1}{t}k_0 X\left(\frac{z_0}{t}\right) \tag{2.7-8}$$

with k_i and z_i, $i = 1,...,M$ being, respectively, the residues and poles of the partial fraction expression in (2.7-4), noting that for even values of M, poles and residues appear in complex-conjugate pairs, and for odd M, only one residue-pole duo (k_0, z_0) is real, with the rest being in complex-conjugate pairs. In what follows, M will be taken as even knowing that odd values can be treated in a similar manner.

C. Accuracy

It has been shown in [SING 93], that the approximation of $\tilde{x}^{[n]}(t)$ is related to the exact $x(t)$ through

$$x(t) - \tilde{x}^{[0]}(t) = \Psi_{N,M} \left.\frac{d^{N+M+1}}{dt^{N+M+1}} x(t)\right|_{t=0} t^{N+M+1} + O\left(t^{N+M+2}\right) \tag{2.7-9}$$

where $\Psi_{N,M}$ is the "truncation constant' given by

$$\Psi_{N,M} = \frac{(-1)^M M!\, N!}{(M+N)!(N+M+1)!} \tag{2.7-10}$$

The choice of the integers N and M is done based on satisfying two main requirements. The first requirement is that the summation in (2.7-7) and (2.7-8) should be equivalent to the integral in (2.7-1), while the second requirement pertains to guaranteeing the numerical stability in the proceeding from one point in time to the next. It has been shown [SING 75] that the two stated requirements are satisfied if, and only if, $N = M - 2$.

2.7.3 Initial Value Mode of the NILT*n*

A. Foundation

A more accurate variant of the NILT, called the NILT*n* (or the modified NILT), has been introduced recently in [TAO 21]. The NILT*n* recovers the time-domain response of $x(t)$ from the derivatives of the Laplace-domain, $X(s)$, w.r.t s, up to the n^{th}-order derivative. For $n=0$, the NILT*n* (NILT0) is equivalent to the classical NILT described in the previous section. It has been shown in [TAO 21] that the NILT*n* multiplies the truncation constant by $1/(n+1)^{N+M}$ effectively reducing the approximation error by several orders-of-magnitudes. This feature made it possible to take longer time steps without sacrificing the accuracy or incurring additional significant computation cost. The general formulation for the initial value mode of the NILT*n* is shown below

$$\tilde{x}^{[n]}(t) = -\frac{p\,p!}{t}\sum_{\boldsymbol{l}\in\Lambda_p^M}\sum_{\substack{i=1\\ l_i\neq 0}}^{M}\frac{\boldsymbol{k}^{\boldsymbol{l}}}{\boldsymbol{l}!}\left[\frac{1}{(l_i-1)!}\sum_{\mu=0}^{l_i-1}\binom{l_i-1}{\mu}\left(\frac{p\,z_i}{t}\right)^{\mu}X\left(\frac{p\,z_i}{t}\right)^{(\mu)}\cdot\left(\sum_{\boldsymbol{v}\in\Lambda_{l_i-1-\mu}^{M-1}}\frac{(l_i-1-\mu)!}{\boldsymbol{v}!}\prod_{\substack{j=1\\ j\neq i}}^{M}\frac{(-1)^{v_j}\prod_{\theta=0}^{v_j-1}(l_j+\theta)}{(z_i-z_j)^{l_j+v_j}}\right)\right] \tag{2.7-11}$$

where $p=n+1$[14], $\boldsymbol{k}=\begin{bmatrix}k_1 & k_2 & \dots & k_M\end{bmatrix}^T$ and

$$X\left(\frac{pz_i}{t}\right)^{(\mu)} = \left.\frac{d^{\mu}X(s)}{ds^{\mu}}\right|_{s=\frac{p\,z_i}{t}} \tag{2.7-12}$$

[14] Where *n* pertains to the "*n*" in the NILT*n*

Of particular interest in this thesis, are the expressions for the initial value modes of the NILT0, NILT1, and NILT2, which are simplifications of (2.7-11) for $n = 0$, $n = 1$ and $n = 2$ respectively. Those expressions are respectively shown for the NILT0

$$\tilde{x}^{[0]}(t) = -\frac{2}{t}\sum_{i=1}^{M/2} \mathcal{R}e\{k_i X(s)\}\Big|_{s=\frac{z_i}{t}} \tag{2.7-13}$$

the NILT1

$$\tilde{x}^{[1]}(t) = -\frac{8}{t}\sum_{i=1}^{M/2} \mathcal{R}e\left\{\frac{(k_i)^2}{t}\frac{dX(s)}{ds} + k_i X(s)\sum_{\substack{j=1\\ j\neq i}}^{M}\frac{k_j}{z_i - z_j}\right\}\Bigg|_{s=\frac{2z_i}{t}} \tag{2.7-14}$$

and the NILT2

$$\tilde{x}^{[2]}(t) = -\frac{9}{t}\sum_{i=1}^{M/2} Re\left\{\frac{3(\tilde{k}_i)^3}{8t^2}\frac{d^2X(s)}{ds^2} + \frac{3(\tilde{k}_i)^2}{2t}\frac{dX(s)}{ds}\sum_{\substack{j=1\\ j\neq i}}^{M}\frac{k_j}{z_i - z_j} + X(s)\left(\tilde{k}_i\sum_{\substack{j=1\\ j\neq i}}^{M}\sum_{\substack{v=1\\ v\neq 1}}^{M}\frac{k_j k_v}{(z_i - z_j)(z_i - z_v)} - \frac{(\tilde{k}_i)^2}{2}\sum_{\substack{j=1\\ j\neq i}}^{M}\frac{k_j}{(z_i - z_j)^2}\right)\right\}\Bigg|_{s=\frac{3z_i}{t},\ \tilde{k}_i = 2k_i} \tag{2.7-15}$$

Of course, as stated earlier, (2.7-13) is the same as (2.7-7) because the NILT0 is the same as the classical NILT.

B. Application of the Initial Value Mode of the NILTn in Circuit Analysis

To implement the NILT*n* for circuit analysis using the initial-value mode, one will need first compute the Laplace-domain derivatives of the circuit variables $\boldsymbol{X}(s)$, up to the n[th]-order at values of s equal to $\frac{z_i}{t}$, $i = 1,...,M/2$. Those derivatives, denoted $\boldsymbol{B}^{[q]}(s)$ are obtained from the well known MNA circuit formulation as follows [VLAC 83]

$$(\boldsymbol{G} + s\boldsymbol{C})\boldsymbol{X}^{(0)}(s) = \boldsymbol{B}^{(0)}(s) + \boldsymbol{C}x(0) \tag{2.7-16}$$

and

$$(\boldsymbol{G} + s\boldsymbol{C})\boldsymbol{X}^{(q)}(s) = \boldsymbol{B}^{(q)}(s) - q\boldsymbol{C}\boldsymbol{X}^{(q-1)}, \quad q = 1,...,n \tag{2.7-17}$$

where $\boldsymbol{x}(0) \equiv x(t)\big|_{t=0}$. After computing those s-domain derivatives, recursively, for values of $s = \frac{pz_i}{t}$, those, (vector-valued derivatives) are substituted in (2.7-11) for the (scalar-valued) $X\left(\frac{pz_i}{t}\right)^{(\mu)}$ to obtain vector-values of the NILT*n*-based approximations for all circuit variables.

2.7.4 Re-Initialized Mode of the NILT*n*

A. Foundation

As stated in the introduction, the initial value NILT*n* solution becomes less accurate (but never unstable) as the value of *t* moves further away from zero. However, the NILT can greatly improve the accuracy of results further out in time, by employing the NILT*n* approach in a time-stepping procedure while maintaining stability. This method is called the re-initialized NILT*n*.

The implementation of the re-initialized NILT*n* is done by creating the approximation of $x(t)$ for values of $t = (r+1)h$, for an integer r where, $r = 0,1,2,...,$ and with given length of time step h. It does so by using the approximation made at previous time point i.e., $t = rh$. The formula of the re-initialized mode of the NILT*n* is similar to the formula initial-value mode of NILT*n* given in (2.7-11). The formula of the re-initialized mode of the NILT*n* is given by

$$\tilde{x}^{[n]}\left((r+1)h\right) = -\frac{pp!}{h}\sum_{\boldsymbol{l}\in\Lambda_p^M}\sum_{\substack{i=1\\ l_i\neq 0}}^{M}\frac{\boldsymbol{k}^{\boldsymbol{l}}}{\boldsymbol{l}!}\left[\frac{1}{(l_i-1)!}\sum_{\mu=0}^{l_i-1}\binom{l_i-1}{\mu}\left(\frac{p}{h}\right)^{\mu}\hat{X}\left(\frac{pz_i}{h}\right)^{(\mu)}\right.$$
$$\left.\cdot\left(\sum_{\boldsymbol{v}\in\Lambda_{l_i-1-\mu}^{M-1}}\frac{(l_i-1-\mu)!}{\boldsymbol{v}!}\prod_{\substack{j=1\\ j\neq i}}^{M}\frac{(-1)^{v_j}\prod_{\theta=0}^{v_j-1}(l_j+\theta)}{(z_i-z_j)^{l_j+v_j}}\right)\right] \tag{2.7-18}$$

where, $\hat{X}\left(\frac{pz_i}{h}\right)^{(\mu)}$ in (2.7-18) is defined by

$$\hat{X}\left(\frac{pz_i}{h}\right)^{(\mu)} = \frac{d^{\mu}}{ds^{\mu}}\left(\hat{X}(s)\right)\Big|_{s=\frac{pz_i}{h}}$$
$$\hat{X}(s) = \mathcal{L}\left\{x\left(\hat{t}+rh\right)\right\}, \tag{2.7-19}$$
$$= \int_0^{\infty} x\left(\hat{t}+rh\right)e^{s\hat{t}}d\hat{t}, \qquad r = 1,2,...$$

Similar to the NILT0, the NILT*n* requires the Laplace expression of the time-domain $x(t)$ shifted by r steps of length h, i.e., $x\left(\hat{t}+rh\right)$. However, a re-initialized NILT*n* requires not simply the Laplace domain expression of the shifted time-domain, but also its s-domain derivatives. The utility of the NILT*n* will be made clearer when examples are presented in terms of circuit simulations.

B. Applications of NILTn – Re-Initialization Mode in Circuit Analysis

Using the re-initialized mode of the NILT*n*, we will need the Laplace-domain version of the time-domain, *rh*-shifted, of all circuit variables. This is carried out by substituting the change of time variable $t \to \hat{t}+rh$ into the time-domain MNA formulation of the circuit equations and taking the Laplace transformation w.r.t $\hat{t}$. The outcome of this process can be expressed through.

$$\boldsymbol{G}\hat{\boldsymbol{x}}\left(\hat{t}\right)+\boldsymbol{C}\frac{d\boldsymbol{x}\left(\hat{t}\right)}{d\hat{t}} = \boldsymbol{b}\left(\hat{t}+rh\right) \tag{2.7-20}$$

$$\left(\boldsymbol{G}+\hat{s}\boldsymbol{C}\right)\hat{\boldsymbol{X}}\left(\hat{s}\right)=\hat{\boldsymbol{B}}\left(\hat{s}\right)+\boldsymbol{C}\hat{\boldsymbol{x}}\left(rh\right) \tag{2.7-21}$$

where $\boldsymbol{x}\left(\hat{t}\right)\equiv\boldsymbol{x}\left(\hat{t}+rh\right)$. $\hat{\boldsymbol{X}}\left(\hat{s}\right)$ in both (2.7-20) and (2.7-21) is the Laplace transform of $\boldsymbol{x}\left(\hat{t}+rh\right)$. Similarly, $\hat{\boldsymbol{B}}\left(\hat{s}\right)$ is the Laplace transform of $\boldsymbol{b}\left(\hat{t}+rh\right)$, w.r.t. $\hat{t}$. $\hat{s}$ was used in the place of s to demonstrate that the Laplace transform was done w.r.t. $\hat{t}$ instead of t.

In order to work with the formula for the NILT*n*, the s-domain derivatives of $\hat{\boldsymbol{X}}\left(\hat{s}\right)$, w.r.t. $\hat{s}$ are needed at values of $\hat{s}$ equal to $\frac{pz_i}{h}$. To make it up to time $\hat{t}=h$, which is equivalent to $t=\left(r+1\right)h$ in the original time-domain, we substitute $\hat{s}=\frac{p\,z_i}{h}$ in those derivatives. The derivatives themselves are obtained by differentiating both sides of (2.7-20) and (2.7-21), w.r.t. $\hat{s}$ n times

$$\left(\boldsymbol{G}+\hat{s}\boldsymbol{C}\right)\hat{\boldsymbol{X}}\left(\hat{s}\right)^{(0)}=\hat{\boldsymbol{B}}^{(0)}\left(\hat{s}\right)+\boldsymbol{C}\hat{\boldsymbol{x}}\left(rh\right) \tag{2.7-20}$$

$$\left(\boldsymbol{G}+\hat{s}\boldsymbol{C}\right)\hat{\boldsymbol{X}}\left(\hat{s}\right)^{(q)}=\hat{\boldsymbol{B}}^{(q)}\left(\hat{s}\right)+\boldsymbol{C}\hat{\boldsymbol{X}}\left(\hat{s}\right)^{(q-1)},\quad q=1,2,...,n \tag{2.7-21}$$

Thus, the NILT*n*-based approximation to circuit variables $\boldsymbol{x}\left(t\right)$ at the time $t=\left(r+1\right)h$, with $r=0,1,2...$, can be written as

$$\tilde{x}^{[n]}\left(\left(r+1\right)h\right)=-\frac{p\;p!}{h}\sum_{\boldsymbol{l}\in\Lambda_p^M}\;\sum_{\substack{i=1\\ l_i\neq 0}}^{M}\frac{\boldsymbol{k}^{\boldsymbol{l}}}{\boldsymbol{l}!}\left[\frac{1}{\left(l_i\text{-}1\right)!}\sum_{\mu=0}^{l_i\text{-}1}\binom{l_i\text{-}1}{\mu}\left(\frac{p}{h}\right)^{\mu}\overbrace{\hat{\boldsymbol{X}}\left(\frac{p\,z_i}{h}\right)^{(q)}}^{(2.7-20)\ \&\ (2.7-21)}\right.$$
$$\left.\cdot\left(\sum_{\boldsymbol{v}\in\Lambda_{l_i\text{-}1\text{-}\mu}^{M\text{-}1}}\frac{\left(l_i\text{-}1-\mu\right)!}{\boldsymbol{v}!}\prod_{\substack{j=1\\ j\neq i}}^{M}\frac{\left(-1\right)^{v_j}\prod_{\theta=0}^{v_j\text{-}1}\left(l_j+\theta\right)}{\left(z_i\text{-}z_j\right)^{l_j+v_j}}\right)\right] \tag{2.7-22}$$

2.7.5 The Explicit Hermite Interpolation

As stated in the introduction and shown above, the high-order approximation of NILT, combined with the L-stability, has allowed NILT to take a larger time step h without losing accuracy. In other words, NILT is capable of approximating a given time-domain waveform at relatively – compared with conventional time stepping methods – sparsely-separated time points. Although this feature yields an overall reduction in the computational cost and CPU time, it does not produce a waveform that is detailed enough to be used in a task such as Fourier transformation to extract its frequency content. The goal of this section is to present how this issue has been addressed though the NILT framework, using the notation of Hermite interpolation [GAD 22].

The idea of the Hermite interpolation is to construct a polynomial that approximates a given function, through interpolating the values, and derivatives that this function are known to have for specific set of points of its independent variables. To illustrate this notion more clearly, assume that the values of a given function of time t, $x(t)$ is known at a set of H time points, $t_1, t_2, ..., t_H$. Furthermore, assume that higher-order derivatives of this function $d^{\beta}x(t)/dt^{\beta}$ are also known at those same points, where $0 \le \beta \le m_i$, (for $\beta = 0, d^{\beta}x(t)/dt^{\beta} \equiv x(t)$), with $i = 1, ..., H$ and m_i being a given integer. Then a polynomial $x_p(t)$ constructed using the expression

$$x_p(t) = \sum_{\alpha=1}^{H} \sum_{\beta=0}^{m_\alpha - 1} \frac{x(t_\alpha)^{(\beta)}}{\beta!} \prod_{\substack{\gamma=1 \\ \gamma \neq \alpha}}^{H} \left(\frac{t - t_\gamma}{t_\alpha - t_\gamma} \right)^{m_\gamma} \sum_{k=\beta}^{m_\alpha - 1} (t - t_\alpha)^k \, z_{k-\beta} \left(\sum_{\gamma \neq \alpha} \frac{m_\gamma}{(t_\gamma - t_\alpha)^r} \middle| r \in [k - \beta] \right) \quad (2.7\text{-}23)$$

matches $x(t)$ and its derivatives at the H time points. More precisely,

$$\left. \frac{d^{\beta_i} x_p(t)}{dt^{\beta_i}} \right|_{t=t_i} = \left. \frac{d^{\beta_i} x(t)}{dt^{\beta_i}} \right|_{t=t_i}, \quad i = 1, 2, ...H, \quad 0 \le \beta_i \le m_i \quad (2.7\text{-}24)$$

the notation used in (2.7-23) is given as,

$$x(t)^{(\beta)} = \frac{d^{\beta} x(t)}{dt^{\beta}} \tag{2.7-25}$$

and $z(\bullet)$ refers to the cycle index polynomial, whose construction is given in more details in [GAD 22].

The use of the Hermite interpolation is well suited to address the problem mentioned in the previous paragraph of this section, provided that NILT paradigm is extended to compute the higher-order derivatives required for the interpolation technique. This computation was developed in [GAD 22] and is briefly summarized in the remainder of this section.

2.7.6 Computing NILT*n*-Based Approximations of Time-Domain Derivatives

[GAD 22] has adapted the NILT*n* to compute time-domain derivatives. In order to allow the above notations to express the notion of derivatives, we will utilize $\tilde{\boldsymbol{x}}^{[n]}(t)^{(\beta)}$ to denote the NILT*n*-based approximation to β^{th}-order derivative of $\boldsymbol{x}(t)$, that is

$$\tilde{\boldsymbol{x}}^{[n]}(t)^{(\beta)} \equiv \text{NILT}n \text{ approximation of } \frac{d^{\beta} \boldsymbol{x}(t)}{dt^{\beta}} \tag{2.7-26}$$

It is important to note, that $\tilde{\boldsymbol{x}}^{[n]}(t)^{(\beta)}$ that are computed therein, will be substituted for $x(t_{\alpha})^{(\beta)}$ in (2.7-23) to construct the Hermite interpolant.

A. Initial Value Mode

The expression for $\tilde{\boldsymbol{x}}^{[n]}(t)^{(\beta)}$ using the initial value mode is

$$\tilde{\boldsymbol{x}}^{[n]}(t)^{(\beta)} = \tilde{\boldsymbol{\Theta}}_1(t)^{(\beta)} \; - \; \tilde{\boldsymbol{\Theta}}_2(t)^{(\beta)} \tag{2.7-27}$$

where,

$$\tilde{\boldsymbol{\Theta}}_1(t)^{(\beta)} = -\frac{pp!}{t}\sum_{\boldsymbol{l}\in\Lambda_p^M}\sum_{\substack{i=1\\ l_i\neq 0}}^{M}\frac{\boldsymbol{k}^{\boldsymbol{l}}}{\boldsymbol{l}!}\left[\frac{1}{(l_i-1)!}\sum_{\mu=0}^{l_i\text{-}1}\binom{l_i\text{-}1}{\mu}\left(\frac{p}{t}\right)^{\mu}\right.$$
$$\left.\cdot\left(\sum_{r=0}^{\min(\beta,\mu)}\binom{\mu}{r}\frac{\beta!}{(\beta-r)!}\left(\frac{pz_i}{t}\right)^{\beta-r}\boldsymbol{X}\left(\frac{pz_i}{t}\right)^{(\mu-r)}\right)\mathcal{W}_{i,\mu}\right] \tag{2.7-28}$$

and the function $\tilde{\boldsymbol{\Theta}}_2(t)^{(\beta)}$ is given by

$$\tilde{\boldsymbol{\Theta}}_2^{[n]}(t)^{(\beta)} = -\frac{p\,p!}{t}\sum_{\theta=1}^{\beta-1}\boldsymbol{x}(0)^{(\theta-1)}\sum_{l\in\Lambda_p^M}\sum_{\substack{i=1\\ l_i\neq 0}}^{M}\frac{\boldsymbol{k}^{\boldsymbol{l}}}{\boldsymbol{l}!}\left[\frac{1}{(l-1)!}\sum_{\mu=0}^{l_i\text{-}1}\binom{l_i\text{-}1}{\mu}\right.$$
$$\left.\cdot\left(\left(\frac{(\beta-\theta)!}{(\beta-\theta-\mu)!}\right)\left(\frac{z_i}{t}\right)^{\beta-\theta-\mu}\right)\mathcal{W}_{i,\mu}\right] \quad \beta>1 \tag{2.7-29}$$

where $\mathcal{W}_{i,\mu}$ is given by

$$\mathcal{W}_{i,\mu} = \sum_{\boldsymbol{v}\in\Lambda_{l_i\text{-}1\text{-}\mu}^{M\text{-}1}}\frac{(l_i\text{-}1\text{-}\mu)!}{\boldsymbol{v}!}\prod_{\substack{j=1\\ j\neq i}}^{M}\frac{(-1)^{v_j}\prod_{\theta=0}^{v_j-1}(l_j+\theta)}{(z_i-z_j)^{l_j+v_j}} \tag{2.7-30}$$

B. Re-initialized Mode

The expression for $\tilde{\boldsymbol{x}}^{[n]}\big((r+1)h\big)^{(\beta)}$ using the re-initialized mode is

$$\tilde{\boldsymbol{x}}^{[n]}\big((r+1)h\big)^{(\beta)} = \tilde{\boldsymbol{\Theta}}_1\big((r+1)h\big)^{(\beta)} - \tilde{\boldsymbol{\Theta}}_2\big((r+1)h\big)^{(\beta)} \tag{2.7-31}$$

where,

$$\tilde{\boldsymbol{\Theta}}_1\left((r+1)h\right)^{(\beta)} = -\frac{pp!}{h}\sum_{\boldsymbol{l}\in\Lambda_p^M}\sum_{\substack{i=1\\ l_i\neq 0}}^{M}\frac{\boldsymbol{k}^{\boldsymbol{l}}}{\boldsymbol{l}!}\left[\frac{1}{(l_i-1)!}\sum_{\mu=0}^{l_i-1}\binom{l_i-1}{\mu}\left(\frac{p}{h}\right)^{\mu}\right.$$
$$\left.\cdot\left(\sum_{r=0}^{\min(\beta,\mu)}\binom{\mu}{r}\frac{\beta!}{(\beta-r)!}\left(\frac{p\,z_i}{h}\right)^{\beta-r}\boldsymbol{X}\left(\frac{p\,z_i}{h}\right)^{(\mu-r)}\right)\mathcal{W}_{i,\mu}\right] \tag{2.7-32}$$

function $\tilde{\boldsymbol{\Theta}}_2\left((r+1)h\right)^{(\beta)}$ is given by

$$\tilde{\boldsymbol{\Theta}}_2^{[n]}\left((r+1)h\right)^{(\beta)} = -\frac{p\,p!}{h}\sum_{\theta=1}^{\beta-1}\tilde{\boldsymbol{x}}^{[n]}(rh)^{(\theta-1)}\sum_{l\in\Lambda_p^M}\sum_{\substack{i=1\\ l_i\neq 0}}^{M}\frac{\boldsymbol{k}^{\boldsymbol{l}}}{\boldsymbol{l}!}\left[\frac{1}{(l-1)!}\sum_{\mu=0}^{l_i-1}\binom{l_i-1}{\mu}\right.$$
$$\left.\cdot\left(\frac{(\beta-\theta)!}{(\beta-\theta-\mu)!}\right)\left(\frac{z_i}{h}\right)^{\beta-\theta-\mu}\mathcal{W}_{i,\mu}\right] \quad \beta>1 \tag{2.7-33}$$

2.8 THE USE OF NILT*n* IN COMPUTATIONAL ELECTROMAGNETICS

Once a TD-EFIE (which contain integrals with retardation terms) has been spatially discretized, the resulting equations have the form of ordinary differential equations, with delay. Any direct solution of such differential equations requires knowledge of the solution at previous times, as evidenced in the resultant MOT schemes described earlier. In electromagnetics, NILT has been used in an FETD framework [TAGG 19], and a TD-EFIE one, albeit in the form of a partial element equivalent circuit (PEEC) implementation in [LORE 23] and [ANTO 23]. The retarded form of the PEEC method (whether in frequency-domain or time-domain form) can be regarded as "mathematically equivalent" [JIN 10, pp.538] to the conventional MoM formulation for the solution of the EFIE [LORE 22]. It differs from the latter in that it is constructed in a manner allowing it to be seamlessly viewed as a generalization of classical circuit theory, which allows lumped elements and very low frequencies (certain geometrical features being electrically extremely small) to be easily included, thus enabling interfacing with circuit simulators. Such a generalized network interpretation is reminiscent of early work in frequency-domain IE work [HARR 68]. Although re-initialization with the NILT/FETD approach [TAGG 19] parallels the ease with which it can be applied in circuit analysis modelling, this is not so when used with the TD-EFIE. This thesis provides, for the first time, a means of exploiting re-initialization when using NILT in the solution of the TD-EFIE.

2.9 CONCLUDING REMARKS

We began this chapter by expressing the interest in this thesis of numerical methods for solution of the TD-EFIE for electromagnetic scattering from PEC objects. Section 2.2 wrote down expressions for the field due to a known surface current density. Section 2.3 gave the general forms of the differentiated and undifferentiated forms of the TD-EFIE, and this was followed by detailed versions thereof, that will be used in later chapters. Some necessary facts about Gaussian pulses were presented in Section 2.4, as these will be the time-domain behaviour of the incident fields to be used in the thesis. It is well-known that one can move from the time to frequency-domain using Fourier transforms, and vice-versa using the inverse of such transforms. Nevertheless, this is stated for the record in Section 2.5. The most widely-used numerical approach to solve the TD-EFIE has been the MoM along with MOT. Although this thesis deliberately sets out to provide an alternative to the use of such an MOT process, we provided a brief review of the afore-mentioned in Section 2.6. All important is the NILT*n* approach as an alternative to the more conventional MOT one. Its use has mainly been applied in the field of lumped circuit analysis, and so we review this, and summarize the key expressions that it utilizes, in the first part of Section 2.7. It is possible to take the values of any physical quantity sampled at successive points in time, and its derivatives with respect to time at these same points, and use special techniques to interpolate its values at other values of time. We will use this, and so in the second part of Section 2.7 provide the principal expressions needed to do so. The NILT*n* route has not been widely used in electromagnetic field problems; its limited use for such purposes was nevertheless briefly referenced in Section 2.8. A major goal of this thesis is to solve a NILT*n*-related issue (the re-initialization problem) that we hope will make its use in computational electromagnetics attractive.

CHAPTER 3 - The Solution of the Time-Domain EFIE Using MoM/NILTn: The 2D Case

3.1 INITIAL REMARKS

It is often the case that, when new techniques in computational electromagnetics are under development, their soundness is tested on established two-dimensional (2D) problems (to be properly defined in the next section) before moving to more general 3D ones. This is the philosophy adopted in the present work.

The earliest studies of the MOT solutions of the TD-EFIE for a PEC object were performed for 2D objects [BENN 70][MITT 76][RAO 99], because it is less demanding on computing resources. Even recently [LU 00][AZAR 14] such 2D cases have been used to test new ideas[15] before the more daunting task of formulating/implementing these for the general 3D case, much like we are doing here for the NILT*n*/MoM approach. We need not implement the MOT procedure. We will instead use the time-domain results provided by [RAO 99], as reference results against which to compare our new 2D NILT*n*/MoM time-domain results.

■ Section 3.2 formulates a TD-EFIE for the 2D problem of plane wave scattering from a PEC cylinder of arbitrary cross-section, with the electric field of the incident plane wave parallel to the cylinder axis (a TM_z problem). This is selected because it reduces to a scalar problem, which is especially easy to deal with. The PEC cylinder may be an open or closed object. The TD-EFIE is used to arrive at the complex frequency-domain form of the EFIE, and thereafter its (very well-known) frequency-domain form. Although this material[16] can be found elsewhere, it was considered appropriate to include this here (and not with the other "known" existing material in Chapter 2) in order to ensure the correct flow of the thesis.

[15] But not the use of NILT*n*/MoM solutions of a 2D TD-EFIE.
[16] That is, material that does not yet make reference to the NILT*n* technique at all.

■ Section 3.3 presents a MoM formulation for solution of the complex frequency EFIE for the said 2D problem, along with its implementation.

■ Section 3.4 presents, as a reference for what is more familiar, a MoM formulation for solution of the frequency-domain EFIE for the said 2D problem, along with its implementation.

■ Section 3.5 next provides the mathematical detail needed for implementation of the initial value NILT*n* approach in conjunction with the solution of the s-domain EFIE for $n \leq 2$.

■ Section 3.6 shows numerical results, along with their careful examination, for both open and closed 2D PEC objects, and highlight some interesting observations.

■ Section 3.7 ponders the difficulties associated with incorporating re-initialization into the NILT*n* approach when, unlike the lumped circuit analysis case, its use in full-wave electromagnetic scattering problems has to deal with the results in the presence of multiple time delay terms. Although the issue is discussed, the actual development of such an ability is postponed to Chapter 5, where it is done for the general 3D problem case.

■ Section 3.8 concludes the chapter.

3.2 TWO-DIMENSIONAL CUSTOMIZATION OF THE TD-EFIE

3.2.1 Definition of the Two-Dimensional (2D) TM_z Problem

Although the derivation of the TD-EFIE for PEC objects in Section 2.3 is quite general, in this chapter we will apply it to two-dimensional (2D) problems only. This will allow us to formulate, implement, and perform numerical experimentation on, an initial NILT*n* method for an electromagnetic field problem that is less complicated than the full 3D one that is the subject of Chapter 4.

If both the PEC object and the source are of a two-dimensional nature, in other words the geometry of the object and the incident field can be completely described in terms of two spatial coordinates (*x* and *y* in our case) and is independent of the third (*z* in our case), then the problem is both physically two-dimensional and so mathematically 2D. As a result, any equivalent current densities and scattered electromagnetic fields will be independent of the spatial coordinate *z*. In fact, if the incident electric field, in addition, only has a z-component, then the induced electric current density only has a z-component as well, and the scattered field has only z-component. The PEC objects are infinitely long cylinders of arbitrary cross-section. Because all quantities are z-independent we can sketch and concern ourselves with the xy-plane. We can have a thin open, or closed, PEC object illuminated as shown in Fig. 3.2-1. The embedding medium is free space, and so $k = \omega\sqrt{\mu_0 \varepsilon_0}$. The 2D position vector is represented by $\bar{\rho} = (x, y)$. As discussed for the general 3D case in Section 2.3, application of the surface equivalence theorem allows us to replace the physical PEC object by an equivalent electric current density $\bar{J}_s(\bar{\rho}) = \hat{z}\, J_z\left(\bar{\rho}\right)$ in free space, located on the contour *C* originally occupied by the PEC object. The incident electric field is that of a z-polarized Gaussian pulse plane wave,

$$\mathscr{E}_z^{inc}(\bar{\rho}, t) = E_o \exp\left(-\frac{\left\{ t - t_o - (\bar{\rho} \cdot \hat{k}^{inc} / c) \right\}^2}{\left\{ T_w / 4 \right\}^2} \right) \tag{3.2-1}$$

with $\hat{k}^{inc}$ its propagation direction. If the incident plane wave is incoming on the PEC object from direction, ϕ^{inc}, then its direction of travel is described by unit vector

$$\hat{k}^{inc} = \hat{x}\cos\phi^{inc} + \hat{y}\sin\phi^{inc} \tag{3.2-2}$$

and so

$$\bar{\rho}\cdot\hat{k}^{inc} = x\cos\phi^{inc} + y\sin\phi^{inc} \tag{3.2-3}$$

Therefore, the Laplace transform of (3.2-1) is

$$E_z^{\,inc}(x,y,s) = \mathcal{L}\left\{\mathcal{E}_z^{inc}(\bar{\rho},t)\right\} = \hat{u}^{inc}\,\frac{E_0 T_w\sqrt{\pi}}{8}\exp\left(-\frac{\left\{t_0 + \dfrac{x\cos\phi^{inc} + y\sin\phi^{inc}}{c}\right\}^2}{\left\{T_w/4\right\}^2}\right) \times \operatorname{erfcx}\left(\frac{sT_w}{8} - \frac{\left\{t_0 + \dfrac{x\cos\phi^{inc} + y\sin\phi^{inc}}{c}\right\}}{\left\{T_w/4\right\}}\right) \tag{3.2-4}$$

Gaussian pulse plane waves were defined in Section 2.4, for arbitrary direction of incidence. In this 2D case we always have $\theta^{inc} = 90^\circ$ and hence we would also arrive at (3.2-4) by simply substituting $\theta^{inc} = 90^\circ$ into expression (2.4-10) of Section 2.4

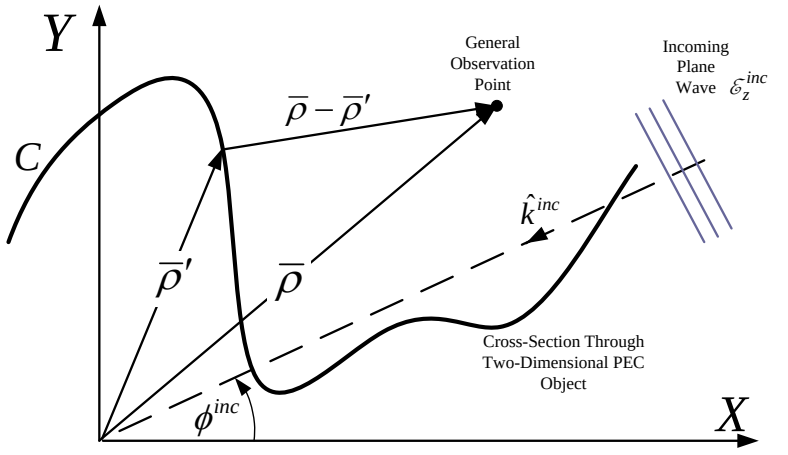

(a)

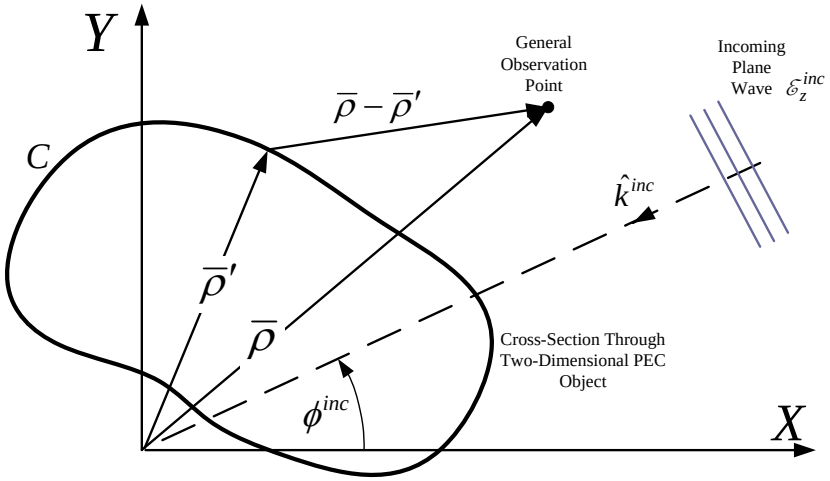

(b)

Fig. 3.2-1: Representation of the two-dimensional (a). Open PEC object, and (b). Closed PEC object.

3.2.2 TD-EFIE for the 2D TM$_z$ Problem

The scattered electric field in terms of the unknown surface current density $\mathcal{J}_z(\bar{\rho},t)$ is[17]

$$\mathcal{E}_z^{scat}\left(\bar{\rho},t\right)=\frac{\partial \mathcal{A}_z^{inc}\left(\bar{\rho},t\right)}{\partial t} \tag{3.2-5}$$

with

$$\mathcal{A}_z\left(\bar{\rho},t\right)=\mu_0\int_C \mathcal{J}_z\left(\bar{\rho}',t\right)*\mathcal{G}\left(\bar{\rho},\bar{\rho}',t\right)dC' \tag{3.2-6}$$

where the time-domain 2D scalar free space Green's function is [MORS 53][NEVE 04]

$$\mathcal{G}\left(\bar{\rho},\bar{\rho}',t\right)=\frac{\mathrm{u}\left(\mathrm{t}-\frac{\left|\bar{\rho}-\bar{\rho}'\right|}{\mathrm{c}}\right)}{2\pi\sqrt{\mathrm{t}^2-\left(\left|\bar{\rho}-\bar{\rho}'\right|/\mathrm{c}\right)^2}} \tag{3.2-7}$$

In the above expressions symbol $*$ continues to denote time convolution, and $u(..)$ is the Heaviside step function[18]. Thus, by requiring that $\mathcal{E}_z^{scat}\left(\bar{\rho},t\right)+\mathcal{E}_z^{inc}\left(\bar{\rho},t\right)=0$ at all points $\bar{\rho}\in C$ we obtain the (un-differentiated) TD-EFIE is

$$\frac{\partial}{\partial t}\left\{\mu_0\int_C \mathcal{J}_z\left(\bar{\rho}',t\right)*\mathcal{G}\left(\bar{\rho},\bar{\rho}',t\right)dC'\right\}=\mathcal{E}_z^{inc}\left(\bar{\rho},t\right)\qquad \bar{\rho}\in C \tag{3.2-8}$$

we will sometimes denote $R=\left|\bar{\rho}-\bar{\rho}'\right|$ in what follows.

[17] These are the equivalents, for the 2D situation under consideration here, of the 3D treatment discussed in Section 2.2 and Section 2.3.

[18] As opposed to the Dirac delta function that occurs in the 3D Green's function in Section 2.2.

3.2.3 Complex-Frequency-Domain EFIE for the 2D TM$_z$ Problem

The complex frequency-domain EFIE for the 2D TM$_z$ problem is found by taking the Laplace transform of both sides of (3.2-8), namely

$$\mathcal{L}\left[\frac{\partial}{\partial \mathrm{t}}\left\{\mu\int_C \mathcal{J}_z(\bar{\rho}',t)*\mathcal{G}(\bar{\rho},\bar{\rho}',t)dC'\right\}\right]=\mathcal{L}\left[\mathcal{E}_z^{inc}(\bar{\rho},t)\right] \tag{3.2-9}$$

In the interest of notational clarity we will write

$$\mathcal{L}\left[\mathcal{E}_z^{inc}(\bar{\rho},t)\right]=E_z^{inc}(\bar{\rho},s) \tag{3.2-10}$$

and[19]

$$\mathcal{L}\left[\frac{\partial}{\partial \mathrm{t}}\left\{\mu\int_C \mathcal{J}_z(\bar{\rho}',t)*\mathcal{G}(\bar{\rho},\bar{\rho}',t)\,dC'\right\}\right]=s\mu\int_C J_z(\bar{\rho}',\mathrm{s})\,G(\bar{\rho},\bar{\rho}',s)dC' \tag{3.2-11}$$

where

$$J_z(\bar{\rho}',\mathrm{s})=\mathcal{L}\left[\mathcal{J}_z(\bar{\rho}',t)\right] \tag{3.2-12}$$

and

$$G(\bar{\rho},\bar{\rho}',s)=\mathcal{L}\left[\mathcal{G}(\bar{\rho},\bar{\rho}',t)\right] \tag{3.2-13}$$

from tables of Laplace transforms [ERDE 54], we have, writing $R=|\bar{\rho}-\bar{\rho}'|$,

$$G(\bar{\rho},\bar{\rho}',s)=\mathcal{L}\left\{\frac{u[t-(R/c)]}{2\pi\sqrt{t^2-(R/c)^2}}\right\}=\frac{1}{2\pi}\left[\frac{\Gamma(1/2)}{\sqrt{\pi}}K_0\left(\frac{R}{c}s\right)\right] \tag{3.2-14}$$

[19] Applying the convolution theorem for Laplace transforms.

since $\Gamma(½) = \sqrt{\pi}$, thus becomes

$$G(\bar{\rho},\bar{\rho}',s) = \frac{1}{2\pi} K_0\left(\frac{R}{c}s\right) \tag{3.2-15}$$

with $K_0(..)$ the modified Bessel function. Therefore, the complex frequency-domain EFIE reads

$$s\frac{\mu}{2\pi}\left\{\int_C J_z(\bar{\rho}') K_0\left(\frac{|\bar{\rho} - \bar{\rho}'|}{c}s\right) dC'\right\} = -E_z^{inc}(\bar{\rho},s) \qquad \bar{\rho} \in C \tag{3.2-16}$$

3.2.4 Frequency-Domain EFIE for the 2D TM_z Problem

The frequency-domain EFIE for the 2D TM_z problem is a well documented problem [VOLA 12]. It can be shown that the equivalent current density $J_z(\bar{\rho})$ - entirely z-directed and only dependent on spatial coordinates *x* and *y* - will produce an electric field magnetic vector potential

$$E_z^{scat}\{\bar{\rho}, J_z(\bar{\rho})\} = -\frac{\omega\mu}{4}\int_C J_z(\bar{\rho}') H_0^{(2)}\left(k|\bar{\rho} - \bar{\rho}'|\right) dC' \tag{3.2-17}$$

with $H_0^{(2)}(...)$ the zeroth order Hankel function of the second kind. The total electric field at any observation point is therefore:

$$E_z\{\bar{\rho}, J_z(\bar{\rho})\} = E_z^{inc}\{\bar{\rho}\} + E_z^{scat}\{\bar{\rho}, J_z(\bar{\rho})\} \tag{3.2-18}$$

The total tangential electric field vanish at all points on the conducting strip becomes the frequency-domain integral equation

$$-j\omega\left\{\frac{\mu}{4j}\int_C J_z(\bar{\rho}') H_0^{(2)}\left(k|\bar{\rho} - \bar{\rho}'|\right) dC'\right\} = -E_z^{inc}\{\bar{\rho}\} \qquad \bar{\rho} \in C \tag{3.2-19}$$

As a point of interest, we should of course be able to find the frequency-domain EFIE by simply replacing s by $j\omega$ in (3.2-16). Because the modified Bessel function is related to the Hankel function by

$$K_0(\xi) = -j\frac{\pi}{2}H_0^{(2)}\left(-j\xi\right) \qquad -\frac{\pi}{2} < \arg\xi \le \pi \tag{3.2-20}$$

one finds that this is indeed so.

3.3 MOMENT METHOD SOLUTION OF THE COMPLEX FREQUENCY-DOMAIN EFIE

The contour *C* is segmented into N_s segments, as illustrated in Fig. 3.3-1. We define a set of pulse expansion functions $J_{zn}(\bar{\rho}) = P_n(\bar{\rho})$, $n = 1, 2, ..., N_s$, with the *n*-th pulse equal to unity over the *n*-th segment (that occupies a portion ΔC_n of the complete contour) and zero elsewhere. A set of delta weighting functions $\delta(\bar{\rho} - \bar{\rho}_m)$, $m = 1, 2, ..., N_s$ is also defined, with $\bar{\rho}_m$ the centroid of the *m*-th segment.

Application of the usual method of moments procedure discretizes the EFIE in (3.2-16) into a matrix equation $[Z(s)][I(s)] = [V(s)]$. Vector $[I(s)]$ is the column matrix of elements $I_n(s)$ that provides the solution for the current density as

$$J_z(\bar{\rho}, s) = \sum_{n=1}^{N_s} I_n(s) P_n(\bar{\rho}) \tag{3.3-1}$$

the elements $Z_{mn}(s)$ of the square interaction matrix $[Z(s)]$ by

$$\begin{aligned} Z_{mn} &= \int_C \delta(\bar{\rho} - \bar{\rho}_m) \left\{ \frac{s\mu}{2\pi} \int_C P_n(\bar{\rho}') \mathrm{K}_0\left(\frac{s}{c} |\bar{\rho}_m - \bar{\rho}'| \right) dC' \right\} dC \\ &= \frac{s\mu}{2\pi} \int_C P_n(\bar{\rho}') \mathrm{K}_0\left(\frac{s}{c} |\bar{\rho}_m - \bar{\rho}'| \right) dC' \\ &= \frac{s\mu}{2\pi} \int_{\Delta C_n} \mathrm{K}_0\left(\frac{s}{c} |\bar{\rho}_m - \bar{\rho}'| \right) dC' \end{aligned} \tag{3.3-2}$$

If we parametrize[20] the *n*-th segment this can be reduced to

$$Z_{mn} = s \frac{\mu_o h_n}{2\pi} \int_0^1 \mathrm{K}_0\left(\frac{s}{c} \sqrt{ \left\{ x_m - x_n^{(1)} - \xi' \left(x_n^{(2)} - x_n^{(1)} \right) \right\}^2 + \left\{ y_m - y_n^{(1)} - \xi' \left(y_n^{(2)} - y_n^{(1)} \right) \right\}^2 } \right) d\xi' \tag{3.3-3}$$

[20] The parametrization follows that done in [MCNA 21], although that reference is concerned with the 2D TM_z problem in the frequency-domain.

where h_n is the length of the *n*-th linear segment. This integral, even for the self-terms Z_{nn} for which the integrand has a logarithmic singularity (due to the modified Bessel function), can be evaluated using the generalized Gaussian quadrature rule [MA 96].

The elements $V_m(s)$ of the excitation vector $[V(s)]$ are given by

$$V_m(s) = -\int_C E_z^{inc}\left(\bar{\rho}, s\right)\delta\left(\bar{\rho} - \bar{\rho}_m\right)dC = -E_z^{inc}\left(\bar{\rho}_m, s\right) \tag{3.3-4}$$

The incident field in the time-domain is given by (3.2-1). It then follows from (3.2-4) that

$$V_m = \frac{E_0 T_w \sqrt{\pi}}{8} exp\left(- \frac{\left\{ t_0 + \frac{x_m \cos\phi^{inc} + y_m \sin\phi^{inc}}{c} \right\}^2}{\left\{T_w / 4\right\}^2} \right) \text{erfcx}\left(\frac{sT_w}{8} - \frac{\left\{ t_0 + \frac{x_m \cos\phi^{inc} + y_m \sin\phi^{inc}}{c} \right\}}{\left\{T_w / 4\right\}} \right) \tag{3.3-5}$$

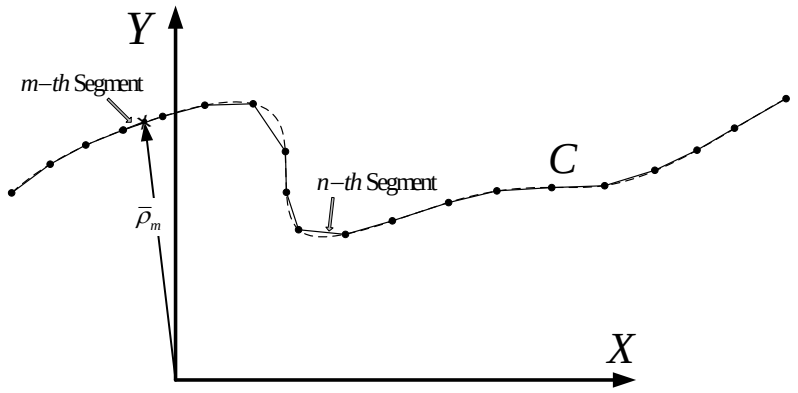

Fig.3.3-1: Diagram showing meshing of contour

3.4 MOMENT METHOD SOLUTION OF THE FREQUENCY-DOMAIN EFIE

The MoM solution of (3.2-19) mimics that of (3.2-16) described in the previous section. The MoM discretizes (3.2-19) into a matrix equation $[Z(\omega)][I(\omega)]=[V(\omega)]$. The incident field is the time-harmonic plane wave

$$E_z^{inc}(\bar{\rho},\omega)=e^{\,j\omega\sqrt{\mu\varepsilon}\,\bar{\rho}\cdot\hat{k}^{inc}}=e^{\,j\omega\sqrt{\mu\varepsilon}\,(x\cos\phi^{inc}+y\sin\phi^{inc})} \tag{3.4-1}$$

and so

$$V_m=-E_z^{inc}\left(\bar{\rho}_m\right)=-e^{\,j\omega\sqrt{\mu\varepsilon}\,(x_m\cos\phi^{inc}+y_m\sin\phi^{inc})} \tag{3.4-2}$$

the elements of the interaction matrix (that we may, in the frequency-domain, correctly refer to as an impedance matrix) are

$$Z_{mn}=-\frac{\omega\mu h_n}{4}\int_0^1 H_0^{(2)}\left\{k\sqrt{\left\{x_m-x_n^{(1)}-\xi'\left(x_n^{(2)}-x_n^{(1)}\right)\right\}^2+\left\{y_m-y_n^{(1)}-\xi'\left(y_n^{(2)}-y_n^{(1)}\right)\right\}^2}\right\}d\xi' \tag{3.4-3}$$

3.5 INCORPORATION OF NILT*n* APPROACH WITH THE MOMENT METHOD SOLUTION OF THE s-DOMAIN EFIE

3.5.1 Implementation of NILT0

The matrix equation $[Z(s_i)][I(s_i)]=[V(s_i)]$ is solved to determine the solution vector $[I(s_i)]$ for each of the complex frequency values s_i, $i=1,2,...,M/2$ [21] dictated by the NILT0 expression (2.7-7) in Section 2.7 for a specific value of time *t*. Recall that each vector $[I(s_i)]$ consists of N_s individual terms, namely $[I(s_i)]=[I_1(s_i),I_2(s_i),.....,I_{N_s}(s_i)]^T$. The individual terms $I_n(s_i)$ in each of the set of solution vectors $[I(s_i)]$ are then substituted into (2.7-7) to obtain the individual terms $i_n(t)$ in the time-domain solution vector $[i(t)]$. That is to say,

$$i_n(t)=-\frac{2}{t}\sum_{i=1}^{M/2}\mathcal{R}e\left\{k_i I_n(s_i)\right\}\Bigg|_{s_i=\frac{z_i}{t}} \tag{3.5-1}$$

which may as well be written in vector form as

$$\left[i(t)\right]=-\frac{2}{t}\sum_{i=1}^{M/2}\mathcal{R}e\left\{\left[k_i I(s_i)\right]\right\}\Bigg|_{s_i=\frac{z_i}{t}} \tag{3.5-2}$$

This is repeated for each value of *t* at which $[i(t)]$ is desired. We are reminded that, for each different value of *t* there is a different set of complex frequency values s_i at which $[I(s_i)]$ must be determined[22].

3.5.2 Implementation of NILT1

The NILT1 expression for the time-domain current density vector $[i(t)]$, suitably adapted to the present fields problem via (2.7-14), reads

---

[21] Recall that the values of s_i are in complex conjugates pairs of one another.

[22] We mention this here in order to contrast it later with what is needed when the so-called re-initialized (time-stepping) mode of operation of the NILT0 (or indeed NILT*n*) method is used in Chapter 5.

$$\left[i(t)\right] = -\frac{8}{t}\sum_{i=1}^{M/2}\left\{\mathcal{R}e\left[\frac{k_i^2}{t}\frac{d\left[I(s_i)\right]}{ds} + k_i^2\left[I(s_i)\right]\sum_{\substack{j=1\\ j\neq i}}^{M}\frac{k_j}{z_i - z_j}\right]\right\}_{s=\frac{2z_i}{t}} \tag{3.5-3}$$

Clearly, in addition to solution vector $[I(s)]$, derivative vector $d\{[I(s)]\}/ds$ is also required. In order to see how this can be obtained we refer once more to the matrix equation $[Z(s)][I(s)] = [V(s)]$, and differentiate both sides with respect to *s* to obtain

$$\frac{d}{ds}\{[Z(s)][I(s)]\} = \frac{d}{ds}\{[V(s)]\} \tag{3.5-4}$$

use of the product rule for differentiation allows (3.5-4) to be written as

$$[I(s)]\frac{d}{ds}\{[Z(s)]\} + [Z(s)]\frac{d}{ds}\{[I(s)]\} = \frac{d}{ds}\{[V(s)]\} \tag{3.5-5}$$

this can then be re-arranged to read

$$[Z(s)]\frac{d}{ds}\{[I(s)]\} = \frac{d}{ds}\{[V(s)]\} - [I(s)]\frac{d}{ds}\{[Z(s)]\} \tag{3.5-6}$$

Expression (3.5-6) is matrix equation that can be solved for $d\{[I(s)]\}/ds$. In order to do this we of course need to know $d\{[V(s)]\}/ds$ and $d\{[Z(s)]\}/ds$. These are found by returning to the fundamental expressions for the individual terms V_m and Z_{mn}, and determining their indicated derivatives analytically, as shown in what follows.

The derivative of $V_m(s)$ can be found by taking the derivative of equation (3.3-5). We will write (3.3-5) as

$$V_m = A_o \ \mathrm{erfcx}\left(B_o s \ - \ D_m\right) \tag{3.5-7}$$

where

$$A_o = \frac{E_0 T_w \sqrt{\pi}}{8} \exp\left(- \frac{\left\{ t_0 + \dfrac{x_m \cos\phi^{inc} + y_m \sin\phi^{inc}}{c} \right\}^2}{\left\{ T_w / 4 \right\}^2} \right) \tag{3.5-8}$$

$$B_o = T_w / 8 \tag{3.5-9}$$

and

$$D_m = \frac{\left\{ t_0 + \dfrac{x_m \cos\phi^{inc} + y_m \sin\phi^{inc}}{c} \right\}}{\left\{ T_w / 4 \right\}} \tag{3.5-10}$$

hence

$$\frac{dV_m}{ds} = A_o \frac{d}{ds} \mathrm{erfcx}(B_o s - D_m) \tag{3.5-11}$$

Now $erfcx(z) = e^{z^2} erfc(z)$, and so we have

$$\frac{d}{dz}\left\{\mathrm{erfcx}(z)\right\} = 2z e^{z^2} \mathrm{erfc}(z) - e^{z^2} \frac{2}{\sqrt{\pi}} e^{-z^2} = 2z \,\mathrm{erfcx}(z) - \frac{2}{\sqrt{\pi}} \tag{3.5-12}$$

and so

$$\frac{d}{ds} \mathrm{erfcx}(B_o s - D_m) = B_o \left\{ 2(B_o s - D_m) \mathrm{erfcx}(B_o s - D_m) - \frac{2}{\sqrt{\pi}} \right\} \tag{3.5-13}$$

thus (3.5-11) becomes

$$\frac{dV_m}{ds} = A_o B_o \left\{ 2(B_o s - D_m)\,\mathrm{erfcx}(B_o s - D_m) - \frac{2}{\sqrt{\pi}} \right\} \tag{3.5-14}$$

Next, the derivative of Z_{mn} can be found by taking the derivative of (3.4-3), namely

$$\frac{d\,Z_{mn}}{ds} = \frac{d}{ds}\left(s\,\frac{\mu_o\, h_n}{2\pi} \int_0^1 \mathrm{K}_0\left(\frac{s}{c}\sqrt{\left\{ x_m - x_n^{(1)} - \xi'\left(x_n^{(2)} - x_n^{(1)} \right) \right\}^2 + \left\{ y_m - y_n^{(1)} - \xi'\left(y_n^{(2)} - y_n^{(1)} \right) \right\}^2} \right) d\xi' \right) \tag{3.5-15}$$

application of the properties of modified Bessel functions, and the usual product and chain rules of differential calculus, allows this to be rewritten as

$$\frac{d\,Z_{mn}}{ds} = \frac{\mu\, h_n}{2\pi} \left\{ \int_0^1 \mathrm{K}_0\left(\frac{s}{c}\,\Psi_{mn}(\xi') \right) d\xi' \;-\; s \int_0^1 \frac{\Psi_{mn}(\xi')}{c}\,\mathrm{K}_1\left(\frac{s}{c}\,\Psi_{mn}(\xi') \right) d\xi' \right\} \tag{3.5-16}$$

where

$$\Psi_{mn}(\xi') = \sqrt{\left\{ x_m - x_n^{(1)} - \xi'\left(x_n^{(2)} - x_n^{(1)} \right) \right\}^2 + \left\{ y_m - y_n^{(1)} - \xi'\left(y_n^{(2)} - y_n^{(1)} \right) \right\}^2} \tag{3.5-17}$$

Although $\mathrm{K}_1(...)$ has a singularity, the singularity of the integrand is weakened by the multiplicative term $\Psi_{mn}(...)$, and so the quadrature rule in [MA 96] can still be used to find all terms in $d\,\{[Z(s)]\}/ds$.

3.5.3 Implementation of NILT2

The NILT2 expression for the time-domain current density vector $[i(t)]$, in terms of the present fields problem via (2.7-15), reads[23]

[23] Recall that $\tilde{k}_i = 2k_i$.

$$\left[i(t)\right] \approx -\frac{9}{t}\sum_{i=1}^{M/2}\left\{\begin{array}{l}\dfrac{3\tilde{k}_i^3}{8t^2}\dfrac{d^2\left[I(s)\right]}{ds^2}+\dfrac{3\tilde{k}_i^2}{2t}\dfrac{d\left[I(s)\right]}{ds}\displaystyle\sum_{\substack{j=1\\ j\neq i}}^{M}\frac{k_j}{z_i - z_j} \\ +\left[I(s)\right]\left(\tilde{k}_i\displaystyle\sum_{\substack{j=1\\ j\neq i}}^{M}\sum_{\substack{v=1\\ v\neq 1}}^{M}\frac{k_j k_v}{\left(z_i - z_j\right)\left(z_i - z_v\right)} - \frac{\tilde{k}_i^2}{2}\sum_{\substack{j=1\\ j\neq i}}^{M}\frac{k_j}{\left(z_i - z_j\right)^2}\right)\end{array}\right\}_{s=\frac{3z_i}{t}} \tag{3.5-18}$$

In addition to solution vector $[I(s)]$, and derivative vector $d\{[I(s)]\}/ds$, we require second derivative vector $d^2\{[I(s)]\}/ds^2$. To do this, we first take the second-order derivative of the matrix product [Z(s)][I(s)], namely

$$\frac{d^2\{[V(s)]\}}{ds^2} = \frac{d^2}{ds^2}\{[Z(s)][I(s)]\} = [Z(s)]\frac{d^2[I(s)]}{ds^2} + 2\frac{d[Z(s)]}{ds}\frac{d[I(s)]}{ds} + \frac{d^2[Z(s)]}{ds^2}[I(s)] \tag{3.5-19}$$

which can be re-arranged as

$$[Z(s)]\frac{d^2[I(s)]}{ds^2} = \frac{d^2[V(s)]}{ds^2} - 2\frac{d[Z(s)]}{ds}\frac{d[I(s)]}{ds} - \frac{d^2[Z(s)]}{ds^2}[I(s)] \tag{3.5-20}$$

expression (3.5-20) is matrix equation that can be solved for $d^2\{[I(s)]\}/ds^2$. In order to accomplish this one must determine expressions for $d^2\{[V(s)]\}/ds^2$ and $d^2\{[Z(s)]\}/ds^2$; expressions for $d\{[I(s)]\}/ds$ and $d\{[Z(s)]\}/ds$ were already found in Section 3.5.2. The additional expressions can be found by taking derivatives of (3.5-14) and (3.5-16). From (3.5-14) we have

$$\begin{aligned}\frac{d^2V_m}{ds^2} &= A_o B_o \frac{d}{ds}\left\{2(B_o s - D_m)\,erfcx(B_o s - D_m) - \frac{2}{\sqrt{\pi}}\right\} \\ &= 2A_o B_o\left[B_o\,erfcx(B_o s - D_m) + (B_o s - D_m)\frac{d}{ds}erfcx(B_o s - D_m)\right]\end{aligned} \tag{3.5-21}$$

the derivative term on the right-hand side of (3.5-21) is already available in (3.5-13), and so (3.5-21) becomes

$$\frac{d^2V_m}{ds^2} = 2A_oB_o\left\{erfcx(B_os - D_m) + 2(B_os - D_m)^2\, erfcx(B_os - D_m) - \frac{2}{\sqrt{\pi}}(B_os - D_m)\right\} \qquad (3.5\text{-}22)$$

if we differentiate (3.5-16) with respect to s we arrive at

$$\frac{d^2Z_{mn}}{ds^2} = -\frac{\mu_o h_n}{2\pi}\int_0^1 \frac{\Psi_{mn}(\xi')}{c}\mathrm{K}_1\left(\frac{s}{c}\Psi_{mn}(\xi')\right)d\xi' - \frac{\mu_o h_n}{2\pi}\int_0^1 \frac{\Psi_{mn}(\xi')}{c}\mathrm{K}_1\left(\frac{s}{c}\Psi_{mn}(\xi')\right)d\xi'$$
$$-\frac{1}{s}s\frac{\mu_o h_n}{2\pi}\int_0^1 \frac{\Psi_{mn}(\xi')}{c}\mathrm{K}_1\left(\frac{s}{c}\Psi_{mn}(\xi')\right)d\xi' + s\frac{\mu_o h_n}{2\pi}\int_0^1 \frac{\Psi^2_{mn}(\xi')}{c^2}\mathrm{K}_2\left(\frac{s}{c}\Psi_{mn}(\xi')\right)d\xi' \qquad (3.5\text{-}23)$$

The grouping of various terms yields

$$\frac{d^2Z_{mn}}{ds^2} = -\frac{3\mu_o h_n}{2\pi}\int_0^1 \frac{\Psi_{mn}(\xi')}{c}\mathrm{K}_1\left(\frac{s}{c}\Psi_{mn}(\xi')\right)d\xi' + s\frac{\mu_o h_n}{2\pi}\int_0^1 \frac{\Psi^2_{mn}(\xi')}{c^2}\mathrm{K}_2\left(\frac{s}{c}\Psi_{mn}(\xi')\right)d\xi' \qquad (3.5\text{-}24)$$

3.6 VALIDATION EXAMPLES

3.6.1 Selection of Examples

In order to validate the new NILT*n*-based formulation for scattering from 2D PEC objects it was implemented and applied to two example geometries, namely a flat PEC strip and a circular PEC cylinder. The results obtained using the NILT*n*-based approach for $n = 0,1,2$ will be compared to those for the same geometries published in [Rao 99], that were computed using the MOT method of Section 2.6.2. In the computed time-domain current densities to be shown below for the above geometries, the z-polarized incident plane wave field has a Gaussian pulse time variation, as described in Section 3.2.1, with its s-domain MoM excitation vector elements given by (3.3-5).

The parameters of this Gaussian plane wave are, in both examples

- $E_0 = 120\pi$
- $T_w = 13.33$ ns
- $t_0 = 20$ ns (Significant frequency content to maximum frequency 200 MHz, λ_o = 1.5m)
- $\hat{k}^{inc} = -\hat{x}$ (so that $\phi^{inc} = 0^\circ$)

and the parameters used in the NILT*n* computations are

- $M = 10$
- $N = 8$

Based on these parameters, it is instructive to briefly examine the sets of complex frequencies s_i required in the NILT*n* based approaches for the two cases to be considered. As explained in Section 2.7, these are given by

$$s_i = \frac{(n+1)\, z_i}{t} = \mathrm{Re}\{s_i\} + \mathrm{Im}\{s_i\} \tag{3.6-1}$$

where *n* is that in NILT*n*. They are plotted in Fig. 3.6-1. Although NILT*n* as described in this chapter need not have *t* values spaced at regular intervals, in the examples discussed here, and

hence in Fig. 3.6-1, the values used were $t = p\Delta t$ with $\Delta t = 0.33\text{ns}$ and $p = 1, 2, ...$[24]. It is obvious from expression (3.6-1) that as *t* increases the s_i values decrease (but will not reach the origin of the complex plane except literally at $t \to \infty$). It can be seen from (3.6-1) that for the same value of *t*, s_i increases if a larger value of *n* in NILT*n* is used.

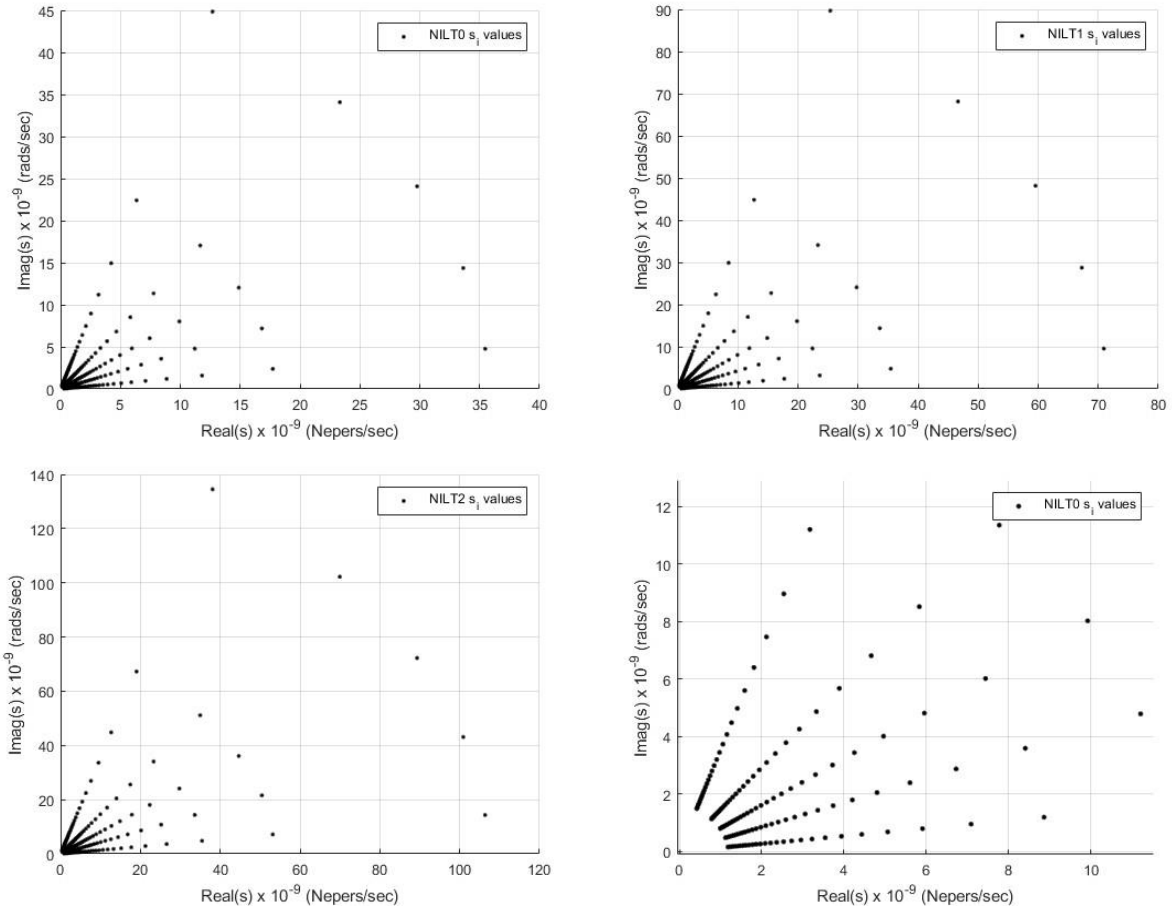

Fig. 3.6-1: The distribution of complex frequencies s_i required in the computation of the NILT0 (top left), NILT1 (top right) and the NILT2 (bottom left) results, and a magnified portion (bottom right) of the plot for the NILT0 case, for larger values of t.

[24] Due to the assumption of causality, it is unnecessary to find values at $t = 0$

3.6.2 Infinitely Long Zero-Thickness Planar PEC Strip (Open Structure)

The first scatterer is the flat PEC strip of width[25] w = 1m shown in Fig. 3.6-2. The induced current density $\mathcal{J}_z(x,y,t)$ is computed using the NILT0 approach for the incident Gaussian plane wave specified in Section 3.6.1. Its value at the location $(x, y) = (0, 0)$, the centre of the strip, is shown in Fig. 3.6-3 using the NILT0 approach. The [RAO 99] result is taken as a reference. It is clear that NILT0 accurately replicates the [RAO 99] time-domain response up to 20 ns, but beyond that they fluctuate around the [RAO 99] results and are thus inaccurate. Use of the NILT1 and NILT2 on the other hand yields the results shown in Fig. 3.6-4, both providing accurate results.

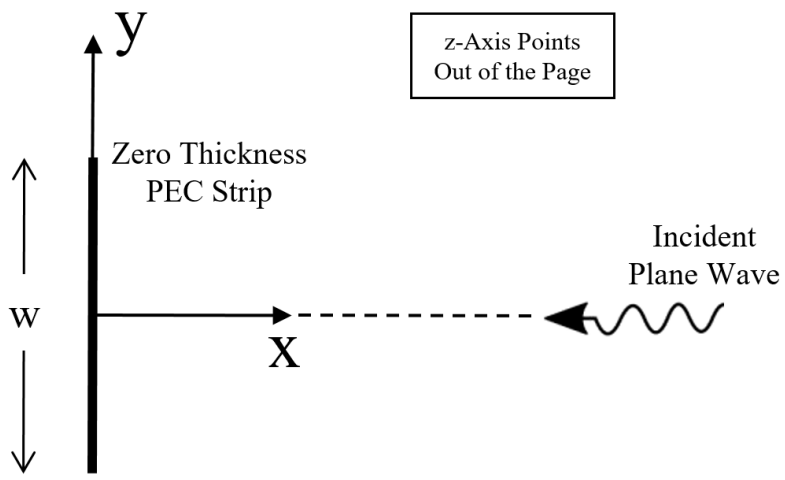

Fig. 3.6-2: Sketch of problem geometry: Plane wave incident on a zero-thickness PEC strip.

[25] This width is $0.67\lambda_o$ at 200 MHz.

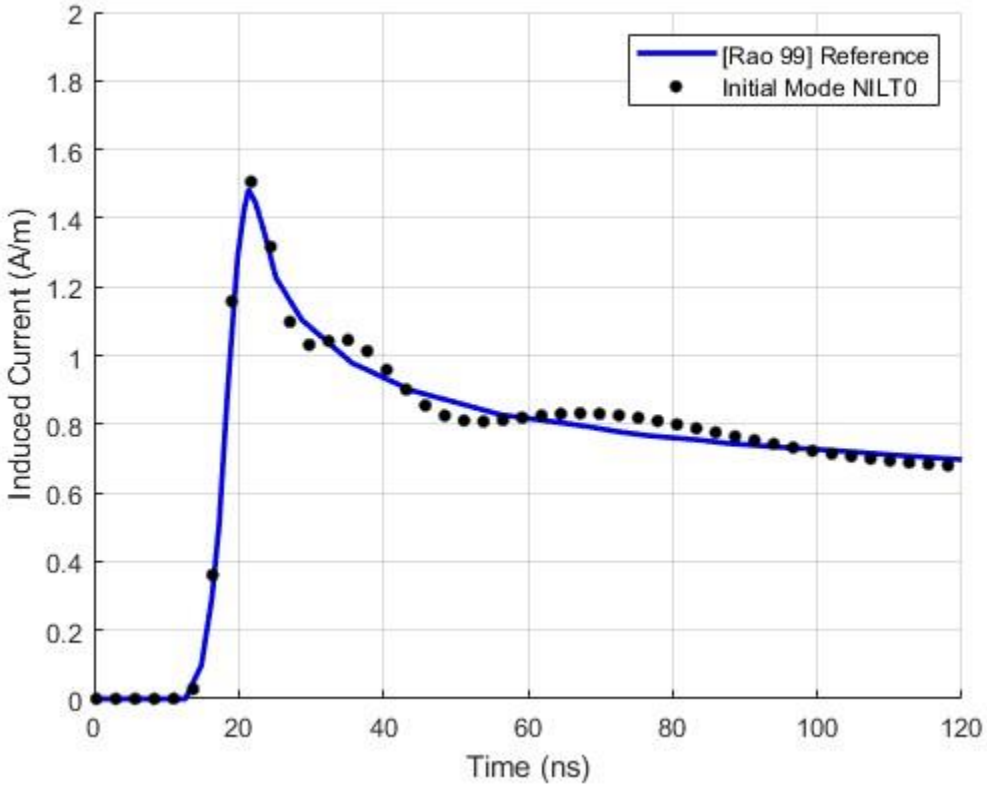

Fig. 3.6-3: The induced current at the centre of a straight strip excited by an incident z-polarized (TM_z) Gaussian plane wave as determined in [Rao 99] (blue line) and NILT0 (black dots). The width of the strip (w) is 1m. Nine expansion functions were used in computing the results shown.

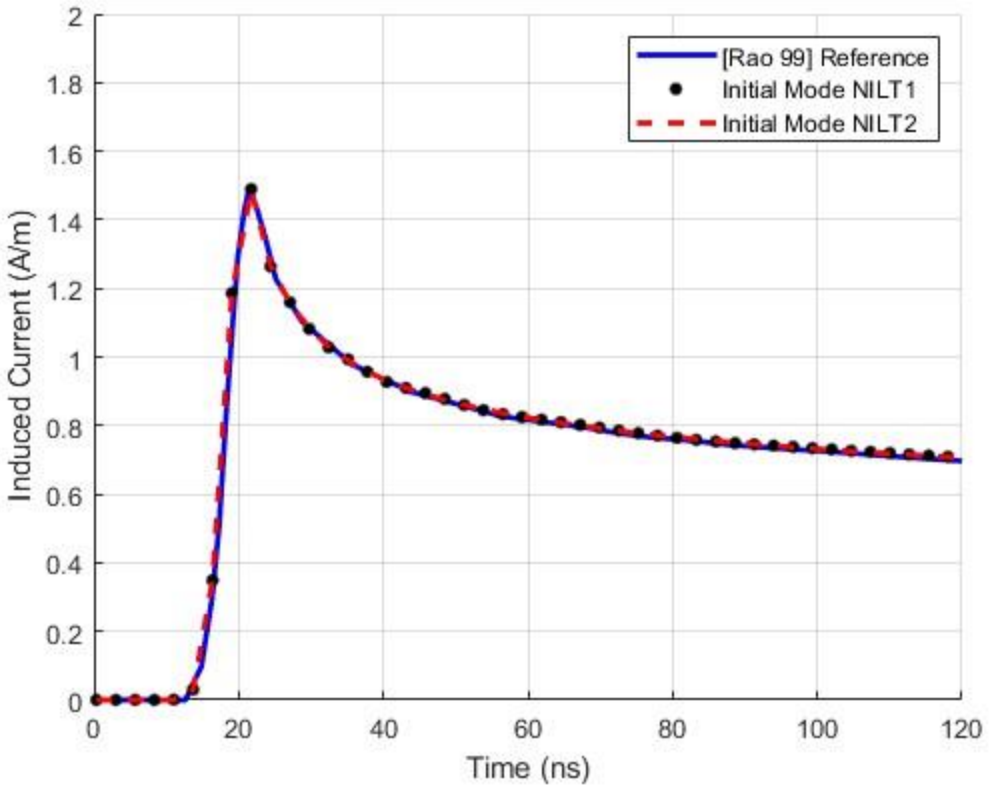

Fig. 3.6-4: The induced current at the centre of a straight strip excited by an incident z-polarized Gaussian plane wave as determined in [Rao 99] (blue line), NILT1 (black dots) and NILT2 (red dashes). The width of the strip (w) is 1m. Nine expansion functions were used in computing the results shown.

3.6.3 Infinitely Long Cylinder of Circular Cross-Section (Closed Structure)

The second scatterer is the circular PEC cylinder of radius[26] a = 1m shown in Fig. 3.6-5. The induced current density $\mathcal{J}_z(x,y,t)$ is computed using the NILT0 approach for the incident Gaussian plane wave specified in Section 3.6.1. Its value at the location $(x,y)=(a,0)$ of the specular point, using the NILT0 approach is shown in Fig. 3.6-6. The [RAO 99] result for this problem is again taken as a reference. As for the previous PEC strip example, NILT0 accurately replicates the [RAO 99] time-domain response up to about 20 ns, but then incorrectly oscillates around the [RAO 99] results. Use of the NILT1 and NILT2 on the other hand yields the results shown in Fig. 3.6-7, both providing accurate results.

[26] A circumference of $4.19\lambda_o$ at 200 MHz.

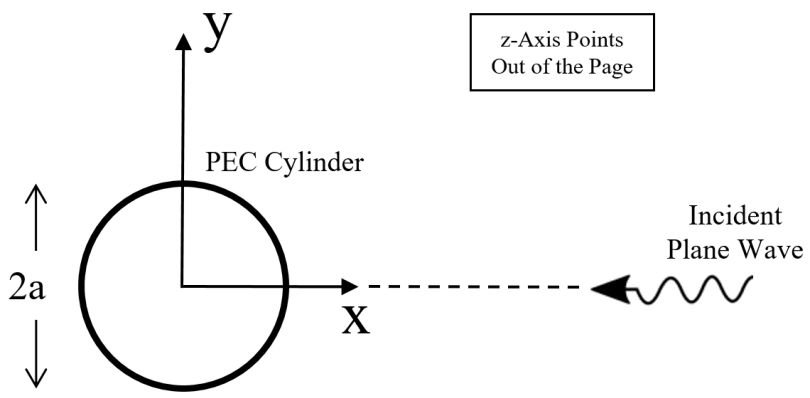

Fig. 3.6-5: Sketch of problem geometry : Plane wave incident on a PEC cylinder of circular cross-section. The cross-sectional radius of the cylinder (*a*) is 1m.

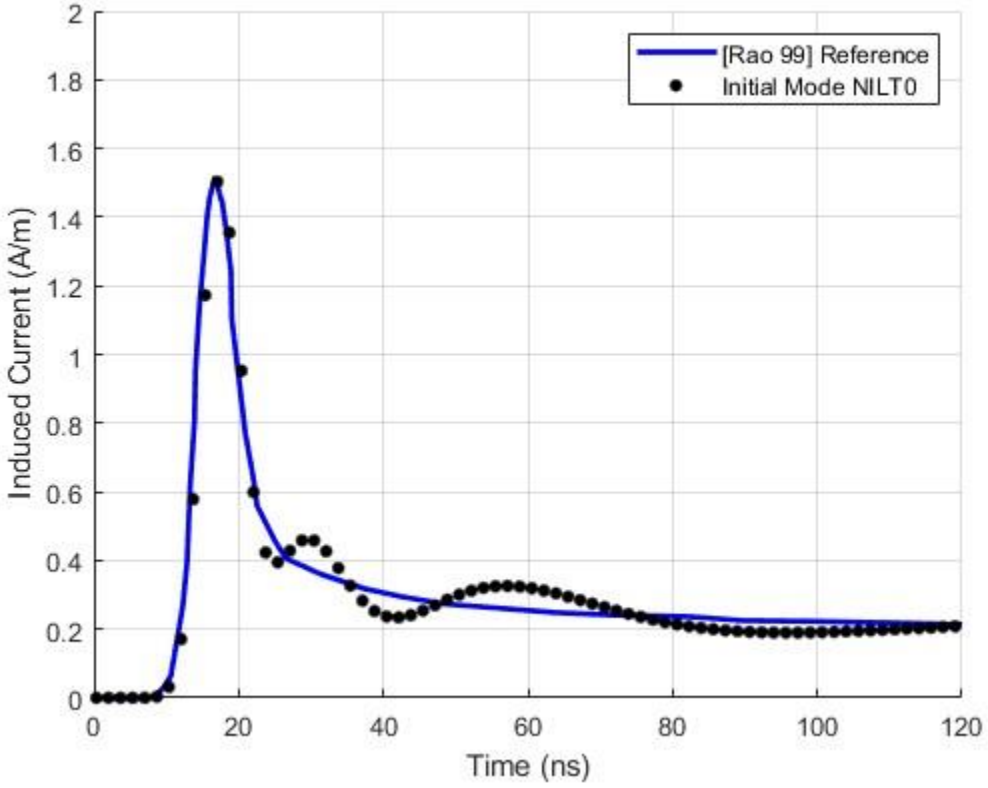

Fig. 3.6-6: The induced current at the centre of a circular PEC cylinder excited by an incident z-polarized Gaussian plane wave as determined in [Rao 99] (blue line) and NILT0 (black dots). The cross-sectional radius of the cylinder (*a*) is 1m. The number of expansion functions (linear segments) used to model the cylinder surface was 24.

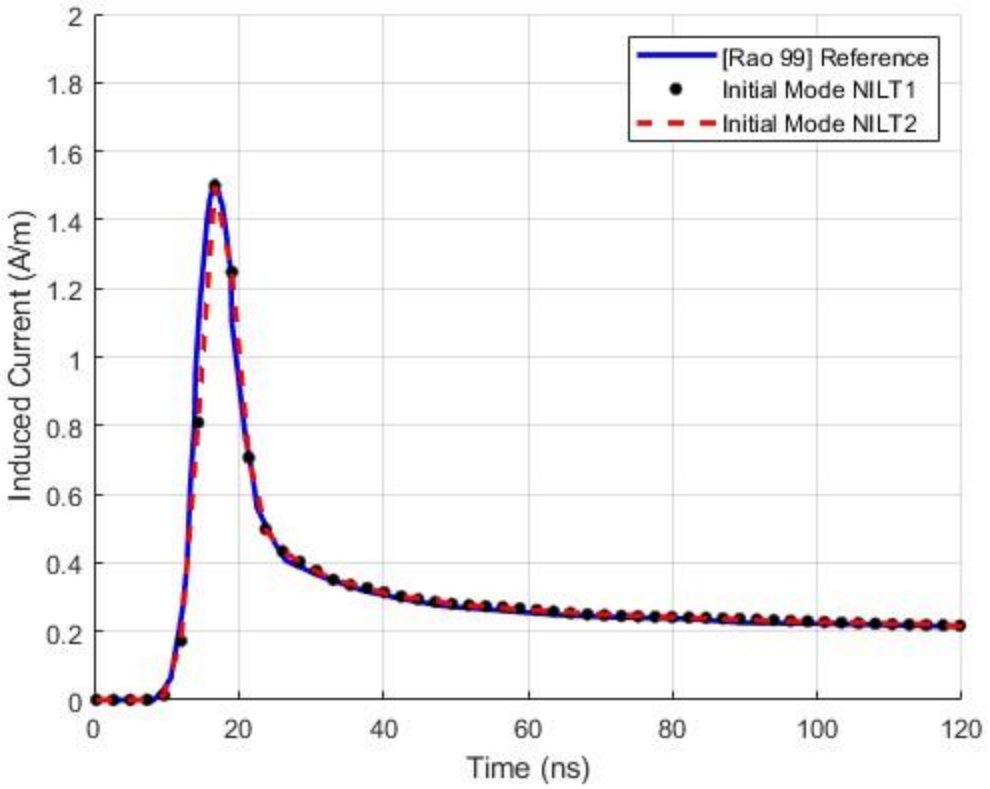

Fig. 3.6-7: The induced current at the centre of the circular PEC cylinder excited by an incident z-polarized Gaussian plane wave as determined in [Rao 99] (blue line), NILT1 (black dots) and NILT2 (red dashes). The cross-sectional radius of the cylinder (*a*) is 1m. The number of expansion functions (linear segments) used to model the cylinder surface was 24.

3.7 ON THE POSSIBILITY OF RE-INITIALIZATION

Section 2.7.3-B observed that, when applied to the analysis of circuits composed of lumped elements, the use of re-initialization to convert the NILT into time-stepping mode provides a robust scheme for accurate time-domain simulation out to very large times. A means of achieving such a conversion in the case of the present use of the NILT in the MoM solution of the TD-EFIE is less straightforward, as we explain here. Before proceeding, we remind ourselves that if we can analytically determine $F(s) = \mathcal{L}\{f(t)\}$, then the Laplace transform of the forward-shifted function $f(t-h)$, $h \geq 0$ is easily found from a well-known identity as $\mathcal{L}\{f(t-h)\} = e^{-sh}F(s)$. Although this identity can apply to forward-shifted functions, there is no similar straightforward identity for finding the Laplace transform of a backward-shifted function $f(t+h)$, $h \geq 0$ [27].

As discussed in Section 2.7.3-B, to obtain a re-initialized NILT formulation, we start by replacing variable t by $\hat{t} + rh$ in the TD-EFIE. Correct mathematical "book-keeping" requires that we identify new quantities $\hat{\mathscr{J}}_z(\bar{\rho}, \hat{t})$, $\hat{\mathcal{G}}(\bar{\rho}, \bar{\rho}', \hat{t})$ and $\hat{\mathscr{E}}_z^{inc}(\bar{\rho}, \hat{t})$. From (3.2-7) we have

$$\hat{\mathcal{G}}(\bar{\rho}, \bar{\rho}', \hat{t}) = \frac{\mathrm{u}\left(\hat{t} + rh - \dfrac{|\bar{\rho} - \bar{\rho}'|}{\mathrm{c}}\right)}{2\pi\sqrt{(\hat{t} + rh)^2 - \left(|\bar{\rho} - \bar{\rho}'| / \mathrm{c}\right)^2}} \tag{3.7-1}$$

and its Laplace transform is thus

$$\hat{G}(\bar{\rho}, \bar{\rho}', s) = \int_0^\infty \frac{\mathrm{u}\left(\hat{t} + rh - \dfrac{|\bar{\rho} - \bar{\rho}'|}{\mathrm{c}}\right)}{2\pi\sqrt{(\hat{t} + rh)^2 - \left(|\bar{\rho} - \bar{\rho}'| / \mathrm{c}\right)^2}} e^{-s\hat{t}}\, d\hat{t} \tag{3.7-2}$$

This is not defined in general due to the "$+rh$" term. A similar roadblock arises when we want to find the Laplace transform

[27] See Appendix III for more details

$$\hat{E}_z^{inc}(\bar{\rho},s) = E_0 \int_0^{\infty} exp\left(-\left[\frac{4}{T_w}\left(\hat{t}+rh-t_0-\frac{\bar{\rho}\cdot\hat{k}}{c}\right)\right]^2\right)e^{-s\hat{t}}d\hat{t} \tag{3.7-3}$$

of the altered

$$\hat{\mathcal{E}}_z^{inc}(\bar{\rho},\hat{t}) = E_o\, exp\left(-\left[\frac{4}{T_w}\left(\hat{t}+rh-t_0-\frac{\bar{\rho}\cdot\hat{k}}{c}\right)\right]^2\right) \tag{3.7-4}$$

obtained from (3.2-1). A more detailed understanding of the process is needed to arrive at a re-initialized form in the case of fields problems. Such a form will be derived in Chapter 5, where we will see that the reason for the difficulty is the presence of delay terms that do not exist in lumped circuit analysis problems.

3.8 CONCLUDING REMARKS

This chapter has formulated, implemented and applied the NILT*n*/MoM approach to find solutions to the TD-EFIE of 2D PEC objects. As declared in Section 3.1, this was largely done to acquire insight in the NILT*n*/MoM. Nevertheless, this appears to be the first time the material presented has been described anywhere, and is significant (quite separate from the goals of the thesis) in that 2D problems continue to be used by researchers to examine new ideas and improvements in the methods of computational electromagnetics. Numerical results for one open and one closed 2D PEC object have been shown and validated. The understanding gained now allows us to proceed naturally to the general 3D case in Chapter 4. It was indicated why the use of re-initialization with the NILT*n*/MoM for fields problems is not as straightforward as when NILT*n* is applied to lumped circuit analysis ones, but that this will be tackled for the general 3D case in Chapter 5.

CHAPTER 4 - The Solution of the Time-Domain EFIE Using MoM/NILTn: The 3D Case

4.1 PRELIMINARY REMARKS

In Chapter 3 we successfully applied NILT*n* methods to find the solutions of the TD-EFIE via scattering from a 2D PEC object. With this experience in hand, we now wish to do the same for general 3D PEC objects. The TD-EFIE for scattering from a PEC object(s) of surface S is given in undifferentiated form in (2.3-3) and (2.3-4) of in Section 2.3.3. We wish to obtain numerical solutions of this particular TD-EFIE in its general form using NILT*n* methods, namely by finding the MoM solutions of the complex frequency EFIE form of the undifferentiated TD-EFIE in Section 2.3.4, and then using the NILT*n* expressions to find the actual time-domain solution[28]. The present chapter attains this goal as follows:

■ Section 4.2 constructs a MoM formulation for solution of the complex frequency-domain EFIE.

■ Section 4.3 develops all the necessary expressions and matrix equations needed to use the results obtained via the formulation in Section 4.2 with NILT*n* to reach the desired time-domain solutions of the TD-EFIE.

■ Section 4.4 provides numerical results obtained using an implementation of the developments in Section 4.2 and Section 4.3.

■ Section 4.5 concludes the chapter.

[28] As in Chapter 3 for the 2D cases, the formulation here in Chapter 4 will also not make use of re-initialization, and will (to contrast it to the re-initialization technique that will be developed in Chapter 5), be referred to as the use of NILT*n* in an *initial-value mode*. The approach in Chapter 5 will be referred to as the use of NILT*n* in a *re-initialized mode*.

4.2 MOMENT METHOD FORMULATION OF THE 3D s-DOMAIN EFIE

4.2.1 Derivation of Expressions for the Interaction Matrix and Excitation Vector

The unknown current density $\bar{J}(\bar{r},s)$ can be determined by meshing the PEC surface S into triangular elements and subsequently expanding the surface current density in the RWG div-conforming expansion functions as

$$\bar{J}(\bar{r},s)=\sum_{n=1}^{N_s} I_n(s)\,\bar{j}_n(\bar{r}) \tag{4.2-1}$$

where a

$$\bar{j}_n(\bar{r})=\begin{cases}\dfrac{l_n}{2A_n^+}\bar{\rho}_n^+ & \bar{r}\in T_n^+\\ \dfrac{l_n}{2A_n^-}\bar{\rho}_n^- & \bar{r}\in T_n^-\\ 0 \qquad Otherwise\end{cases} \tag{4.2-2}$$

is associated with every edge shared by two triangles, as indicated in Fig. 4.2-1. Quantity l_n is the length of the n^{th} edge in the mesh, and $A_n^{\pm}$ represents the areas of the triangles associated with the n^{th} edge. We assume there are N_s such edges, and hence expansion functions. Using a Galerkin approach, a set of testing functions $\bar{j}_m(\bar{r})$, $m=1,2,...,N_s$, identical to the expansion functions, is chosen [RAO 91][RAO 20].

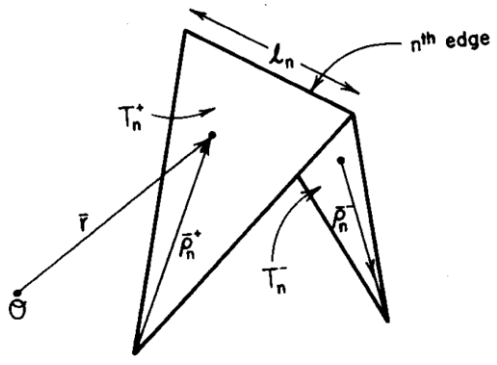

Fig. 4.2-1: Rao-Wilton-Glisson (RWG) expansion function [RAO 82].

The usual MoM procedure is then followed. The expansion (4.2-1) for the unknown $\bar{J}(\bar{r},s)$ is inserted into the s-domain EFIE in (2.3-13), that involves an integration over S with respect to the primed coordinates. Next a dot product of each side of the resulting expression is taken with the m-th testing function $\bar{j}_m(\bar{r})$, and both sides integrated over S with respect to the unprimed coordinate, to obtain (with some judicious use of vector analysis)[29]

$$\begin{aligned}\frac{\mu}{4\pi}\sum_{n=1}^{N_s}\sum_{p=1}^{N_g}\sum_{q=1}^{N_g}\sum_{(\kappa_1,\kappa_2)} w_p w_q\, I_n(s)\, s\, e^{-s\tau_{mnpq}^{\kappa_1\kappa_2}} L_{mnpq}^{\kappa_1\kappa_2} \\ + \frac{1}{4\pi\varepsilon_0}\sum_{n=1}^{N_s}\sum_{p=1}^{N_g}\sum_{q=1}^{N_g}\sum_{(\kappa_1,\kappa_2)} w_p w_q\, I_n(s)\frac{e^{-s\tau_{mnpq}^{\kappa_1\kappa_2}}}{s} C_{mnpq}^{\kappa_1\kappa_2} \\ = \sum_{q=1}^{N_g}\sum_{(\kappa_1,\kappa_2)} w_p \bar{j}_m\left(\bar{r}_{pm}^{\kappa_1}\right)\cdot \bar{E}^{inc}\left(\bar{r}_{pm}^{\kappa_2}, s\right)\end{aligned} \tag{4.2-3}$$

where

$$\tau_{mnpq}^{\kappa_1\kappa_2} = \frac{\left|\bar{r}_{pm}^{\kappa_1\kappa_2} - \bar{r}'^{\kappa_1\kappa_2}_{qn}\right|}{c} \tag{4.2-4}$$

$$L_{mnpq}^{\kappa_1\kappa_2} = \frac{\bar{j}_m\left(\bar{r}_{pm}^{\kappa_1\kappa_2}\right)\cdot \bar{j}_n\left(\bar{r}'^{\kappa_1\kappa_2}_{qn}\right)}{\left|\bar{r}_{pm}^{\kappa_1\kappa_2} - \bar{r}'^{\kappa_1\kappa_2}_{qn}\right|} \tag{4.2-5}$$

and

$$C_{mnpq}^{\kappa_1\kappa_2} = \frac{\left(\nabla\cdot \bar{j}_m\left(\bar{r}_{pm}^{\kappa_1\kappa_2}\right)\right)\left(\nabla'\cdot \bar{j}_n\left(\bar{r}'^{\kappa_1\kappa_2}_{qn}\right)\right)}{\left|\bar{r}_{pm}^{\kappa_1\kappa_2} - \bar{r}'^{\kappa_1\kappa_2}_{qn}\right|} \tag{4.2-6}$$

where the w_p, w_q, $\bar{r}_{pm}^{\kappa_1}$ and $\bar{r}_{qn}^{\kappa_2}$ are the weights and sampling points (on the respective triangles), respectively, for the particular quadrature rule used. Dummy symbols κ_i represent either a plus or a minus sign. If this is done for each of the testing functions in turn, a set of N_s

[29] Explanatory details of how one reaches (4.2-3) are provided in Appendix II.

linear equations in the N_s unknowns $I_n(s)$ results, which is written as a matrix equation $[Z(s)][I(s)]=[V(s)]$. The elements V_m of excitation vector $[V(s)]$ can be written down by inspection of (4.2-3) as

$$V_m(s)=\sum_{p=1}^{N_g}\sum_{(\kappa_1,\kappa_2)} w_p\ \bar{j}_m\left(\bar{r}_{pm}^{\kappa_1}\right)\cdot\bar{E}^{inc}\left(\bar{r}_{pm}^{\kappa_2},s\right) \tag{4.2.7}$$

whereas the elements Z_{mn} of $[Z(s)]$

$$Z_{mn}=\frac{\mu}{4\pi}\sum_{p=1}^{N_g}\sum_{q=1}^{N_g}\sum_{(\kappa_1,\kappa_2)} w_p w_q\, s\, e^{-s\tau_{mnpq}^{\kappa_1\kappa_2}} L_{mnpq}^{\kappa_1\kappa_2} + \frac{1}{4\pi\varepsilon_0}\sum_{p=1}^{N_g}\sum_{q=1}^{N_g}\sum_{(\kappa_1,\kappa_2)} w_p w_q \frac{e^{-s\tau_{mnpq}^{\kappa_1\kappa_2}}}{s} C_{mnpq}^{\kappa_1\kappa_2} \tag{4.2-8}$$

4.2.2 Expression for the Excitation Vector Elements for Antenna-Like Excitation

If we excite the PEC object as an antenna, with the excitation concentrated as a "delta-gap" source [JOHN 90] across the *m*-th edge, then (4.2-7) reduces to

$$V_m(s)=\ell_m V_m^{imp}(s) \tag{4.2-9}$$

where

$$V_m^{imp}(s)=\mathcal{L}\left[v_m^{imp}(t)\right] \tag{4.2-10}$$

and $v_m^{imp}(t)$ is the time-variation (in our cases Gaussian) of the voltage impressed across the *m*-th edge. In this chapter we will use

$$v^{imp}(t)=V_0 e^{-\left[\frac{4}{T_w}(t-t_0)\right]} \tag{4.2-11}$$

and so

$$V_m^{imp}(s) = \frac{V_0 T_w \sqrt{\pi}}{8} e^{\left(-\frac{(t_0)^2}{\left(\frac{1}{4}T_w\right)^2} \right)} erfcx\left(\frac{sT_w}{8} - \frac{t_0}{\frac{1}{4}T_w} \right) \qquad (4.2\text{-}12)$$

To simplify (4.3-12), we shall re-write it as

$$V_m^{imp}(s) = -A_o erfcx\left(B_o s - D_m\right) \qquad (4.2\text{-}13)$$

where

$$A_o = \frac{V_0 T_w \sqrt{\pi}}{8} exp\left(- \frac{\{t_0\}^2}{\{T_w / 4\}^2} \right) \qquad (4.2\text{-}14)$$

$$B_o = T_w / 8 \qquad (4.2\text{-}15)$$

and

$$D_m = \frac{\{t_0\}}{\{T_w / 4\}} \qquad (4.2\text{-}16)$$

4.3 INCORPORTION OF NILT*n* APPROACH WITH THE MOMENT METHOD SOLUTION OF THE s-DOMAIN EFIE

4.3.1 Initial Remarks

The steps needed here are almost identical to those in Section 3.5 for the 2D problem. Solution vectors $[I(s)]$, and their derivatives $d[I(s)]/ds$ and $d^2[I(s)]/ds^2$, are used in the same way in the NILT expressions whether they arise in 2D or 3D problems. We will therefore not need to repeat all the explanatory material already available there. The details of some expressions in the matrix equations used to find $d[I(s)]/ds$ and $d^2[I(s)]/ds^2$ are different in the general 3D case, and so are derived here.

4.3.2 Implementation of NILT0

No new expressions are needed for the NILT0 case. The procedure follows that in Section 3.5.1.

4.3.3 Implementation of NILT1

As explained in Section 3.5.2, we need expressions for the matrix elements dV_m/ds and dZ_{mn}/ds. Starting from (4.2-9), for the case of antenna-like excitation, we have

$$\frac{dV_m(s)}{ds} = \ell_m \frac{d}{ds}\left\{V_m^{imp}(s)\right\} = \ell_m \frac{d}{ds}\left\{A_o \text{erfcx}\left(B_o s - D_m\right)\right\} \tag{4.3-1}$$

Following the derivation that was done in Section 3.5.2, it can be shown that (4.3-1) becomes:

$$\frac{dV_m(s)}{ds} = \ell_m A_o B_o \left\{2\left(B_o s - D_m\right)\text{erfcx}\left(B_o s - D_m\right) - \frac{2}{\sqrt{\pi}}\right\} \tag{4.3-2}$$

Next, the derivative of Z_{mn} can be found by taking the derivative of (4.2-8), namely,

$$\frac{dZ_{mn}}{ds} = \frac{d}{ds}\left\{ \frac{\mu}{4\pi} \sum_{p=1}^{N_g} \sum_{q=1}^{N_g} \sum_{(\kappa_1,\kappa_2)} w_p w_q \, s\, e^{-s\,\tau_{mnpq}^{\kappa_1\kappa_2}} L_{mnpq}^{\kappa_1\kappa_2} \right\}$$
$$+ \frac{d}{ds}\left\{ \frac{1}{4\pi\varepsilon_0} \sum_{p=1}^{N_g} \sum_{q=1}^{N_g} \sum_{(\kappa_1,\kappa_2)} w_p w_q \, \frac{e^{-s\tau_{mnpq}^{\kappa_1\kappa_2}}}{s} C_{mnpq}^{\kappa_1\kappa_2} \right\} \tag{4.3-3}$$

that results in:

$$\frac{dZ_{mn}}{ds} = \frac{\mu}{4\pi} \sum_{p=1}^{N_g} \sum_{q=1}^{N_g} \sum_{(\kappa_1,\kappa_2)} w_p w_q \left(1 - s\,\tau_{mnpq}^{\kappa_1\kappa_2}\right) e^{-s\,\tau_{mnpq}^{\kappa_1\kappa_2}} L_{mnpq}^{\kappa_1\kappa_2}$$
$$- \frac{1}{4\pi\varepsilon_0} \sum_{p=1}^{N_g} \sum_{q=1}^{N_g} \sum_{(\kappa_1,\kappa_2)} w_p w_q \left(\frac{1}{s} + \tau_{mnpq}^{\kappa_1\kappa_2}\right) \frac{e^{-s\tau_{mnpq}^{\kappa_1\kappa_2}}}{s} C_{mnpq}^{\kappa_1\kappa_2} \tag{4.3-4}$$

4.3.4 Implementation of NILT2

As explained in Section 3.5.3, we need expressions for d^2V_m / ds^2 and d^2Z_{mn} / ds^2. We take the derivative *d/ds* of both sides of (4.3-2) to obtain:

$$\frac{d^2V_m}{ds^2} = 2\ell_m A_o B_o \left\{ \operatorname{erfcx}(B_o s - D_m) + 2(B_o s - D_m)^2 \operatorname{erfcx}(B_o s - D_m) - \frac{2}{\sqrt{\pi}}(B_o s - D_m) \right\} \tag{4.3-5}$$

Next to find d^2Z_{mn} / ds^2 we take the derivative *d/ds* of both sides of (4.3-4), to obtain

$$\frac{d^2Z_{mn}}{ds^2} = \frac{\mu}{4\pi} \sum_{p=1}^{N_g} \sum_{q=1}^{N_g} \sum_{(\kappa_1,\kappa_2)} w_p w_q \, \tau_{mnpq}^{\kappa_1\kappa_2} \left(s\,\tau_{mnpq}^{\kappa_1\kappa_2} - 2\right) e^{-s\,\tau_{mnpq}^{\kappa_1\kappa_2}} L_{mnpq}^{\kappa_1\kappa_2}$$
$$+ \frac{1}{4\pi\varepsilon_0} \sum_{p=1}^{N_g} \sum_{q=1}^{N_g} \sum_{(\kappa_1,\kappa_2)} w_p w_q \left(\frac{2}{s^2} + \frac{2\tau_{mnpq}^{\kappa_1\kappa_2}}{s} + (\tau_{mnpq}^{\kappa_1\kappa_2})^2 \right) \frac{e^{-s\tau_{mnpq}^{\kappa_1\kappa_2}}}{s} C_{mnpq}^{\kappa_1\kappa_2} \tag{4.3.6}$$

4.4 VALIDATION EXAMPLES

4.4.1 Selection of Antenna Geometries

In order to validate the implementation of the initial-value mode NILT0, NILT1, and NILT2 for the solution of the TD-EFIE in 3D cases we consider three different antenna geometries:

- Centre-fed strip dipole antenna.
- Centre-fed bowtie dipole antenna.
- Air-substrate patch antenna.

Apart from the fact that they involve 3D PEC objects, these examples differ from those in Chapter 3 in that they are excited as antennas (with concentrated excitations) instead of incoming plane waves. In order to have reference results against which to compare the time-domain (TD) results obtained via the initial-value NILT*n* technique, we use the frequency-domain method of moments (FD-MoM) formulation for the 3D PEC objects[30] being analysed, at a set of frequencies, and then perform an inverse Fourier transform to obtain time-domain responses (which we will refer to as the IDFT[31] results).

Comments on the sets of complex frequencies s_i required in the initial-value NILT*n* approaches for the three examples to be considered, are like those for the initial-value NILT*n* mode used for the 2D cases in Chapter 3, and as given in Section 3.6.1. Nevertheless, after the discussion of the three examples, we will show these for each of the three examples for the NILT2 case, knowing (as discussed in Section 3.6.1) that the frequency distribution of such complex frequencies will be smaller for the NILT1 and NILT0 cases.

4.4.2 Centre-Fed Strip Dipole Antenna

The first antenna is a PEC strip dipole antenna shown in Fig. 4.4-1, excited at a centre-feedpoint with a Gaussian voltage pulse. The antenna size parameters, as well as those of the

[30] This is achieved by setting $s = j\omega$ in the complex frequency-domain formulation implemented in Section 4.2.

[31] An acronym for "inverse discrete Fourier transform".

excitation pulse, are provided in Table 4.4-1. The reference IDFT-based responses to be shown used the FD-MoM method to find frequency-domain results for the antenna terminal current between 0.0 GHz[32] and 1.0 GHz in frequency steps of 1.95 MHz, that were then converted to the time-domain using the IDFT.

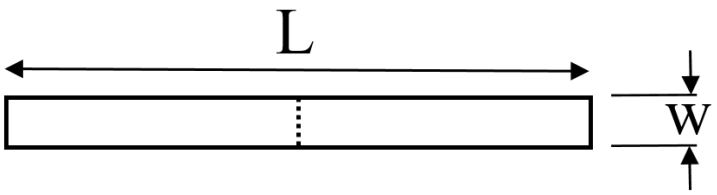

Fig. 4.4-1: Centre-fed strip dipole antenna geometry. The dashed line shows the location of the feedpoint where the Gaussian voltage pulse is injected.

Table 4.4-1: Parameters of the strip dipole antenna and the Gaussian voltage pulse.

L	2m
w	0.02m
Gaussian pulse width (T_w)	10 ns
Gaussian pulse delay t_o	20 ns
M	6
N	4
Time between samples	3.33 ns
Endtime	200 ns
Number of triangles in mesh[33]	86

Fig. 4.4-2 shows that the initial-value mode NILT0 only follows the IDFT results up to 20 ns, and then deviates from it substantially. To accurately predict responses out to later times the NILT1 and NILT2 routes (of Section 4.3) in their initial-value modes were applied, producing the results in Fig. 4.4-3 and Fig. 4.4-4, respectively. As expected, these allow the NILT-based results to match those of the IDFT out to later times (namely 40 ns and 45 ns respectively) compared to the NITL0 in Fig. 4.4-2. However, the use of using NILTn ($n > 0$) in their initial-value modes represents only a marginal improvement over the NILT0 in its initial-value mode.

[32] Albeit not at 0 GHz itself, instead assuming that at DC frequency, the magnitude of the current is zero.
[33] See APPENIDX IV for an explanation on the mesh density selection

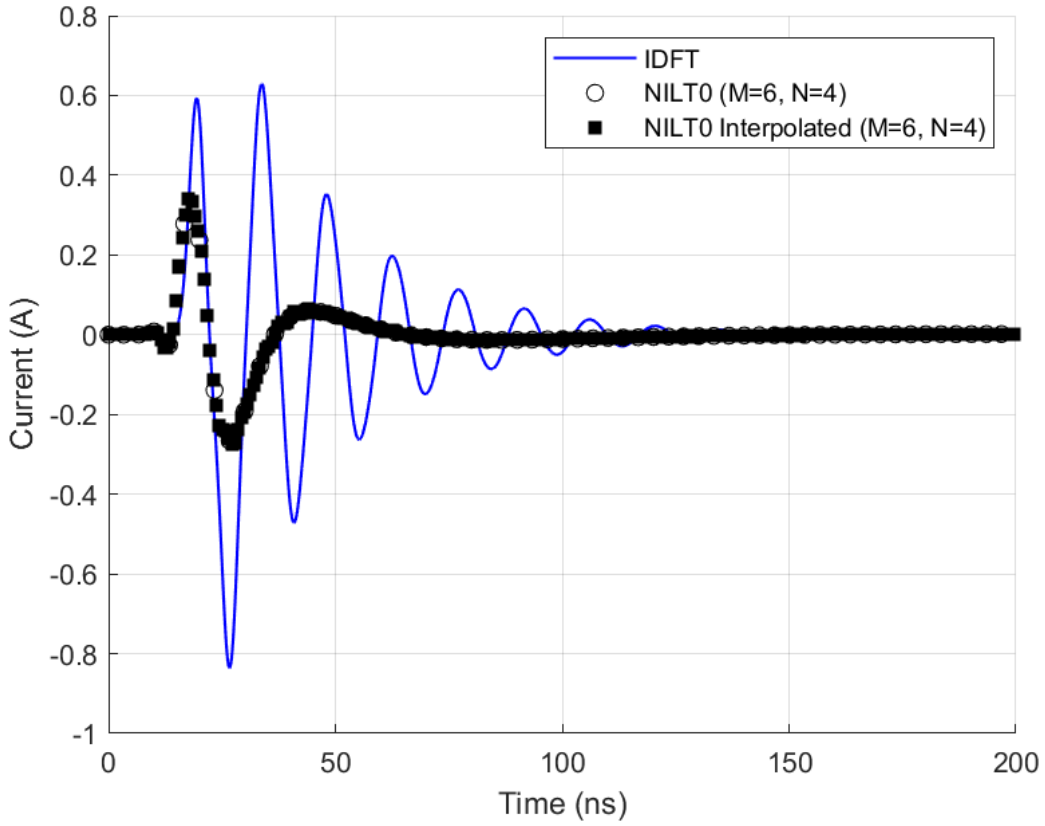

Fig. 4.4-2: The current at the feedpoint of the strip dipole antenna when excited by a Gaussian pulse located at the feedpoint. The blue line represents the TD results obtained using an IDFT. The black circles represent the TD current obtained using the NILT0 in the initial-value mode. The black squares represent the interpolated results obtained using the information available from the NILT0 predictions.

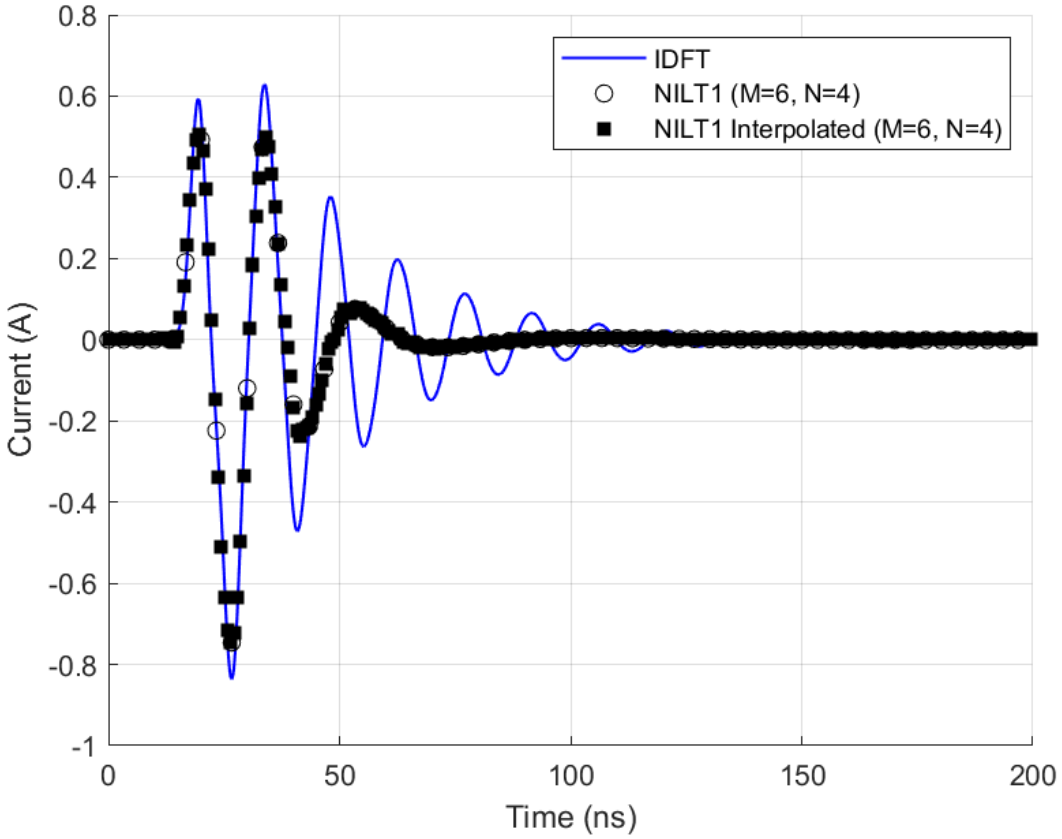

Fig. 4.4-3: The current at the feedpoint of the strip dipole antenna when excited by a Gaussian pulse located at the feedpoint. The blue line represents the TD results obtained using an IDFT. The black circle represents the TD current obtained using the NILT1 in the initial-value mode. The black squares represent the interpolated results obtained using the information available from the NILT1 predictions.

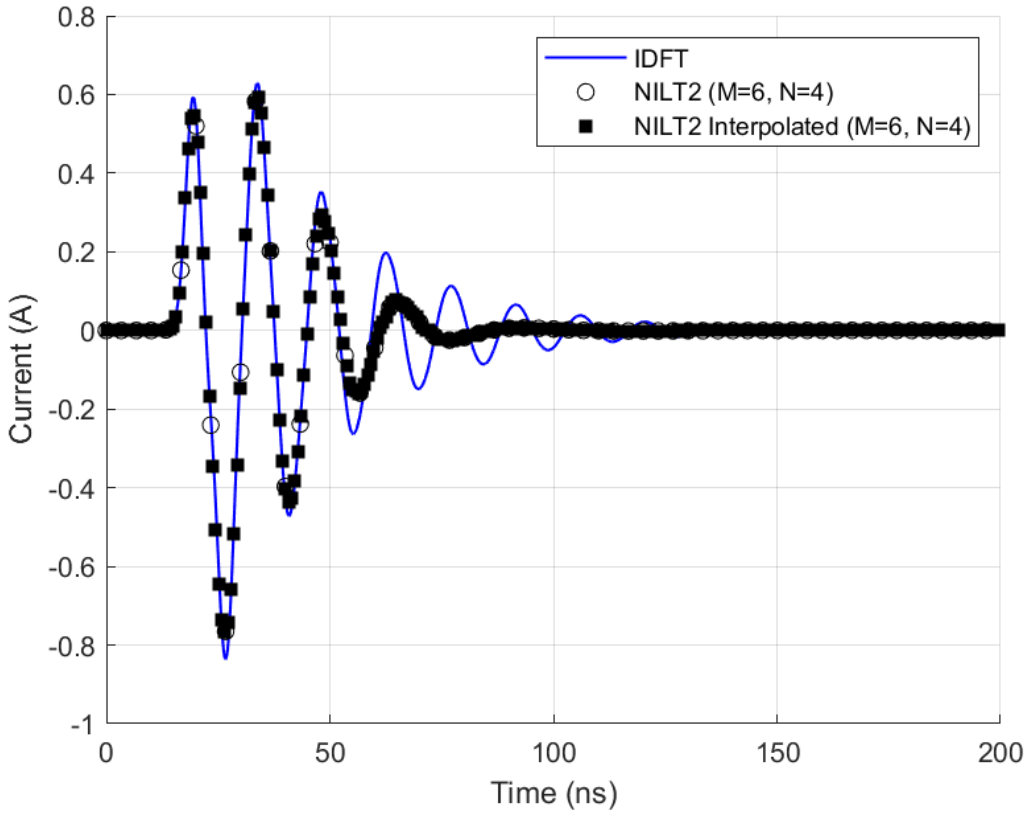

Fig. 4.4-4: The current at the feedpoint of the strip dipole antenna when excited by a Gaussian pulse located at the feedpoint. The blue line represents the TD results obtained using an IDFT. The black circle represents the TD current obtained using the NILT2 in the initial-value mode. The black squares represent the interpolated results obtained using the information available from the NILT2 predictions.

4.4.3 Centre-Fed Bowtie Dipole Antenna

The second antenna tested was the PEC bowtie dipole antenna shown Fig. 4.4-5. The dimensions, Gaussian pulse excitation parameters, and mesh information, are provided in Table 4.4-2. The reference IDFT-based responses to be shown used the FD-MoM method to find frequency-domain results for the antenna terminal current between 0.0 GHz and 1.0 GHz in frequency steps of 1.25 MHz, that were then converted to the time-domain using the IDFT.

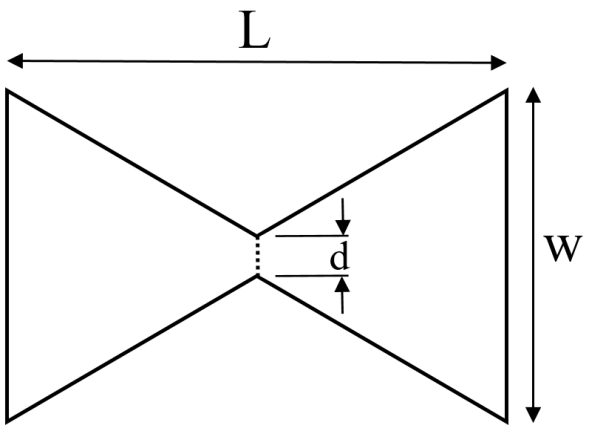

Fig. 4.4-5: Centre-fed bowtie dipole antenna geometry. The dashed line is the location of the feedpoint where the Gaussian voltage pulse is injected.

Table 4.4-2: Parameters of the bowtie dipole antenna and the Gaussian voltage pulse.

L	2m
w	2.1m
d	0.1m
Gaussian pulse width (T_w)	30 ns
Gaussian pulse delay t_o	60 ns
M	6
N	4
Time between samples	10 ns
Endtime	335 ns
Number of triangles in mesh[34]	148

[34] See APPENIDX IV for an explanation on the mesh density selection

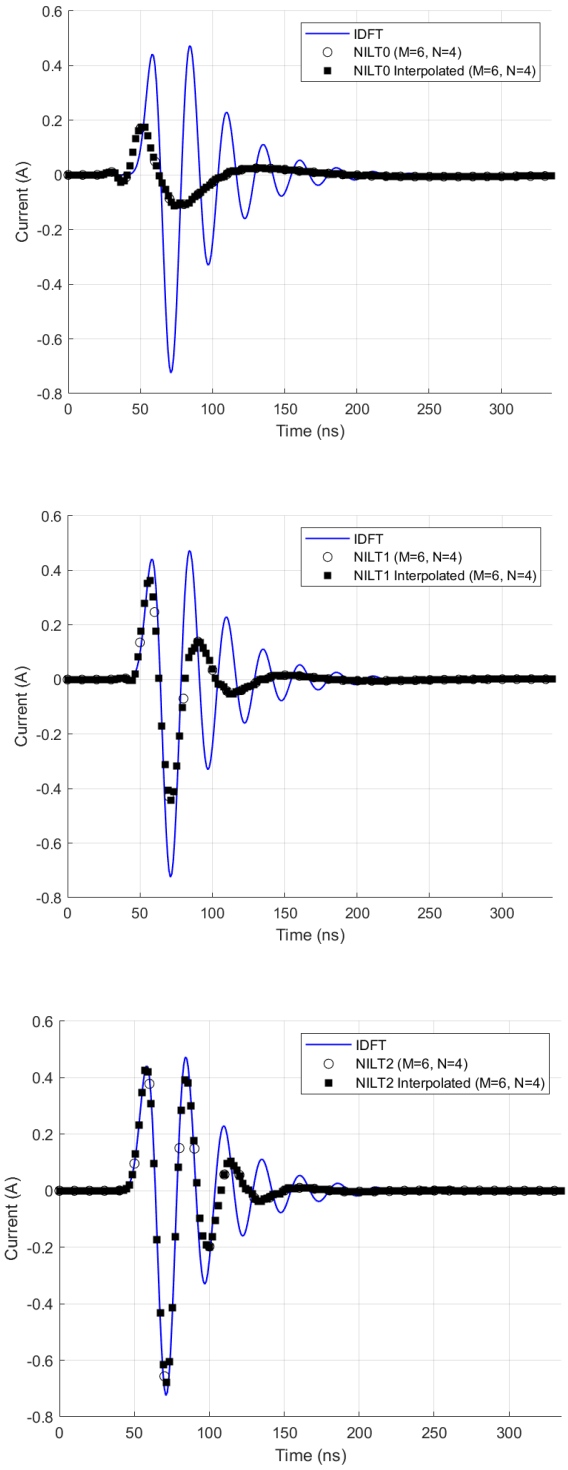

Fig. 4.4-6: The induced current at the feedpoint of the bowtie dipole antenna when excited by a Gaussian pulse located at the feedpoint. The blue lines represent the TD results obtained using an IDFT approach. The black circles represent the TD current obtained using the initial-value modes of the NILT0 (top), NILT1 (middle) and the NILT2 (bottom). The black squares represent the interpolated results of the same.

The observations from Fig. 4.4-6 are similar to those for the strip-dipole case. These initial-value mode NILT*n* results follow that the IDFT ones out to increasingly larger times (namely 45ns, 55ns and 90ns, for $n = 0,1,2$), but are unsatisfactory in the sense that the IDFT results are still at significant values well beyond the point where the NILT*n*-based ones fail.

4.4.4 Patch Antenna with Air Substrate

The third antenna modelled was the PEC patch antenna with an "air-substrate" (this is the terminology used in the literature), based on such an antenna described in [HERS 98], but not identical to it. Its geometry is shown in Fig. 4.4-7. Its dimensions, the parameters of the Gaussian pulse excitation used, and mesh information, is that listed in Table 4.4-3. The reference IDFT-based responses to be shown used the FD-MoM method to find frequency-domain results for the antenna terminal current between 0.0 GHz and 20.0 GHz in frequency steps of 3.33 MHz, that were then converted to the time-domain using the IDFT.

Table 4.4-3: Parameters of the patch antenna with air substrate antenna and the Gaussian voltage pulse.

w_1	17.40 mm
w_2	53.00 mm
w_3	27.95 mm
h_1	49.10 mm
h_2	8.90 mm
h_3	16.20 mm
d_1	76.2 mm
d_2	50.1 mm
a	18.40 mm
b	3.80 mm
Gaussian pulse width (T_w)	2.5 ns
Gaussian pulse delay t_o	5 ns
M	6
N	4
Time between samples	5/6 ns
Endtime	135 ns
Number of triangles in mesh[35]	163

[35] See APPENDIX IV for an explanation on the mesh density selected

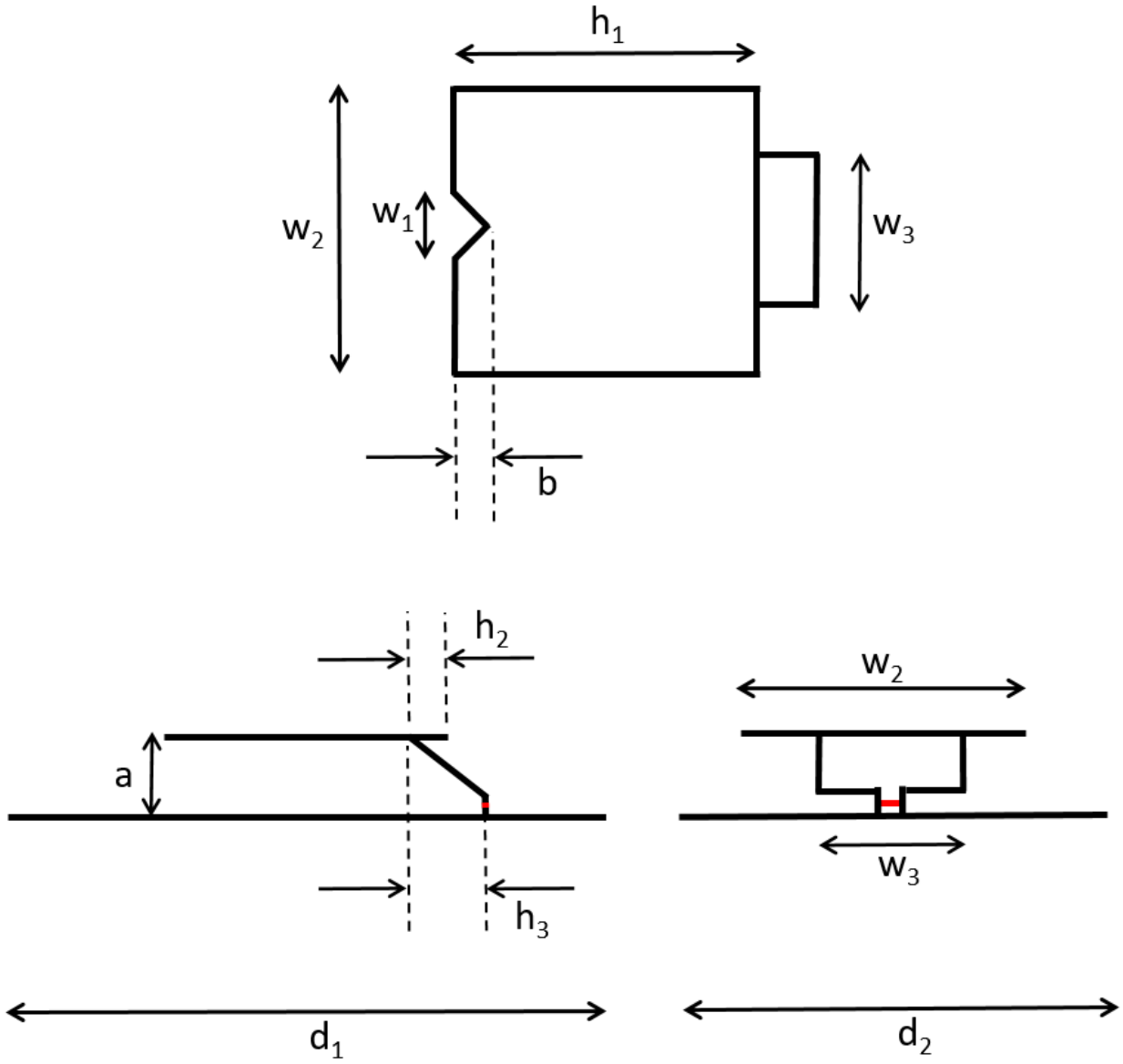

Fig. 4.4-7: The geometry of the patch antenna with an air substrate. The red line is the location of the feedpoint where the Gaussian voltage pulse is injected.

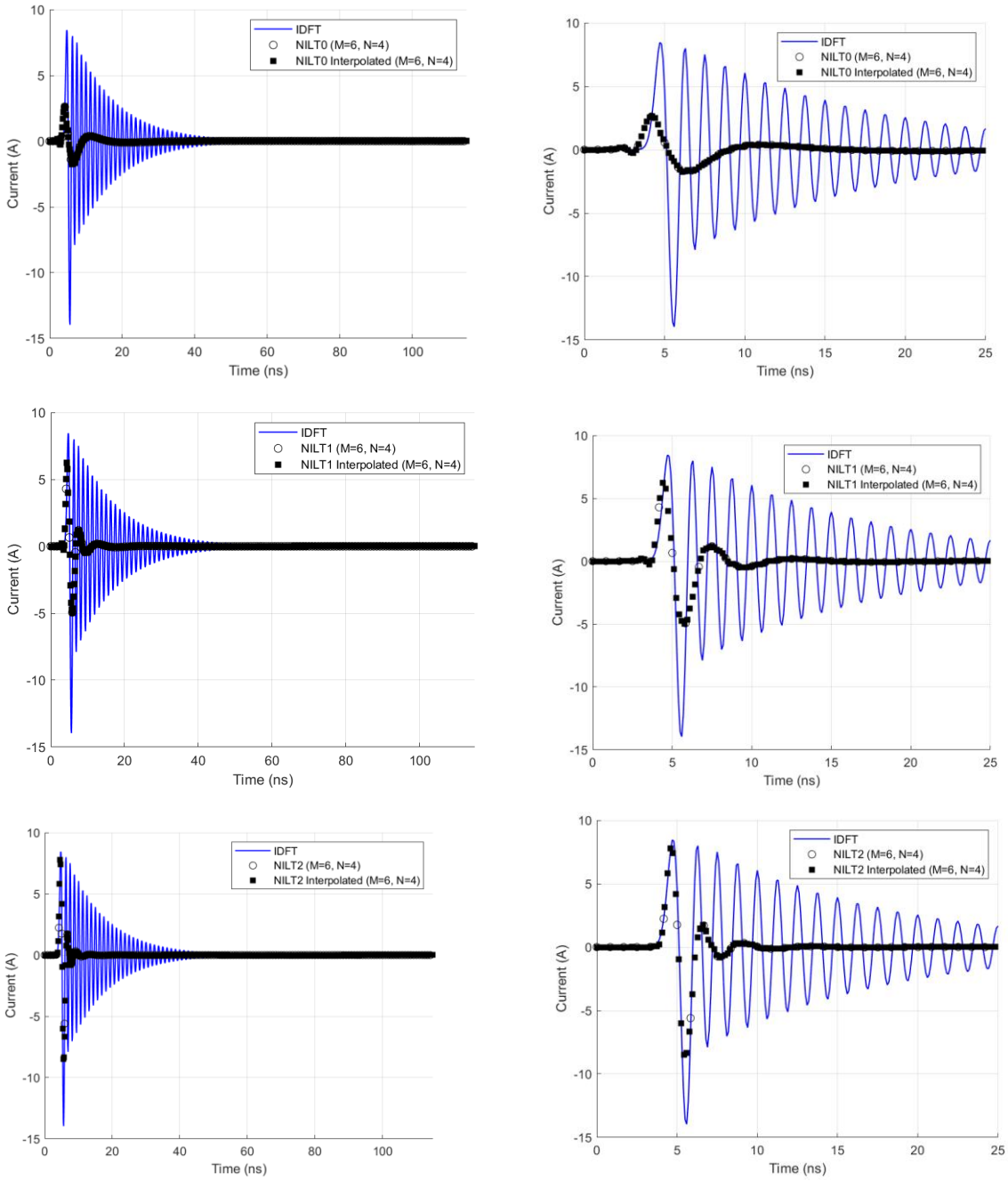

Fig. 4.4-8: The induced current at the feedpoint of the patch antenna when excited by a Gaussian pulse at its feedpoint. The blue lines represent the TD results obtained using an IDFT approach. The black circles represent the TD current obtained using the initial-value modes of the NILT0 (top), NILT1 (middle) and the NILT2 (bottom). The black squares represent the interpolated results of the same. Zoomed-in depictions (right) are shown for the results shown (left).

Similar comments on the NILT*n* results can be made here as done for the strip-dipole and bowtie-dipole in the two previous sub-sections. That is to say, we find here again that the NILT*n*-based results (with interpolation), used in the initial-value mode, match those of the IDFT one out to increasingly later times (namely 3ns, 4ns and 5ns for $n = 0, 1$ and 2, respectively), but the $n = 1, 2$ values provide only marginal improvement over NILT0. It is unmistakably clear that, in order to substantially improve the ability of NILT*n*-based methods, the use of re-initialization is needed. This is formulated and discussed in the next chapter.

Finally, Fig. 4.4-9 shows the sets of s_i values needed for the NILT2 results (in the initial-value mode) needed for the three different geometries. The sets are different simply because different sample times were used in each case.

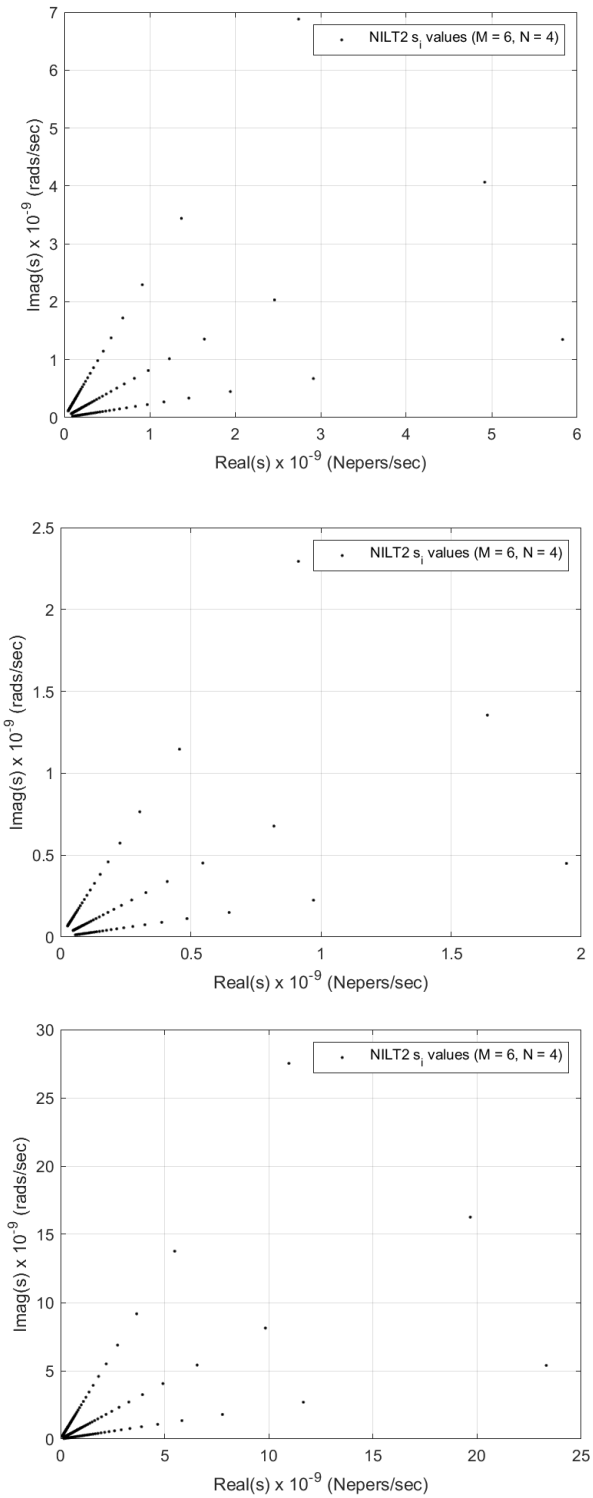

Fig. 4.4-9: The distribution of complex frequencies used in the calculation of the NILT2 results for the strip dipole (top), bowtie dipole (middle) and patch (bottom) antennas. Recall that as the time gets larger, the real and imaginary component of the s_i used in the calculation gets smaller.

4.5 CONCLUSIONS

This chapter has formulated, implemented and applied the NILT*n*/MoM approach in its initial-value mode to find solutions to the TD-EFIE of 3D PEC objects. Numerical results for open 3D PEC objects have been shown and validated. This has extended what was done in Chapter 3, for 2D objects, to 3D objects. The numerical experiments have been found to support what was observed for the 2D cases in Chapter 3, namely that although the use of NILT*n* approaches (for $n > 0$) permit prediction out to larger value of t, this improvement is only marginal. It is clear that in order to substantially improve the ability of NILT*n*-based methods, the use of re-initialization is needed. This will be formulated for the general 3D case in Chapter 5.

CHAPTER 5 - The Incorporation of Re-Initialization in Time-Domain Integral Equation Models Solved Using the NILT/MM

5.1 INITIAL REMARKS

Amongst other things, Chapter 2 provided the established background on the NILT*n* method needed to conduct the research reported in this thesis. It was pointed out in Section 2.7 that the NILT*n* can be used in two different ways. The first, referred to as the initial value form, is not a marching-on-in-time type method. The second, called the re-initialized form, is a recursive method that finds the time-domain solution in a recursive time-stepping manner. Chapter 3 formulated and applied, in its initial value form, the NILT*n* technique(s) to the solution of the TD-EFIE for a 2D problem. It also explained the difficulty in applying re-initialization to TD-EFIE problems, in essence due to the occurrence of delay terms (because of the full-wave character of the TD-EFIE) that are not present in the analysis of lumped circuits. Chapter 4 then formulated and demonstrated the successful use of the initial NILT*n*-based solution to TD-EFIE problems for open PEC objects. However, the numerical experiments in Chapter 4 make it clear that a re-initialized form of the NILT*n* technique is needed. Chapter 5 now tackles the problem of incorporating such re-initialization, in the following sections:

■ Section 5.2 performs a spatial discretization of the TD-EFIE, thereby converting it into a set of time-domain partial differential equations. It then converts these into what is an s-domain form of TD-EFIE, but (unlike that in Chapter 4) in a manner that permits the use of re-initialization in spite of the multiplicity of delay terms. This is done for the NILT0 approach in the re-initialization mode.

■ Section 5.3 first carefully outlines the steps of the re-initialized NILT0 approach, and then extends what was described in Section 5.2 so that we have what is needed to implement NILT1 and NILT2 in the re-initialization mode.

■ Section 5.4 implements the newly devised and derived formulations of Section 5.2 and Section 5.3 to the same three examples presented in Section 4.4 (but there only possible using these

NILT*n*-based methods in the initial-value mode). The enormous advantages of being able to use these in the re-initialized mode developed in this chapter will be evident.

■ Section 5.5 examines the re-initialized NILT*n*-based techniques in terms of their computational complexity.

■ Section 5.6 concludes the chapter by putting into context what has been achieved.

5.2 A FORMULATION FOR INCORPIRATING RE-INITIALIZATION INTO THE NILT*n*/MoM SOLUTION OF THE 3D TD-EFIE

5.2.1 Spatial Discretization of the TD-EFIE

The first step is to discretize the differentiated[36] TD-EFIE[37] [38] in (2.3-14) with respect to the spatial coordinates but *not* the time variable. A similar MoM procedure to that used in Section 4.2.1, is followed with the exception that, the unknown current density is considered to be expressed as[39]

$$\bar{\mathscr{J}}_s(\bar{r},t) = \sum_{n=1}^{N_s} i_n(t)\,\bar{j}_n(\bar{r}) \tag{5.2-1}$$

The expansion functions $\bar{j}_n(\bar{r})$ are the same RWG ones used in Section 4.2.1, with an identical set forming the testing functions. Expression (5.2-1) is inserted into (2.3-14), which involves integration over *S* with respect to the primed coordinates. Next a dot product of each side of the resulting expression is taken with the *m*-th testing function $\bar{j}_m(\bar{r})$, and both sides integrated over S with respect to the unprimed coordinate, to obtain (once more with some judicious use of vector analysis)

$$\begin{aligned}
&\frac{\mu}{4\pi}\sum_{n=1}^{N_s}\sum_{p=1}^{N_g}\sum_{q=1}^{N_g}\sum_{(\kappa_1,\kappa_2)} w_p w_q L_{mnpq}^{\kappa_1\kappa_2}\frac{\partial^2}{\partial t^2}\int_{-\infty}^{\infty} i_n(t')\,\delta\left(t-t'-\tau_{mnpq}^{\kappa_1\kappa_2}\right)dt' \\
&\qquad + \frac{1}{4\pi\varepsilon}\sum_{n=1}^{N_s}\sum_{p=1}^{N_g}\sum_{q=1}^{N_g}\sum_{(\kappa_1,\kappa_2)} w_p w_q C_{mnpq}^{\kappa_1\kappa_2}\int_{-\infty}^{\infty} i_n(t')\,\delta\left(t-t'-\tau_{mnpq}^{\kappa_1\kappa_2}\right)dt' \\
&\qquad\qquad = \frac{\partial}{\partial t}\sum_{p=1}^{N_g} w_p\,\bar{j}_m\left(\bar{r}_{pm}^{\kappa_1}\right)\cdot\bar{\mathscr{E}}^{inc}\left(\bar{r}_{pm}^{\kappa_2},t\right)
\end{aligned} \tag{5.2-2}$$

---

[36] See annex II for more details, noting that it similar steps can be taken for the differentiated TD-EFIE
[37] Chapter 4 did this but for the *s*-domain EFIE and *not* the *t*-domain EFIE (that is, TD-EFIE).
[38] Readers curious in knowing why the differentiated TD-EFIE was used instead of the previously used undifferentiated form are encouraged to read Appendix V.
[39] Observe that $i_n(t)$ is the coefficient of the *n*-th expansion function, and is a continuous function of time.

as described in Section 2.7-3 and Section 3.7, an essential move for re-initialization is to implement the change of variable[40] $t = \hat{t} + rh$ in (5.2-2). This yields

$$\frac{\mu}{4\pi}\sum_{n=1}^{N_s}\sum_{p=1}^{N_g}\sum_{q=1}^{N_g}\sum_{(\kappa_1,\kappa_2)} w_p w_q L_{mnpq}^{\kappa_1\kappa_2}\frac{\partial^2}{\partial t^2}\int_{-\infty}^{\infty} i_n(t')\delta\left(\hat{t}+rh-t'-\tau_{mnpq}^{\kappa_1\kappa_2}\right)dt'$$
$$+\frac{1}{4\pi\varepsilon}\sum_{n=1}^{N_s}\sum_{p=1}^{N_g}\sum_{q=1}^{N_g}\sum_{(\kappa_1,\kappa_2)} w_p w_q C_{mnpq}^{\kappa_1\kappa_2}\int_{-\infty}^{\infty} i_n(t')\delta\left(\hat{t}+rh-t'-\tau_{mnpq}^{\kappa_1\kappa_2}\right)dt'$$
$$=\frac{\partial}{\partial t}\sum_{p=1}^{N_g} w_p\,\bar{j}_m\left(\bar{r}_{pm}^{\kappa_1}\right)\cdot\bar{\mathcal{E}}^{inc}\left(\bar{r}_{pm}^{\kappa_2},\hat{t}+rh\right) \tag{5.2-3}$$

the sifting property of the delta function makes the two identical convolution terms in (5.2-3)

$$\int_{-\infty}^{\infty} i_n(t')\delta\left(\hat{t}+rh-t'-\tau_{mnpq}^{\kappa_1\kappa_2}\right)dt' = i_n\left(\hat{t}+rh-\tau_{mnpq}^{\kappa_1\kappa_2}\right) \tag{5.2-4}$$

also, the time derivative operation on the left-hand side of (5.2-3) acts only on the incident field $\bar{\mathcal{E}}^{inc}(\bar{r}_{pm}^{\kappa_2},\hat{t}+rh)$. Thus (5.2-3) becomes

$$\frac{\mu}{4\pi}\sum_{n=1}^{N_s}\sum_{p=1}^{N_g}\sum_{q=1}^{N_g}\sum_{(\kappa_1,\kappa_2)} w_p w_q L_{mnpq}^{\kappa_1\kappa_2}\frac{\partial^2}{\partial t^2} i_n\left(\hat{t}+rh-\tau_{mnpq}^{\kappa_1\kappa_2}\right)$$
$$+\frac{1}{4\pi\varepsilon}\sum_{n=1}^{N_s}\sum_{p=1}^{N_g}\sum_{q=1}^{N_g}\sum_{(\kappa_1,\kappa_2)} w_p w_q C_{mnpq}^{\kappa_1\kappa_2}\, i_n\left(\hat{t}+rh-\tau_{mnpq}^{\kappa_1\kappa_2}\right) \tag{5.2-5}$$
$$=\sum_{p=1}^{N_g} w_p\,\bar{j}_m\left(\bar{r}_{pm}^{\kappa_1}\right)\cdot\frac{\partial}{\partial t}\bar{\mathcal{E}}^{inc}\left(\bar{r}_{pm}^{\kappa_2},\hat{t}+rh\right)$$

We must then take the Laplace-transform of both sides of (5.2-5) with respect to $\hat{t}$, an operation we will denote by $\hat{\mathcal{L}}$ to distinguish it from $\mathcal{L}$ that signifies the transform with respect to *t*. In other words

[40] Note that $r = 0,1,2,3.....$ is an integer and is unrelated to any distance in space. Observe also that $\partial/\partial\hat{t} \to \partial/\partial t$.

$$\frac{\mu}{4\pi}\sum_{n=1}^{N_s}\sum_{p=1}^{N_g}\sum_{q=1}^{N_g}\sum_{(\kappa_1,\kappa_2)} w_p w_q L_{mnpq}^{\kappa_1\kappa_2}\,\hat{\mathcal{L}}\left\{\frac{\partial^2}{\partial t^2} i_n\left(\hat{t}+rh-\tau_{mnpq}^{\kappa_1\kappa_2}\right)\right\}$$
$$+\frac{1}{4\pi\varepsilon}\sum_{n=1}^{N_s}\sum_{p=1}^{N_g}\sum_{q=1}^{N_g}\sum_{(\kappa_1,\kappa_2)} w_p w_q C_{mnpq}^{\kappa_1\kappa_2}\,\hat{\mathcal{L}}\left\{i_n\left(\hat{t}+rh-\tau_{mnpq}^{\kappa_1\kappa_2}\right)\right\}$$
$$=\sum_{p=1}^{N_g} w_p\,\bar{j}_m\left(\bar{r}_{pm}^{\kappa_1}\right)\cdot\hat{\mathcal{L}}\left\{\frac{\partial}{\partial t}\bar{\mathcal{E}}^{inc}\left(\bar{r}_{pm}^{\kappa_2},\hat{t}+rh\right)\right\} \tag{5.2-6}$$

5.2.2 The Challenge in Re-Initializing NILTn for Solution of the TD-EFIE

We would need to find the Laplace transform of the incident field term on the right-hand side of (5.2-6), which is not straightforward for reasons given in the first paragraph of Section 3.7. Even more challenging is the fact that the two Laplace transform terms on the left hand side of (5.2-6), namely $\hat{\mathcal{L}}\left\{i_n\left(\hat{t}+rh-\tau_{mnpq}^{\kappa_1\kappa_2}\right)\right\}$ and $\hat{\mathcal{L}}\left\{\frac{\partial^2}{\partial\hat{t}^2} i_n\left(\hat{t}+rh-\tau_{mnpq}^{\kappa_1\kappa_2}\right)\right\}$ need to be represented in terms of a single Laplace-domain-based unknown that is coupled with, and simultaneously solved for, with the other N_s-1 unknown coefficients. Closer examination, however, reveals that this is not possible. To demonstrate this statement, we consider the definition of the first term,

$$\hat{\mathcal{L}}\left\{i_n\left(\hat{t}+rh-\tau_{mnpq}^{\kappa_1\kappa_2}\right)\right\}=\int_0^\infty i_n\left(\hat{t}+rh-\tau_{mnpq}^{\kappa_1\kappa_2}\right)e^{-s\hat{t}}d\hat{t} \tag{5.2-7}$$

and refer to Fig. 5.2-1. If we were to regard the above integral as an unknown, to be solved for in the course of a MoM analysis, then one should note here that it is an unknown that will depend on the values of indices *m*, *n*, *p* and *q*, and whether those indices belong the + or − side of the *m*- and *n*-th (edge) basis function. This is depicted in the sketch shown in Fig. 5.2-1. This figure shows that whatever comes out of the integral in 5.2-7 is something that is determined by *m*, *p*, *q* and κ_1 κ_2, and not only on *n* or *s*. Therefore, it is not possible to account for the integral by simply denoting it by $\hat{I}_n(s)$. Instead, the correct notation should involve all of the preceding indices, e.g. $\hat{I}_{mnpq}^{\kappa_1\kappa_2}(s)$. Proceeding further with this idea, $\hat{I}_{mnpq}^{\kappa_1\kappa_2}(s)$ cannot be factored out from

under the summation, as $\sum_{p}\sum_{q}\sum_{(\kappa_1,\kappa_2)}$ runs over the quadrature points in (5.2-6). Furthermore, one cannot take $\hat{I}_{mnpq}^{\kappa_1\kappa_2}(s)$ to mean the same unknown for all values of *m*. In other words, it will not be possible to continue and formulate a system of N_s independent equations in N_s Laplace-based unknowns, as is possible in the analysis of lumped circuit analysis devoid of distributed delay terms.

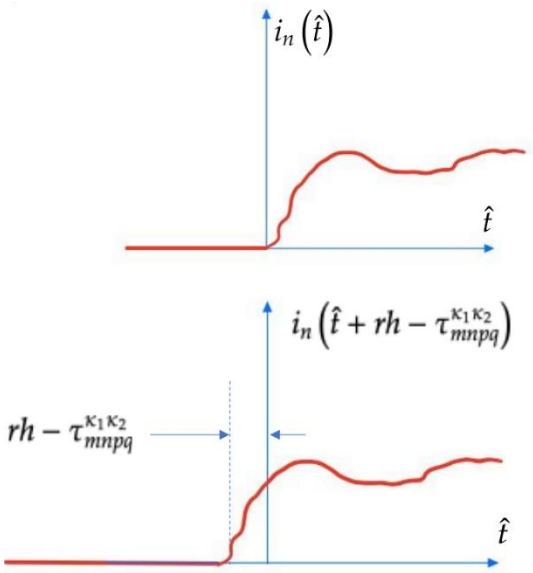

Fig. 5.2-1: Graphical representation highlighting the dependence of the integral in (5.2-7) on the actual value of $\tau_{mnpq}^{\kappa_1\kappa_2}$.

5.2.3 Development of the Basic Idea

In order to facilitate continued development of the idea, we shall assume that $i_n(t)$ has already been computed for all values of $t = h,2h,3h,...,rh$, and that the objective is to compute $i_n\left((r+1)h\right)$.

The idea of the proposed re-initialization process starts by partitioning the integral in (5.2-7) as[41]

[41] A full explanation of the steps leading from (5.2-7) to (5.2-8) is available in Appendix VI

$$\int_0^{\infty} i_n\left(\hat{t}+rh-\tau_{mnpq}^{\kappa_1\kappa_2}\right)e^{-s\hat{t}}d\hat{t}=e^{-s\tau_{mnpq}^{\kappa_1\kappa_2}}\int_0^{\infty} i_n\left(\hat{t}+rh\right)e^{-s\hat{t}}d\hat{t}\;+\;e^{-s\tau_{mnpq}^{\kappa_1\kappa_2}}\int_{-\tau_{mnpq}^{\kappa_1\kappa_2}}^{0} i_n\left(\hat{t}+rh\right)e^{-s\hat{t}}d\hat{t} \qquad (5.2\text{-}8)$$

The first integral on the right-side of equation (5.2-8) is independent of *m*, *p*, *q* and $\kappa_1\kappa_2$. Thus, it can rightfully be denoted as the unknown $\hat{I}_n(s)$, in line with the notation used in lumped circuit simulation that assigns a caret symbol to the Laplace domain quantities of the time-shifted variable.

The integrand $i_n(\hat{t}+rh)e^{-s\hat{t}}$ of the second integral on the right-hand side (5.2-8) is accessible through its past time values, which are assumed to have been computed. Indeed, the limits on the second integral indicate that the values of $i_n(rh-\tau_{mnpq}^{\kappa_1\kappa_2})$ up to $i_n(rh)$, which are on the temporal path that lies in the past (before $t = rh$), contribute to its computation. This observation suggests that the second integral on the right-side of (5.2-8), multiplied by $e^{-s\tau_{mnpq}^{\kappa_1\kappa_2}}$, be denoted by $U_{mnpq}^{\kappa_1\kappa_2}(\mathrm{s})$ and also counted as a known quantity, although it still not obvious how it can be computed. Thus, (5.2-8) can be written

$$\hat{\mathcal{L}}\left\{i_n\left(\hat{t}+rh-\tau_{mnpq}^{\kappa_1\kappa_2}\right)\right\}=e^{-s\tau_{mnpq}^{\kappa_1\kappa_2}}\left(\underbrace{\hat{I}_n(s)}_{\substack{\text{The Unknown}\\ \text{"Now"}}}\;+\;\underbrace{U_{mnpq}^{\kappa_1\kappa_2}(s)}_{\substack{\text{The Known}\\ \text{"Antecedent"}}}\right) \qquad (5.2\text{-}9)$$

The focus of the development will now be directed to the second term in (5.2-9), $U_{mnpq}^{\kappa_1\kappa_2}(\mathrm{s})$, which will be referred to as the antecedent term.

5.2.4 Piecewise Polynomial Representation of $i_n(t)$

Preparing the ground for the handling of the antecedent term necessitates considering the past ($t < rh$) behavior of $i_n(t)$ and modelling it as a piecewise polynomial. That task will draw on the results reported in [GAD 22] to construct the desired polynomial. To motivate the discussions in this, Fig. 5.2-2 graphically illustrates the situation at the present time instant $t = rh$. As shown, $i_n(t)$, taken to be of a given, but arbitrary form, is assumed to have been successfully computed at discrete times $t = h,2h,3h,...,rh$ and the goal is to advance by another step *h* so as to compute

$i_n((r+1)h)$. This assumption is obviously true for at least the case $r=1$ using the process established in Chapter 4. In addition to the past *r* discrete points found on function $i_n(t)$, using past applications of NILT, we will assume that $i_n(t)$ is also represented as a continuous function of time built from piecewise polynomials, all with degree *u*, mainly to simplify the notation, for the whole interval $0 \le t \le rh$. To be more precise, $i_n(t)$ is given the representation,

$$i_n(t) = \sum_{i=0}^{r-1} \sum_{k=0}^{u} a_{k,n}^{(r-i)} \left(t - (r-i)h\right)^k \qquad (5.2\text{-}10)$$

with the coefficients $a_{k,n}^{(i)}$, $k = 0,1,...,u$ that correspond to the *i*-th polynomial that interpolates the sub-interval that extends from $t = \left(r - (i+1)\right)h$ to $t = (r-i)h$, for the *n*-th current density coefficient. This representation is reflected in Fig. 5.2-2.

The task of computing the polynomial coefficients $a_{k,n}^{(r-i)}$ was the subject of a previous work [GAD 22] that hinged on two main facts. The first is that high-order derivatives (with respect to time) of $i_n(t)$ at $t = rh$, $r = 1,2,3,...$ can be obtained with truly negligible additional computational cost from the NILT results, namely the $I_n(z_i / h)$ already used to compute $i_n(rh)$. The second is that such derivatives can be incorporated to create the Hermite interpolating polynomial. The coefficients of the Hermite interpolant are found explicitly from the derivatives at *rh*, that is to say the $d^k i_n(t)/dt^k$ at *t* = *rh*. The high-order approximation characteristics of NILT, used in computing $i_n(rh)$, are extended to computing its high-order derivatives, enabling the resulting polynomial to capture the behavior of $i_n(t)$ in the intervals between the points at *t* = *rh* with very high accuracy, as demonstrated in [GAD 22]. In what follows, we can confidently assume that the coefficients of the Hermite interpolant $a_{k,n}^{(r-i)}$ are known.

5.2.5 Derivation of the Closed-Form for the *Antecedent* Term

The primary purpose of the polynomial representation in Section 5.2.3 is to facilitate development of closed-form representations for the integrals of the antecedent term $U_{mnpq}^{\kappa_1\kappa_2}(s)$. In

fact, the form representing this term will depend on the relation between $\tau_{mnpq}^{\kappa_1\kappa_2}$ and the time step size *h*, and will be characterized through an integer $\zeta_{mnpq}^{\kappa_1\kappa_2}$ defined by

$$\zeta_{mnpq}^{\kappa_1\kappa_2} = \left\lfloor \frac{\tau_{mnpq}^{\kappa_1\kappa_2}}{h} \right\rfloor \tag{5.2-11}$$

where $\lfloor ... \rfloor$ denotes the floor function, that is equal to the greatest integer less than its argument. There are three values of interest for $\zeta_{mnpq}^{\kappa_1\kappa_2}$, shown in Table 5.2-1. For each one of the three cases, $U_{mnpq}^{\kappa_1\kappa_2}(s)$ will have a particular expression. These expressions will be derived next, making reference to Fig. 5.2-2 for illustration.

Table 5.2-1: Different cases for $\zeta_{mnpq}^{\kappa_1\kappa_2}$.

Case#	$\zeta_{mnpq}^{\kappa_1\kappa_2}$ Value
1	$\zeta_{mnpq}^{\kappa_1\kappa_2} = 0$
2	$0 < \zeta_{mnpq}^{\kappa_1\kappa_2} \le r$
3	$r < \zeta_{mnpq}^{\kappa_1\kappa_2}$

1) $U_{mnpq}^{\kappa_1\kappa_2}(s)$ for Case#1 : $\zeta_{mnpq}^{\kappa_1\kappa_2} = 0$

In this case $\tau_{mnpq}^{\kappa_1\kappa_2} < h$ and the integration in $U_{mnpq}^{\kappa_1\kappa_2}(s)$ is computed from the values of $i_n(\hat{t} + rh)e^{-s\hat{t}}$ under the right-most blue interval of Fig. 5.2-2. The polynomial representing $i_n(t)$ in this strip is given by

$$i_n(t) = \sum_{k=0}^{u} a_{k,n}^{(r)} (t - rh)^k, \quad (r-1)h \le t \le rh \tag{5.2-12}$$

the above polynomial can then be used to represent $i_n(\hat{t} + rh)$ as

$$i_n(\hat{t} + rh) = \sum_{k=0}^{u} a_{k,n}^{(r)} \hat{t}^k, \quad -h \le \hat{t} \le 0 \tag{5.2-13}$$

substituting (5.2-13) into the second integral in (5.2-8), reveals that $U_{mnpq}^{\kappa_1\kappa_2}(\mathrm{s})$ can be expressed as

$$U_{mnpq}^{\kappa_1\kappa_2}(\mathrm{s}) = e^{-s\tau_{mnpq}^{\kappa_1\kappa_2}} \sum_{k=0}^{u} a_{k,n}^{(r)} \int_{-\tau_{mnpq}^{\kappa_1\kappa_2}}^{0} \hat{t}^k e^{-s\hat{t}} d\hat{t} \tag{5.2-14}$$

The integral in (5.2-14) can be found analytically to be

$$e^{-s\tau_{mnpq}^{\kappa_1\kappa_2}} \int_{-\tau_{mnpq}^{\kappa_1\kappa_2}}^{0} t^k e^{-s\hat{t}} d\hat{t} = \frac{k!}{s^{k+1}} \left(\sum_{v=0}^{k} \frac{\left(-\tau_{mnpq}^{\kappa_1\kappa_2}\right)^v}{s^{-v} v!} - e^{-s\tau_{mnpq}^{\kappa_1\kappa_2}} \right) \tag{5.2-15}$$

This can be proved through simple induction. First, it is obviously true for $k = 0$. Secondly, if it is assumed to be true for $k = l - 1$, l being an integer ($l \geq 1$), then it can be proved to be true for $k = l$. Thus, $U_{mnpq}^{\kappa_1\kappa_2}(\mathrm{s})$ has the closed-form expression

$$U_{mnpq}^{\kappa_1\kappa_2}(\mathrm{s}) = \sum_{k=0}^{u} a_{k,n}^{(r)} \frac{k!}{s^{k+1}} \left(\sum_{v=0}^{k} \frac{\left(-\tau_{mnpq}^{\kappa_1\kappa_2}\right)^v}{s^{-v} v!} - e^{-s\tau_{mnpq}^{\kappa_1\kappa_2}} \right) \tag{5.2-16}$$

the above expression can be computed numerically for a given value of *s*.

2) $U_{mnpq}^{\kappa_1\kappa_2}(s)$ for Case#2 : $0 < \zeta_{mnpq}^{\kappa_1\kappa_2} \leq r$

This case is represented by the yellow interval shown in Fig. 5.2-2, where the value of $-\tau_{mnpq}^{\kappa_1\kappa_2}$ is located. $U_{mnpq}^{\kappa_1\kappa_2}(\mathrm{s})$ can then be derived from

$$U_{mnpq}^{\kappa_1\kappa_2}(\mathrm{s}) = e^{-s\,\tau_{mnpq}^{\kappa_1\kappa_2}} \sum_{k=0}^{u} a_{k,n}^{\left(r-\zeta_{mnpq}^{\kappa_1\kappa_2}\right)} \int_{-\zeta_{mnpq}^{\kappa_1\kappa_2}}^{-\zeta_{mnpq}^{\kappa_1\kappa_2} h} \left(\hat{t} + \zeta_{mnpq}^{\kappa_1\kappa_2} h\right)^k e^{-s\hat{t}}\, d\hat{t}$$

$$+ e^{-s\,\zeta_{mnpq}^{\kappa_1\kappa_2}} \sum_{i=0}^{\zeta_{mnpq}^{\kappa_1\kappa_2}-1} \sum_{k=0}^{u} a_{k,n}^{(r-i)} \int_{-(i+1)h}^{-ih} \left(\hat{t} + ih\right)^k e^{-s\hat{t}}\, d\hat{t} \tag{5.2-17}$$

following steps similar to that in Case#1, the closed-form expression for $U_{mnpq}^{\kappa_1\kappa_2}(\mathrm{s})$ in this Case#2 can be found to be

$$U_{mnpq}^{\kappa_1\kappa_2}(\mathrm{s}) = \sum_{k=0}^{u} a_{k,n}^{\left(r-\zeta_{mnpq}^{\kappa_1\kappa_2}\right)} \frac{k!}{s^{(k+1)}} \left(\sum_{v=0}^{k} \frac{\left(-\left(\tau_{mnpq}^{\pm} - \zeta_{mnpq}^{\kappa_1\kappa_2} h\right)\right)^v}{s^{-v} v!} - e^{-s\left(\tau_{mnpq}^{\kappa_1\kappa_2} - \zeta_{mnpq}^{\kappa_1\kappa_2} h\right)} \right)$$

$$+ \sum_{i=0}^{\zeta_{mnpq}^{\kappa_1\kappa_2}-1} \sum_{k=0}^{u} a_{k,n}^{(r-i)} \frac{k!}{s^{k+1}} \left(\sum_{v=0}^{k} \frac{(-h)^v}{s^{-v} v!} e^{-s\left(\tau_{mnpq}^{\kappa_1\kappa_2} - (i+1)h\right)} - e^{-s\left(\tau_{mnpq}^{\kappa_1\kappa_2} - ih\right)} \right) \tag{5.2-18}$$

3) $U_{mnpq}^{\kappa_1\kappa_2}(s)$ for Case#3 : $\zeta_{mnpq}^{\kappa_1\kappa_2} > r$

This case has $\tau_{mnpq}^{\kappa_1\kappa_2} > rh$ and, as a result, the integral appearing in $U_{mnpq}^{\kappa_1\kappa_2}(\mathrm{s})$ includes time $t < 0$. Given that we are considering only causal currents, the integrand will be identically zero between $t = -\tau_{mnpq}^{\kappa_1\kappa_2}$ and $t = 0$, or equivalently between $\hat{t} = -\tau_{mnpq}^{\kappa_1\kappa_2} - rh$ and $\hat{t} = -rh$. Therefore,

$$U_{mnpq}^{\kappa_1\kappa_2}(\mathrm{s}) = e^{-s\,\tau_{mnpq}^{\kappa_1\kappa_2}} \int_{-\tau_{mnpq}^{\kappa_1\kappa_2}}^{0} i_n\left(\hat{t} + rh\right) e^{-s\hat{t}}\, d\hat{t} = e^{-s\,\tau_{mnpq}^{\kappa_1\kappa_2}} \int_{-rh}^{0} i_n\left(\hat{t} + rh\right) e^{-s\hat{t}}\, d\hat{t} \tag{5.2-19}$$

using the piecewise-polynomial representation of $i_n(\hat{t} + rh)$ in the interval $-rh \le \hat{t} \le 0$, and proceeding in a manner similar to what was done in the previous two cases, the above integral can be found in closed-form as

$$U_{mnpq}^{\kappa_1\kappa_2}(\mathrm{s}) = \sum_{i=0}^{r-1} \sum_{k=0}^{u} a_{k,n}^{(r-i)} \frac{k!}{s^{k+1}} \left(\sum_{v=0}^{k} \frac{(-h)^v}{s^{-v} v!} e^{-s\left(\tau_{mnpq}^{\kappa_1\kappa_2} - (i+1)h\right)} - e^{-s\left(\tau_{mnpq}^{\kappa_1\kappa_2} - ih\right)} \right) \tag{5.2-20}$$

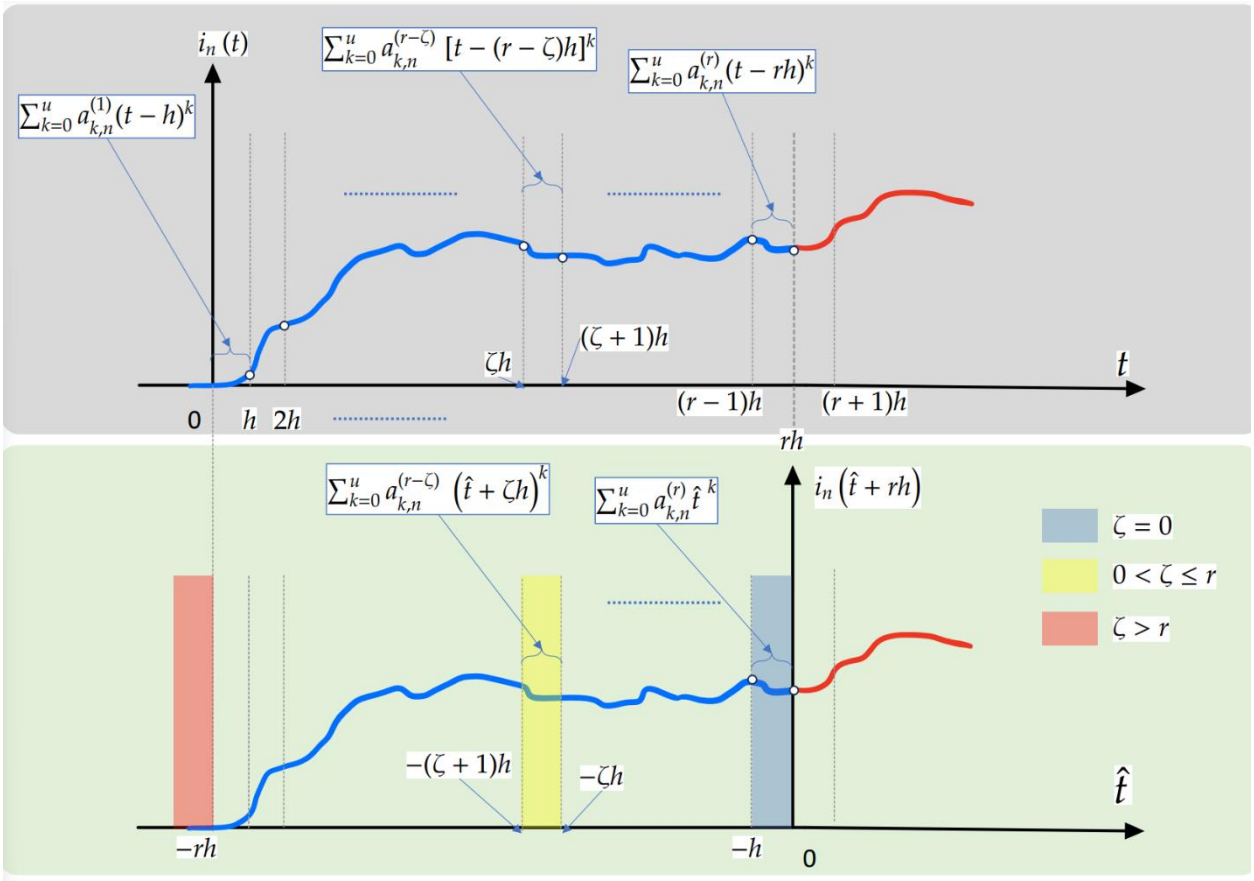

Fig. 5.2-2: A sketch used to illustrate the possiblities involved in the derivation of the antecedent term $U_{mnpq}^{\kappa_1\kappa_2}(s)$. The upper graph assumes an arbitrary temporal waveform $i_n(t)$, with the lower graph mapping it to the shifted domain $\hat{t}$. The circles on the blue part of the graph identify points that have been computed from past applications of NILT, while the red part refers to future points that are yet to be computed.

We can together write all three cases as

$$U_{mnpq}^{\kappa_1\kappa_2}(\mathrm{s}) = \begin{cases} \sum_{k=0}^{u} a_{k,n}^{\left(r-\zeta_{mnpq}^{\kappa_1\kappa_2}\right)} \dfrac{k!}{s^{(k+1)}} \left(\sum_{v=0}^{k} \dfrac{\left(-\tau_{mnpq}^{\kappa_1\kappa_2}\right)^{v}}{s^{-v}v!} - e^{-\left(s\,\tau_{mnpq}^{\kappa_1\kappa_2}\right)} \right) & \zeta_{mnpq}^{\kappa_1\kappa_2} = 0 \\ \dfrac{\sum_{k=0}^{u} a_{k,n}^{\left(r-\zeta_{mnpq}^{\kappa_1\kappa_2}\right)} \dfrac{k!}{s^{(k+1)}} \left(\sum_{v=0}^{k} \dfrac{\left(-\left(\tau_{mnpq}^{\kappa_1\kappa_2} - \zeta_{mnpq}^{\kappa_1\kappa_2} h\right)\right)^{v}}{s^{-v}v!} - e^{-s\left(\tau_{mnpq}^{\kappa_1\kappa_2} - \zeta_{mnpq}^{\kappa_1\kappa_2} h\right)} \right)}{+\sum_{i=0}^{\zeta_{mnpq}^{\kappa_1\kappa_2}-1} \sum_{k=0}^{u} a_{k,n}^{(r-i)} \dfrac{k!}{s^{k+1}} \left(\sum_{v=0}^{k} \dfrac{(-h)^{v}}{s^{-v}v!} e^{-s\left(\tau_{mnpq}^{\kappa_1\kappa_2} - (i+1)h\right)} - e^{-s\left(\tau_{mnpq}^{\kappa_1\kappa_2} - ih\right)} \right)} & 0 < \zeta_{mnpq}^{\kappa_1\kappa_2} \le r \\ \sum_{i=0}^{r-1} \sum_{k=0}^{u} a_{k,n}^{(r-i)} \dfrac{k!}{s^{k+1}} \left(\sum_{v=0}^{k} \dfrac{(-h)^{v}}{s^{-v}v!} e^{-s\left(\tau_{mnpq}^{\kappa_1\kappa_2} - (i+1)h\right)} - e^{-s\left(\tau_{mnpq}^{\kappa_1\kappa_2} - ih\right)} \right) & \zeta_{mnpq}^{\kappa_1\kappa_2} > r \end{cases}$$

(5.2-21)

Since the first and second order derivatives of (5.2-21) with respect to s will be needed in Section 5.3, we will write them down below. However, since the derivation of the derivatives are not difficult, but tedious, we will simply write down the final expressions[42] :

[42] We ask the reader to zoom in on the electronic copy of the document to clearly see the details.

$$\frac{dU_{mnpq}^{\kappa_1\kappa_2}(s)}{ds} = \begin{cases} \displaystyle\sum_{k=0}^{u} a_{k,n}^{\left(r-\zeta_{mnpq}^{\kappa_1\kappa_2}\right)} \frac{k!}{s^{(k+1)}} \left(\sum_{v=0}^{k} \frac{-(k+1-v)\left(-\tau_{mnpq}^{\kappa_1\kappa_2}\right)^{v}}{s^{(-v+1)}v!} + \left(\frac{k+1}{s} + \tau_{mnpq}^{\kappa_1\kappa_2}\right) e^{-\left(s\,\tau_{mnpq}^{\kappa_1\kappa_2}\right)} \right) & \zeta_{mnpq}^{\kappa_1\kappa_2} = 0 \\ \displaystyle\sum_{k=0}^{u} a_{k,n}^{\left(r-\zeta_{mnpq}^{\kappa_1\kappa_2}\right)} \frac{k!}{s^{(k+1)}} \left(\sum_{v=0}^{k} \frac{-(k+1-v)\left(-\left(\tau_{mnpq}^{\kappa_1\kappa_2} - \zeta_{mnpq}^{\kappa_1\kappa_2} h\right)\right)^{v}}{s^{(-v+1)}v!} + \left(\frac{k+1}{s} + \left(\tau_{mnpq}^{\kappa_1\kappa_2} - \zeta_{mnpq}^{\kappa_1\kappa_2} h\right)\right) e^{-s\left(\tau_{mnpq}^{\kappa_1\kappa_2} - \zeta_{mnpq}^{\kappa_1\kappa_2} h\right)} \right) \\ \quad + \displaystyle\sum_{i=0}^{\zeta_{mnpq}^{\kappa_1\kappa_2}-1} \sum_{k=0}^{u} a_{k,n}^{(r-i)} \frac{k!}{s^{k+1}} \left(\sum_{v=0}^{k} \left\{ \left(\frac{-(k+1-v)}{s} - \left(\tau_{mnpq}^{\kappa_1\kappa_2} - (i+1)h\right) \right) \frac{(-h)^{v}}{s^{-v}v!} e^{-s\left(\tau_{mnpq}^{\kappa_1\kappa_2} - (i+1)h\right)} \right\} \right. & 0 < \zeta_{mnpq}^{\kappa_1\kappa_2} \le r \\ \quad \left. + \left(\frac{k+1}{s} + \left(\tau_{mnpq}^{\kappa_1\kappa_2} - ih\right)\right) e^{-s\left(\tau_{mnpq}^{\kappa_1\kappa_2} - ih\right)} \right) & \\ \displaystyle\sum_{i=0}^{r-1} \sum_{k=0}^{u} a_{k,n}^{(r-i)} \frac{k!}{s^{k+1}} \left(\sum_{v=0}^{k} \left\{ \left(\frac{-(k+1-v)}{s} - \left(\tau_{mnpq}^{\kappa_1\kappa_2} - (i+1)h\right) \right) \frac{(-h)^{v}}{s^{-v}v!} e^{-s\left(\tau_{mnpq}^{\kappa_1\kappa_2} - (i+1)h\right)} \right\} - \left(\frac{k+1}{s} + \left(\tau_{mnpq}^{\kappa_1\kappa_2} - ih\right)\right) e^{-s\left(\tau_{mnpq}^{\kappa_1\kappa_2} - ih\right)} \right) & \zeta_{mnpq}^{\kappa_1\kappa_2} > r \end{cases}$$

(5.2-22)

$$\frac{d^2U^{\kappa_1\kappa_2}_{mnpq}(s)}{ds^2} = \begin{cases} \displaystyle\sum_{k=0}^{u} a_{k,n}^{\left(r-\zeta^{\kappa_1\kappa_2}_{mnpq}\right)} \frac{k!}{s^{(k+1)}} \left(\sum_{v=0}^{k} \frac{(k+1-v)(k+2-v)\left(-\tau^{\kappa_1\kappa_2}_{mnpq}\right)^v}{s^{(-v+2)}v!} - \left(\frac{(k+1)(k+2)}{s^2} + \frac{2\tau^{\kappa_1\kappa_2}_{mnpq}(k+1)}{s} + \left(\tau^{\kappa_1\kappa_2}_{mnpq}\right)^2 \right) e^{-\left(s\,\tau^{\kappa_1\kappa_2}_{mnpq}\right)} \right) & \zeta^{\kappa_1\kappa_2}_{mnpq} = 0 \\ \displaystyle\sum_{k=0}^{u} a_{k,n}^{\left(r-\zeta^{\kappa_1\kappa_2}_{mnpq}\right)} \frac{k!}{s^{(k+1)}} \left(\sum_{v=0}^{k} \frac{(k+1-v)(k+2-v)\left(-\left(\tau^{\kappa_1\kappa_2}_{mnpq} - \zeta^{\kappa_1\kappa_2}_{mnpq}h\right)\right)^v}{s^{(-v+2)}v!} - \left(\frac{(k+1)(k+2)}{s^2} + \frac{2\left(\tau^{\kappa_1\kappa_2}_{mnpq} - \zeta^{\kappa_1\kappa_2}_{mnpq}h\right)(k+1)}{s} + \left(\tau^{\kappa_1\kappa_2}_{mnpq} - \zeta^{\kappa_1\kappa_2}_{mnpq}h\right)^2 \right) e^{-s\left(\tau^{\kappa_1\kappa_2}_{mnpq} - \zeta^{\kappa_1\kappa_2}_{mnpq}h\right)} \right) \\ \quad + \displaystyle\sum_{i=0}^{\zeta^{\kappa_1\kappa_2}_{mnpq}-1} \sum_{k=0}^{u} a_{k,n}^{(r-i)} \frac{k!}{s^{k+1}} \left[\sum_{v=0}^{k} \left\{ \left(\frac{(k+2-v)(k+1-v)}{s^2} + \frac{2(k+1-v)\left(\tau^{\kappa_1\kappa_2}_{mnpq} - (i+1)h\right)}{s} + \left(\tau^{\kappa_1\kappa_2}_{mnpq} - (i+1)h\right)^2 \right) \frac{(-h)^v}{s^{-v}v!} e^{-s\left(\tau^{\kappa_1\kappa_2}_{mnpq} - (i+1)h\right)} \right\} \right. & 0 < \zeta^{\kappa_1\kappa_2}_{mnpq} \le r \\ \qquad \left. - \left(\frac{(k+1)(k+2)}{s^2} + \frac{(k+1)\left(\tau^{\kappa_1\kappa_2}_{mnpq} - ih\right)}{s} + \left(\tau^{\kappa_1\kappa_2}_{mnpq} - ih\right)^2 \right) e^{-s\left(\tau^{\kappa_1\kappa_2}_{mnpq} - ih\right)} \right] \\ \displaystyle\sum_{i=0}^{r-1} \sum_{k=0}^{u} a_{k,n}^{(r-i)} \frac{k!}{s^{k+1}} \left[\sum_{v=0}^{k} \left\{ \left(\frac{(k+2-v)(k+1-v)}{s^2} + \frac{2(k+1-v)\left(\tau^{\kappa_1\kappa_2}_{mnpq} - (i+1)h\right)}{s} + \left(\tau^{\kappa_1\kappa_2}_{mnpq} - (i+1)h\right)^2 \right) \frac{(-h)^v}{s^{-v}v!} e^{-s\left(\tau^{\kappa_1\kappa_2}_{mnpq} - (i+1)h\right)} \right\} \right. & \zeta^{\kappa_1\kappa_2}_{mnpq} > r \\ \qquad \left. - \left(\frac{(k+1)(k+2)}{s^2} + \frac{(k+1)\left(\tau^{\kappa_1\kappa_2}_{mnpq} - ih\right)}{s} + \left(\tau^{\kappa_1\kappa_2}_{mnpq} - ih\right)^2 \right) e^{-s\left(\tau^{\kappa_1\kappa_2}_{mnpq} - ih\right)} \right] \end{cases}$$

(5.2-23)[43]

[43] Note that the square brackets in this expression do not denote matrices.

5.2.5 Laplace Transform $\hat{\mathcal{L}}$ of the Second-Order Derivative Term

The treatment of the three cases in Section 5.2.4 indicated how a term such as $i_n(\hat{t} + rh - \tau_{mnpq}^{\kappa_1\kappa_2})$, namely the 2nd term on the left-hand side of (5.2-6), can have a Laplace-based representation that is amenable for use in the context of the re-initialized NILT. We now consider the representation of the Laplace transform of the second order derivative term on the left-hand side of (5.2-6). We use integration by parts twice to simply this term as

$$\begin{aligned}
&\hat{\mathcal{L}}\left\{\frac{\partial^2}{\partial\hat{t}^2} i_n\left(\hat{t} + rh - \tau_{mnpq}^{\kappa_1\kappa_2}\right)\right\} \\
&\quad = \int_0^\infty \frac{\partial^2}{\partial\hat{t}^2} i_n\left(\hat{t} + rh - \tau_{mnpq}^{\kappa_1\kappa_2}\right) e^{-s\hat{t}}\, d\hat{t} \\
&\quad\quad = -s\, i_n\left(rh - \tau_{mnpq}^{\kappa_1\kappa_2}\right) - \frac{\partial}{\partial\hat{t}} i_n\left(\hat{t} + rh - \tau_{mnpq}^{\kappa_1\kappa_2}\right)\Big|_{\hat{t}=0} \\
&\quad\quad\quad + s^2 \underbrace{\int_0^\infty i_n\left(\hat{t} + rh - \tau_{mnpq}^{\kappa_1\kappa_2}\right) e^{-s\hat{t}}\, d\hat{t}}_{e^{-s\tau_{mnpq}^{\kappa_1\kappa_2}}\hat{I}_n(s) + U_{mnpq}^{\kappa_1\kappa_2}(s)}
\end{aligned} \tag{5.2-24}$$

where (5.2-9) was substituted for the integral in the third term. The other two terms in (5.2-24) can also be obtained through the piecewise-polynomial interpolatory representation. More specifically, computing $\zeta_{mnpq}^{\kappa_1\kappa_2}$ from (5.2-11), those terms are obtained from

$$i_n(rh - \tau_{mnpq}^{\kappa_1\kappa_2}) = \sum_{k=0}^{u} a_{k,n}^{(r-\zeta_{mnpq}^{\kappa_1\kappa_2})} (\gamma_{mnpq}^{\kappa_1\kappa_2})^k \tag{5.2-25}$$

and

$$\frac{\partial}{\partial\hat{t}} i_n\left(\hat{t} + rh - \tau_{mnpq}^{\kappa_1\kappa_2}\right)\Big|_{\hat{t}=0} = \sum_{k=0}^{u} k\, a_{k,n}^{(r-\zeta_{mnpq}^{\kappa_1\kappa_2})} (\gamma_{mnpq}^{\kappa_1\kappa_2})^{k-1} \tag{5.2-26}$$

where

$$\gamma_{mnpq}^{\kappa_1\kappa_2} = -\tau_{mnpq}^{\kappa_1\kappa_2} - \zeta_{mnpq}^{\kappa_1\kappa_2} \tag{5.2-27}$$

5.2.6 Steps in the Implementation of the Re-Initialized Mode of the NILT Approach

The previous derivations can now be organized to describe the full implementation steps of the proposed re-initialized NILT method. Using (5-2.9), (5.21), and (5.24) and implementing them into (5.2-6) gives us the Laplace domain differentiated EFIE.

$$\frac{\mu}{4\pi}\sum_{n=1}^{N_s}\sum_{p=1}^{N_g}\sum_{q=1}^{N_g}\sum_{(\kappa_1,\kappa_2)} w_p w_q L_{mnpq}^{\kappa_1\kappa_2}\left\{-s i_n\left(rh-\tau_{mnpq}^{\kappa_1\kappa_2}\right)-\frac{\partial}{\partial\hat{t}} i_n\left(\hat{t}+rh-\tau_{mnpq}^{\kappa_1\kappa_2}\right)\Big|_{\hat{t}=0}+s^2\left(e^{-s\tau_{mnpq}^{\kappa_1\kappa_2}}\hat{I}_n(\mathrm{s})+U_{mnpq}^{\kappa_1\kappa_2}(\mathrm{s})\right)\right\}$$
$$+\frac{1}{4\pi\varepsilon}\sum_{n=1}^{N_s}\sum_{p=1}^{N_g}\sum_{q=1}^{N_g}\sum_{(\kappa_1,\kappa_2)} w_p w_q C_{mnpq}^{\kappa_1\kappa_2}\,\hat{\mathcal{L}}\left\{e^{-s\tau_{mnpq}^{\kappa_1\kappa_2}}\hat{I}_n(s)+U_{mnpq}^{\kappa_1\kappa_2}(s)\right\}$$
$$=\sum_{p=1}^{N_g} w_p\,\bar{j}_m\left(\bar{r}_{pm}^{\kappa_1}\right)\cdot\left\{(s)\hat{\bar{E}}(\bar{r}_{pm}^{\kappa_2},s)-\bar{\mathcal{E}}^{inc}\left(\bar{r}_{pm}^{\kappa_2},rh\right)\right\} \tag{5.2-28}$$

We can then re-write (5.2-28) to be in the form of our typical matrix equation $\left[Z(s)\right]\left[\hat{I}(s)\right]=\left[\Xi(s)\right]$, noting that the $[\Xi(s)]$a column vector. The elements Z_{mn} of $[Z(s)]$ are

$$Z_{mn}=\frac{\mu}{4\pi}\sum_{p=1}^{N_g}\sum_{q=1}^{N_g}\sum_{(\kappa_1,\kappa_2)} w_p w_q\, s^2 e^{-s\tau_{mnpq}^{\kappa_1\kappa_2}} L_{mnpq}^{\kappa_1\kappa_2}$$
$$+\frac{1}{4\pi\varepsilon_0}\sum_{p=1}^{N_g}\sum_{q=1}^{N_g}\sum_{(\kappa_1,\kappa_2)} w_p w_q e^{-s\tau_{mnpq}^{\kappa_1\kappa_2}} C_{mnpq}^{\kappa_1\kappa_2} \tag{5.2-29}$$

Noting that (5.2-29) is the same as the (4.2-8), when the right side is multiplied by s. The unknown is $\left[\hat{I}(s)\right]$, and the column vector $\left[\Xi(s)\right]$is the sum of three separate parts,

$$[\Xi(s)]=-[U(s)]+(s)[i]+[\dot{i}]+[V(s)] \tag{5.2-30}$$

the vectors on the right hand side of (5.2-30) are all complex vectors of size $N_s\times 1$, and are given as follows:

■ the antecedent terms

$$\left[U(s)\right] = \left[\sum_{n=1}^{N_s} \sum_{p=1}^{N_g} \sum_{q=1}^{N_g} \sum_{(\kappa_1,\kappa_2)} w_p w_q \left\{ (s)^2 L_{mnpq}^{\kappa_1\kappa_2} + C_{mnpq}^{\kappa_1\kappa_2} \right\} U_{mnpq}^{\kappa_1\kappa_2}(s) \right]_{m=1}^{N_s} \tag{5.2-31}$$

■ the delayed currents $[i]$ from the past time point

$$\left[i\right] = \left[\sum_{n=1}^{N_s} \sum_{p=1}^{N_g} \sum_{q=1}^{N_g} \sum_{(\kappa_1,\kappa_2)} w_p w_q L_{mnpq}^{\kappa_1\kappa_2} \sum_{k=0}^{u} a_{k,n}^{(r-\zeta_{mnpq}^{\kappa_1\kappa_2})} (\gamma_{mnpq}^{\kappa_1\kappa_2})^k \right]_{m=1}^{N_s} \tag{5.2-32}$$

■ the delayed current derivatives $[\dot{i}]$ from the past time point

$$\left[\dot{i}\right] = \left[\sum_{n=1}^{N_s} \sum_{p=1}^{N_g} \sum_{q=1}^{N_g} \sum_{(\kappa_1,\kappa_2)} w_p w_q L_{mnpq}^{\kappa_1\kappa_2} \sum_{k=0}^{u} a_{k,n}^{(r-\zeta_{mnpq}^{\kappa_1\kappa_2})} (\gamma_{mnpq}^{\kappa_1\kappa_2})^{k-1} \right]_{m=1}^{N_s} \tag{5.2-33}$$

■ and the excitation vector

$$[V(s)] = \sum_{p=1}^{N_g} w_p \, \bar{j}_m\left(\bar{r}_{pm}^{\kappa_1}\right) \cdot \left\{ s\,\hat{\bar{E}}(\bar{r}_{pm}^{\kappa_1}, s) - \bar{\mathcal{E}}^{inc}\left(\bar{r}_{pm}^{\kappa_1}, rh\right) \right\} \tag{5.2-34}$$

here, $\hat{\bar{E}}(\bar{r}_{pm}^{\kappa_1}, s)$ is the Laplace transform of the time-shifted incident field

$$\hat{\bar{E}}(\bar{r}_{pm}^{\kappa_1}, s) = \hat{\mathcal{L}}\left\{ \bar{\mathcal{E}}^{inc}\left(\bar{r}_{pm}^{\kappa_1}, \hat{t} + rh\right) \right\} \tag{5.2-35}$$

5.3 INCORPORTION OF REINITIALIZED NILT*n* APPROACH WITH THE MOMENT METHOD SOLUTION OF THE s-DOMAIN EFIE

Although the steps required for the implementation of re-initialized NILT*n* are somewhat similar to the initial-value NILT*n* approach, there are important details that require some attention. For instance, the derivatives with respect to s, of the matrix equation $\left[Z\left(s_i\right)\right]\left[\hat{I}\left(s_i\right)\right]=\left[\Xi(s_i)\right]$, are slightly different from what applies in the initial-value NILT*n* case. This is not only so because we are now using the re-initialized NILT*n*, but also because we are now using the differentiated TD-EFIE as the basis.

5.3.1 Implementation of NILT0

Similar to the initial-value mode NILT0, described in Section 3.5.1 and Section 4.3.2, there are no major changes required for the implementation re-initialized NILT0. The expression for re-initialized NILT0 is derived from the initial NILT0 shown in (2.7-13), with some minor changes. Mainly the t on the left side of the (2.7-13), is substituted with $t=(r+1)h$, and the t on the right side of (2.7-13), is substituted with $t=h$.

$$[i((r+1)h]=-\frac{2}{h}\sum_{i=1}^{M/2}\mathcal{R}e\left\{k_i\ [\hat{I}\left(s_i\right)]\right\}\Big|_{s_i=z_i/h} \tag{5.3-1}$$

where

$$[\hat{I}\left(s_i\right)]=\left[Z\left(s_i\right)\right]^{-1}\left[\Xi(s_i)\right] \tag{5.3-2}$$

At $t=h$, the first step, $[i(h)]$ is obtained from (5.3-1), noting that $r=0$. Proceeding to compute the current at the next temporal sample point, $t=2h$, we set $r=1$, and then compute $[i\left((r+1)h\right)]$ using, again, (5.3-1). Note that matrix equation $\left[Z\left(s_i\right)\right]\left[\hat{I}\left(s_i\right)\right]=\left[\Xi(s_i)\right]$ is solved to determine the solution vector $\left[\hat{I}(s_i)\right]$ for each of the complex frequency values s_i, $i=1,2,...,M/2$. We select the time-step h so that the NILT0 result there is known to be

accurate[44]. When we march-on-steps to values of time $t=(r+1)h$, $r=0,1,2,3,.....$ the set of complex frequency values s_i, $i=1,2,...,M/2$ at which solution vectors $[I(s_i)]$ are required do not change. Thus, the interaction matrices $[Z(s_i)]$ need not be re-computed. However, the terms in the column vector $[\Xi(z_i/h)]$ do change, as is evident from (5.2-30), and hence at each time-step, the matrix equation $[Z(s_i)][I(s_i)]=[V(s_i)]$ must be solved for $[I(s_i)]$ for $i=1,2,...,M/2$. This is one case where explicit computation and storage of the $[Z(s_i)]^{-1}$ might be computationally worthwhile.

However, since the expressions for $\left[Z(s_i)\right]$ and $\left[\Xi(s_i)\right]$ are described in (2.5-29) and (5.2-30), no further explanations are required.

5.3.2 Implementation of NILT1

The expression for re-initialized NILT1 is derived from the initial NILT1 shown in (2.7-14), with some minor changes. Mainly the t on the left side of the (2.7-14), is substituted with $t=(r+1)h$, and the t on the right side of (2.7-14), is substituted with $t=h$. Applying these modifications results in the expression used for re-initialized NILT1

$$\left[i\left((r+1)h\right)\right]=-\frac{8}{h}\sum_{i=1}^{M/2}\left\{\Re e\left[\frac{k_i^2}{h}\frac{d\left[\hat{I}(s_i)\right]}{ds}+k_i^2\left[\hat{I}(s_i)\right]\sum_{\substack{j=1\\ j\neq i}}^{M}\frac{k_j}{z_i-z_j}\right]\right\}_{s_i=\frac{2z_i}{h}} \qquad (5.3\text{-}3)$$

As was stated in Section 3.5.2 and Section 4.3.3, in addition to the solution vector $\left[\hat{I}(s_i)\right]$, the derivative vector $d\left[\hat{I}(s_i)\right]/ds$ is also required.

[44] See comments in Appendix IV

$d\left[\hat{I}(s_i)\right]/ds$ can be found simply by differentiating both sides of the matrix equation $\left[Z(s_i)\right]\left[\hat{I}(s_i)\right]=\left[\Xi(s_i)\right]$ by s. However, since a similar operation was done in Section 3.5.2, we shall simply state the solution to this operation

$$[Z(s)]\frac{d}{ds}\{[I(s)]\}=\frac{d}{ds}\{[\Xi(s)]\}-[I(s)]\frac{d}{ds}\{[Z(s)]\} \tag{5.3-3}$$

There are two new expressions to be found in (5.3-3). Firstly $\frac{d}{ds}\{[Z(s)]\}$ is unknown. However, the elements of this equation can be found by differentiating both sides of (5.2-29)

$$\frac{dZ_{mnpq}(s)}{ds}=\sum_{n=1}^{N_s}\sum_{p}\sum_{q}\left\{-w_p w_q \tau_{mnpq}^{\kappa_1\kappa_2} e^{-s\tau_{mnpq}^{\kappa_1\kappa_2}}\left(\frac{\mu}{4\pi}s^2 L_{mnpq}^{\kappa_1\kappa_2}+\frac{1}{4\pi\varepsilon}C_{mnpq}^{\kappa_1\kappa_2}\right)\right.$$
$$\left.+w_p w_q e^{-s\tau_{mnpq}^{\kappa_1\kappa_2}}\left(\frac{2\mu}{4\pi}sL_{mnpq}^{\kappa_1\kappa_2}\right)\right\} \tag{5.3-4}$$

Secondly, $\frac{d}{ds}\{[\Xi(s)]\}$ is not known, thus again, we can differentiate both sides of (5.2-30) to get

$$\frac{d}{ds}\{[\Xi(s)]\}=-\frac{d[U(s)]}{ds}+\frac{d[i]}{ds}+[i]+\frac{d[\dot{i}]}{ds}+\frac{d[V(s)]}{ds} \tag{5.3-5}$$

However, the delayed currents $[i]$ and the delayed current derivatives $[\dot{i}]$ have no dependence on s, hence (5.3-5) simplifies to

$$\frac{d}{ds}\{[\Xi(s)]\}=-\frac{d[U(s)]}{ds}+[i]+\frac{d[V(s)]}{ds} \tag{5.3-6}$$

■ The first order derivative with respect to *s* for the antecedent terms is

$$\frac{d\left[U(s)\right]}{ds}=\left[\sum_{n=1}^{N_s}\sum_{p=1}^{N_g}\sum_{q=1}^{N_g}\sum_{(\kappa_1,\kappa_2)}w_p w_q\left(\left\{(2s)L_{mnpq}^{\kappa_1\kappa_2}\right\}U_{mnpq}^{\kappa_1\kappa_2}(s)+\left\{(s)^2 L_{mnpq}^{\kappa_1\kappa_2}+C_{mnpq}^{\kappa_1\kappa_2}\right\}\frac{dU_{mnpq}^{\kappa_1\kappa_2}(s)}{ds}\right)\right]_{m=1}^{N_s} \tag{5.3-7}$$

where $dU_{mnpq}^{\kappa_1\kappa_2}(s)/ds$ is shown in (5.2-22).

■ The first order derivative with respect to *s* for the excitation vector is

$$\frac{d[V(s)]}{ds}=\sum_{p=1}^{N_g}w_p\,\bar{j}_m\left(\bar{r}_{pm}^{\kappa_1}\right)\cdot\left\{\hat{\bar{E}}^{inc}(\bar{r}_{pm}^{\kappa_1},s)+s\,\frac{d\hat{\bar{E}}^{inc}(\bar{r}_{pm}^{\kappa_1},s)}{ds}\right\} \tag{5.3-8}$$

5.3.3 Implementation of NILT2

The expression for re-initialized NILT2 is derived from the initial NILT2 shown in (2.7-15), with some minor changes. Mainly the t on the left side of the (2.7-15), is substituted with $t=(r+1)h$, and the t on the right side of (2.7-15), is substituted with $t=h$. Applying these modifications results in the expression used for re-initialized NILT2

$$\left[\left[i\left((r+1)h\right)\right]\right]\approx-\frac{9}{h}\sum_{i=1}^{M/2}\left\{\frac{3\tilde{k}_i^3}{8h^2}\frac{d^2\left[I(s_i)\right]}{ds^2}+\frac{3\tilde{k}_i^2}{2h}\frac{d\left[I(s_i)\right]}{ds}\sum_{\substack{j=1\\ j\neq i}}^{M}\frac{k_j}{z_i-z_j}\right.$$
$$\left.+\left[I(s_i)\right]\left(\tilde{k}_i\sum_{\substack{j=1\\ j\neq i}}^{M}\sum_{\substack{v=1\\ v\neq 1}}^{M}\frac{k_j k_v}{(z_i-z_j)(z_i-z_v)}-\frac{\tilde{k}_i^2}{2}\sum_{\substack{j=1\\ j\neq i}}^{M}\frac{k_j}{(z_i-z_j)^2}\right)\right\}_{s_i=\frac{3z_i}{t},\,\tilde{k}_i=2k_i} \tag{5.3-9}$$

In addition to solution vector $[I(s)]$, and derivative vector $d\{[I(s)]\}/ds$, we require second derivative vector $d^2\{[I(s)]\}/ds^2$. To enable us to do this, we take the second-order derivative of $\left[Z(s_i)\right]\left[\hat{I}(s_i)\right]=\left[\Xi(s_i)\right]$ by s. However, since a similar operation was done in Section 3.5.3, we shall simply state the solution to this operation

$$[Z(\mathrm{s})]\frac{d^2[\hat{I}(\mathrm{s})]}{ds^2} = \frac{d^2[V(\mathrm{s})]}{ds^2} - 2\frac{d[Z(\mathrm{s})]}{ds}\frac{d[\hat{I}(\mathrm{s})]}{ds} - \frac{d^2[Z(\mathrm{s})]}{ds^2}[\hat{I}(\mathrm{s})] \tag{5.3-10}$$

There are two new expressions to be found in (5.3-10). Firstly $\frac{d^2}{ds^2}\{[Z(s)]\}$ is unknown. However, the elements of this equation can be found by differentiating both sides of (5.3-4) to obtain

$$\frac{d^2 Z_{mnpq}(s)}{ds^2} = \sum_{n=1}^{N_s}\sum_{p}\sum_{q}\left\{ w_p w_q \left(\tau_{mnpq}^{\kappa_1\kappa_2}\right)^2 e^{-s\tau_{mnpq}^{\kappa_1\kappa_2}}\left(\frac{\mu}{4\pi}s^2 L_{mnpq}^{\kappa_1\kappa_2} + \frac{1}{4\pi\varepsilon}C_{mnpq}^{\kappa_1\kappa_2}\right)\right.$$
$$\left. - 2w_p w_q \tau_{mnpq}^{\kappa_1\kappa_2} e^{-s\tau_{mnpq}^{\kappa_1\kappa_2}}\left(\frac{2\mu}{4\pi}sL_{mnpq}^{\kappa_1\kappa_2}\right) + w_p w_q e^{-s\tau_{mnpq}^{\kappa_1\kappa_2}}\left(\frac{2\mu}{4\pi}L_{mnpq}^{\kappa_1\kappa_2}\right)\right\} \tag{5.3-11}$$

Secondly, $\frac{d}{ds}\{[\Xi(s)]\}$ is not known, however again, we can differentiate both sides of (5.3-6) to get

$$\frac{d}{ds}\{[\Xi(s)]\} = -\frac{d^2[U(s)]}{ds^2} + \frac{d^2[V(s)]}{ds^2} \tag{5.3-12}$$

■ The second order derivative with respect to *s* for the antecedent terms is

$$\frac{d^2[U(s)]}{ds^2} = \left[\sum_{n=1}^{N_s}\sum_{p=1}^{N_g}\sum_{q=1}^{N_g}\sum_{(\kappa_1,\kappa_2)} w_p w_q \left(\{(2)L_{mnpq}^{\kappa_1\kappa_2}\}U_{mnpq}^{\kappa_1\kappa_2}(s) + \{(4s)L_{mnpq}^{\kappa_1\kappa_2}\}\frac{dU_{mnpq}^{\kappa_1\kappa_2}(s)}{ds}\right.\right.$$
$$\left.\left. + \{(s)^2 L_{mnpq}^{\kappa_1\kappa_2} + C_{mnpq}^{\kappa_1\kappa_2}\}\frac{d^2U_{mnpq}^{\kappa_1\kappa_2}(s)}{ds^2}\right)\right]_{m=1}^{N_s} \tag{5.3-13}$$

with $d^2U_{mnpq}^{\kappa_1\kappa_2}(s)\big/ds^2$ shown in (5.2-23).

■ The second order derivative with respect to s for the excitation vector is

$$\frac{d^2[V(s)]}{ds^2} = \sum_{p=1}^{N_g} w_p \, \bar{j}_m\left(\bar{r}_{pm}^{\kappa_1}\right) \cdot \left\{ 2\frac{d\hat{\bar{E}}^{inc}(\bar{r}_{pm}^{\kappa_1}, s)}{ds} + s\frac{d^2\hat{\bar{E}}^{inc}(\bar{r}_{pm}^{\kappa_1}, s)}{ds^2} \right\} \tag{5.3-14}$$

5.4 VALIDATION EXAMPLES

5.4.1 Example Geometries

In order to validate the implementation of the re-initialized NILT0, NILT1, and NILT2 for the 3D TD-EFIE, computations are performed for the same three examples used as in Section 4.4. This validation was carried out by comparing the outcomes of a number of different simulations. Although the lengthy descriptive terms defined below (and used in all figure captions) may appear burdensome at first, we have found that this is the best way to ensure complete clarity. It is important that there is no ambiguity when comparing the different sets of results. We wish to demonstrate the significant (and theoretically expected) improvement in the obtained responses, namely the ability to accurately find time-domain responses out to much larger values of time, and the ease of densely interpolating these responses on the time axis (so as to allow accurate and fine Fourier transformation to the frequency-domain) using time-derivative information innately available from the NILT*n* process.

(1) As was done in Section 4.4, to have reference results against which to compare the time-domain (TD) results obtained via the re-initialized NILT*n* technique, we use the frequency-domain method of moments (FD-MoM) formulation, for the 3D PEC objects being analysed, at a set of frequencies, and then perform an inverse Fourier transform to obtain the time-domain currents at the antenna terminals. We again refer these as the "**IDFT results**".

(2) The time-domain currents at the antenna terminals, obtained utilizing the NILT*n* approaches used in the re-initialized mode developed in the present chapter will be referred to as the "**re-initialized NILT*n* results**". The coefficients of the interpolating polynomials $a_{k,n}^{(r)}$ of these re-initialized NILT*n* results, a by-product of the NILT process, are generated from the re-initialized NILT0, NILT1 and NILT2 simulations, and these are referred to as the "**interpolated re-initialized NILT*n* results**".

(3) In addition to the time-domain terminal currents we show frequency-domain results, namely the input impedance (strip and bowtie dipoles) and terminal current (patch antenna), obtained through a re-initialized NILT*n* route. The re-initialized NILT*n* results (which are time-domain ones) are Fourier transformed (DFT) to obtain the input impedance of the antennas; we call these

the "**FD/non-interpolated re-initialized NILT*n* results**". The densely-sampled interpolated re-initialized NILT*n* results are then also Fourier transformed to get the input impedance, and are called the "**FD/interpolated re-initialized NILT*n* results**".

(4) In order to have reference results against which to compare the frequency-domain results obtained via the re-initialized NILT*n* technique, we use the frequency-domain method of moments (FD-MoM) formulation directly for the same 3D PEC objects being analysed. We will refer to these as the "**FD-EFIE results**".

The time-domain terminals currents for the Gaussian pulse input, and the input impedance (a frequency-domain quantity) found from Fourier transformation of the time-domain results, will be shown below for each of the three geometries. However, these have shown that when the re-initialized NILTn approach is used, the NILT0, NILT1 and NILT2 results are largely the same. Thus only the NILT0 results will be shown for each of the geometries, with the NILT1 and NILT2 outcomes catalogued in Appendix VII for completeness. Even then, the results presented might be perceived as somewhat repetitive. In a sense this is purposefully so, as we wish to demonstrate that the substantial advantages afforded by the re-initialized form of NILT*n* does precisely what the theory promises, and the actual numerical results are not merely a fluke for a single specially-selected geometry.

5.4.2 Centre-Fed Strip Dipole Antenna

This is the same physical problem as that described in Section 4.4.2, with parameters the same as those provided in Table 4.4-1. The reference IDFT responses are also the same as those given in Section 4.4.2.

The re-initialized NILT0 results for the terminal current in the time-domain matches the reference IDFT ones very well, as is evident from Fig. 5.4-1.

Figs. 5.4-2 and 5.4-3 reveal that the non-interpolated re-initialized NILT0 results on their own do not produce an accurate picture of the input impedance of the strip dipole after Fourier (DFT) transformation, due to the lack of a sufficient number of time-domain points. However, after Fourier transformation, the interpolated re-initialized NILT0 results do match the FD-EFIE ones

very closely up to the highest frequency component of the Gaussian pulse. It would of course be possible to use a smaller step size h when applying the re-initialized NILT0 and not use interpolation, but this would require more MoM runs, and take away the advantage of re-initialized NILT*n* (the ability to take relative large time steps, while recreating the time-domain response)

As intimated above, the results for the same problem, using the re-initialized NILT1 and NILT2 approaches, are much the same as for the NILT0 case shown here. In other words, the re-initialized NILT0 approach is sufficient. One could envisage problem parameters for which the re-initialized NILT1 and NILT2 methods do provide more than the re-initialized NILT0 one.

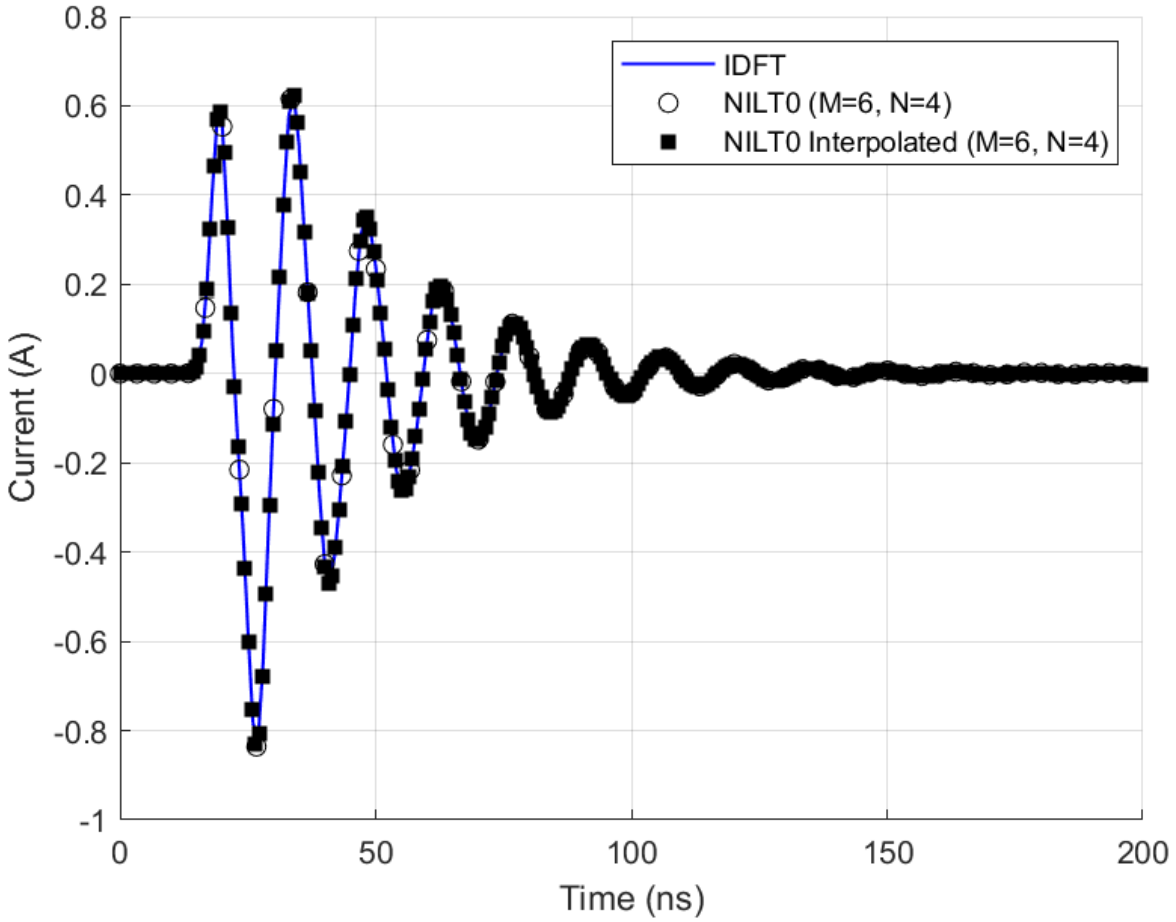

Fig. 5.4-1: The induced current at the feedpoint of the strip dipole antenna when excited by a Gaussian pulse at the feedpoint. The blue line represents the IDFT results. The black circles represent the re-initialized NILT0 results, and the black squares the interpolated re-initialized NILT0 results.

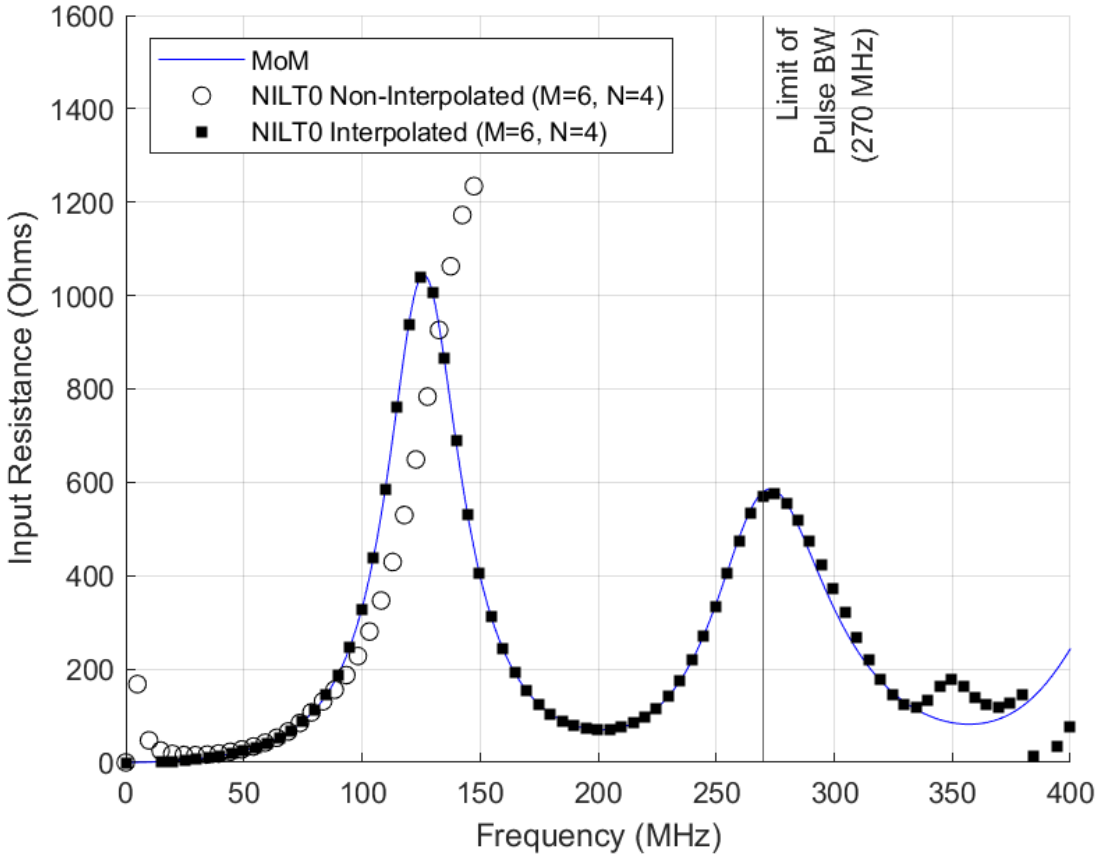

Fig. 5.4-2: The input resistance of the strip dipole. The blue line represents the FD-EFIE results. The black circles represent the FD/non-interpolated re-initialized NILT0 results. The black squares represent FD/interpolated re-initialized NILT0 results.

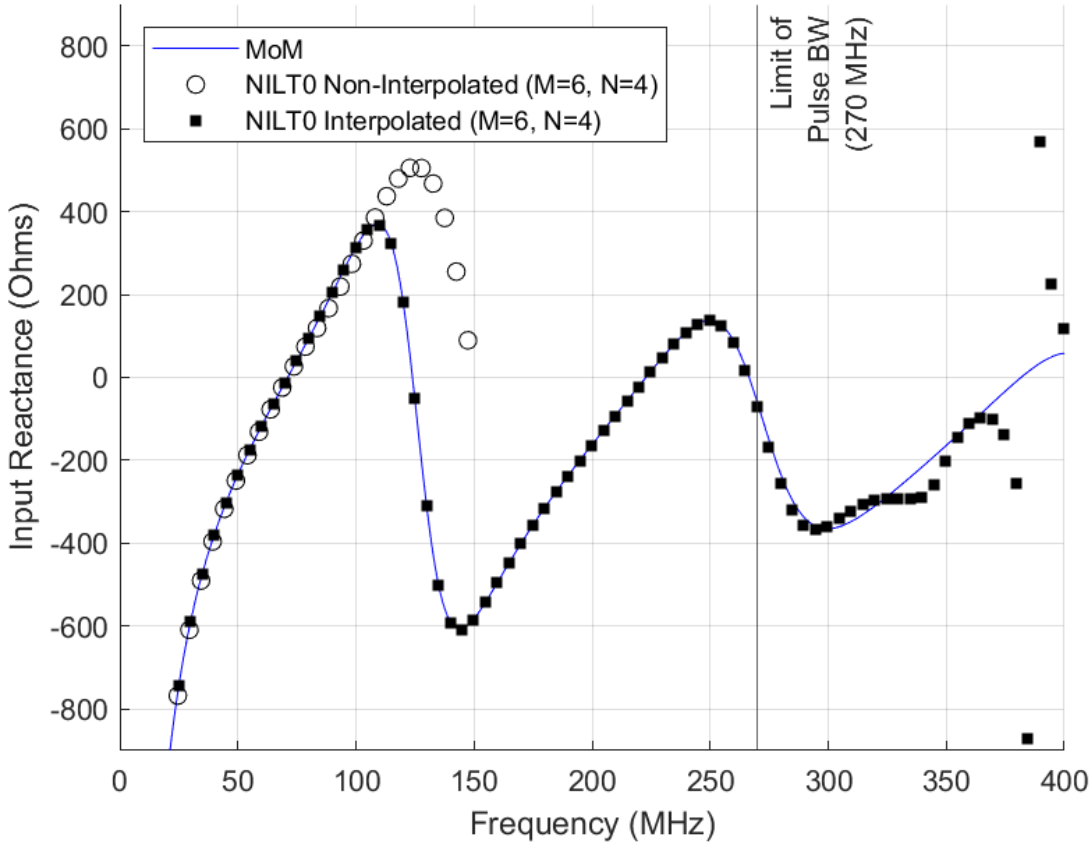

Fig. 5.4-3: The input reactance of the strip dipole. The blue line represents the FD-EFIE results. The black circles represent the FD/non-interpolated re-initialized NILT0 results. The black squares represent FD/interpolated re-initialized NILT0 results.

5.4.3 Centre-Fed Bowtie Dipole Antenna

This is the same physical problem as that described in Section 4.4.3, with parameters the same as that provided in Table 4.4-2. The reference IDFT-based responses are also the same as those given in Section 4.4.3. Comments made for the strip dipole in Section 5.4.2 apply word-for-word for this bowtie dipole case, except that it is Fig. 5.4-4 and Fig. 5.4-5 that should be referred to.

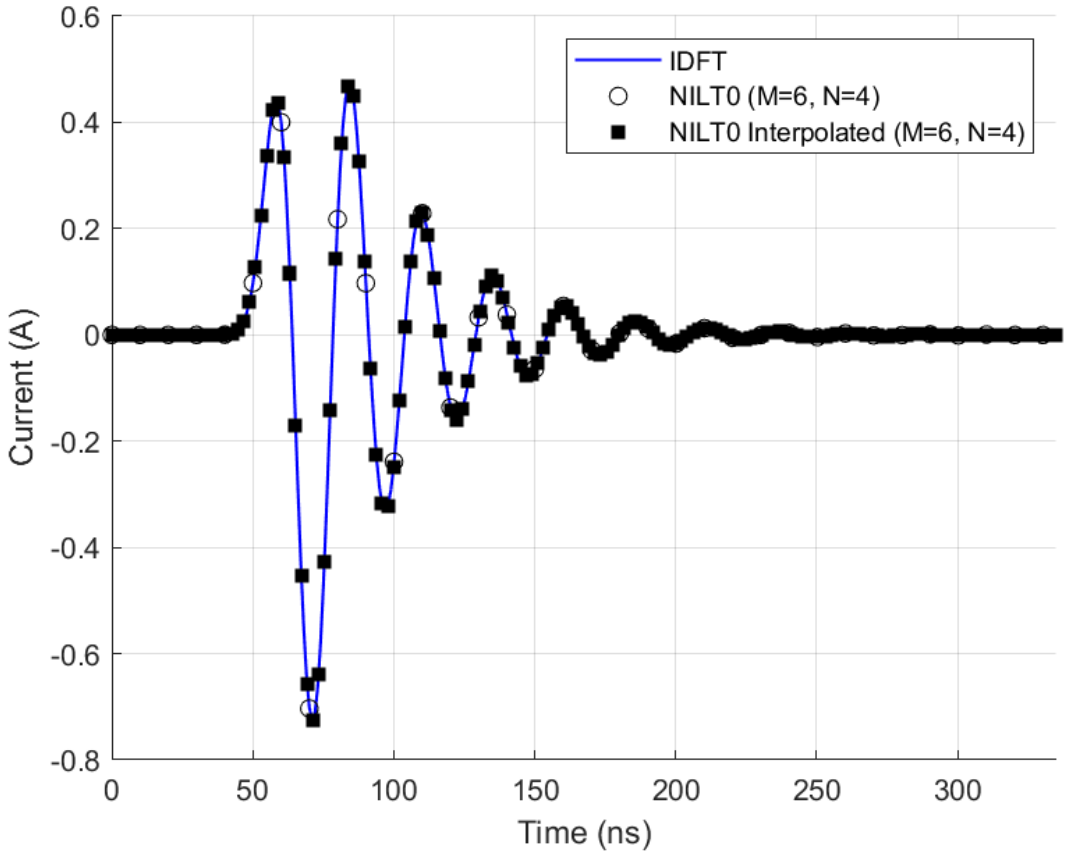

Fig. 5.4-4: The induced current at the feedpoint of the bowtie dipole antenna when excited by a Gaussian pulse at the feedpoint. The blue line represents the IDFT results. The black circles represent the re-initialized NILT0 results, and the black squares the interpolated re-initialized NILT0 results.

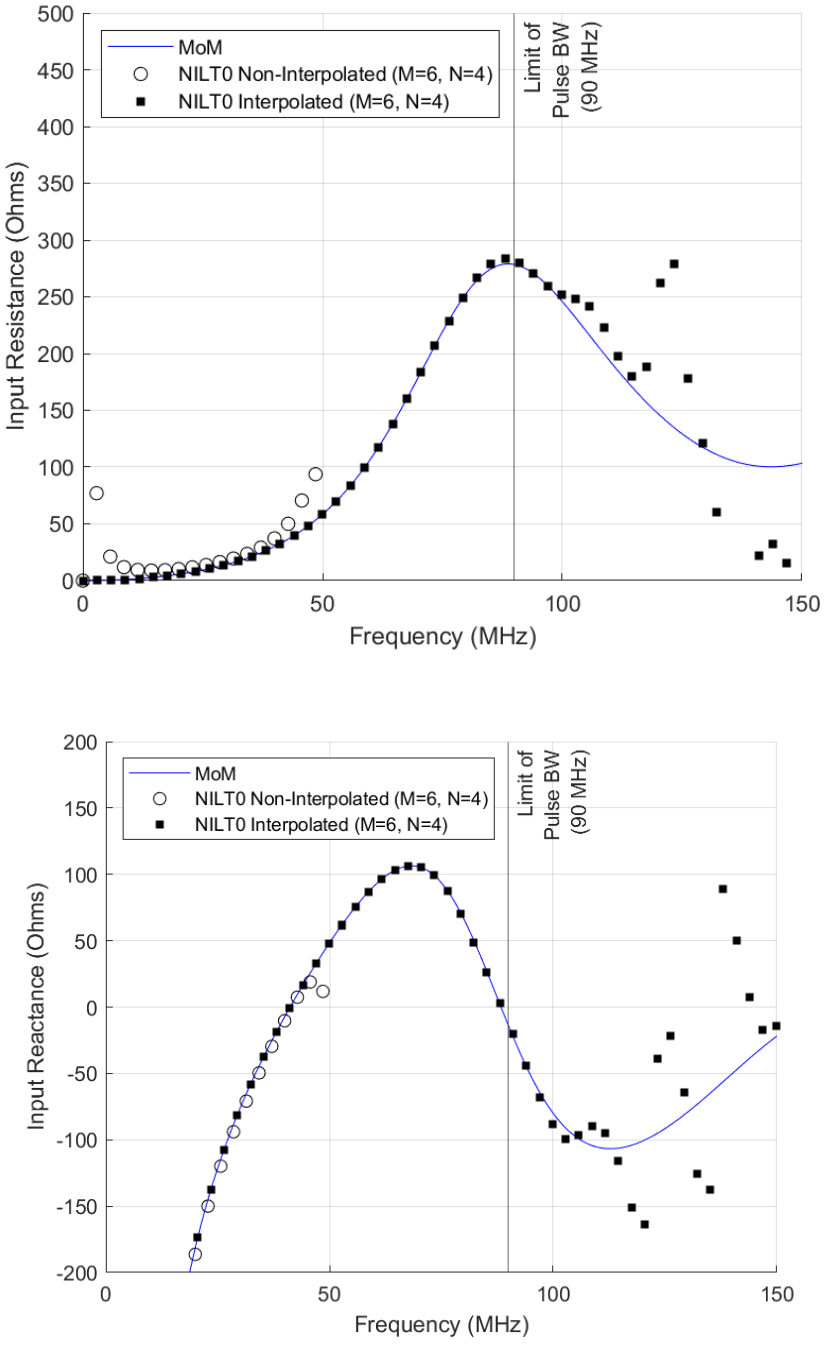

Fig. 5.4-5: The input resistance (top) and input reactance (bottom) of the bowtie dipole. The blue line represents the FD-EFIE results. The black circles represent the FD/non-interpolated re-initialized NILT0 results. The black squares represent FD/interpolated re-initialized NILT0 results.

5.4.4 Patch Antenna with Air Substrate

This is the same physical problem as that described in Section 4.4.4, with parameters the same as that provided in Table 4.4-3. The reference IDFT-based responses are also the same as those given in Section 4.4.4. Comments made for the strip dipole in Section 5.4.2 apply word-for-word for this patch antenna case, except that it is Fig. 5.4-6, Fig. 5.4-7 and Fig. 5.4-8 apply. Fig. 5.4-7 has been included to provide a clearer view of the details in the early-time region of Fig. 5.4-6.

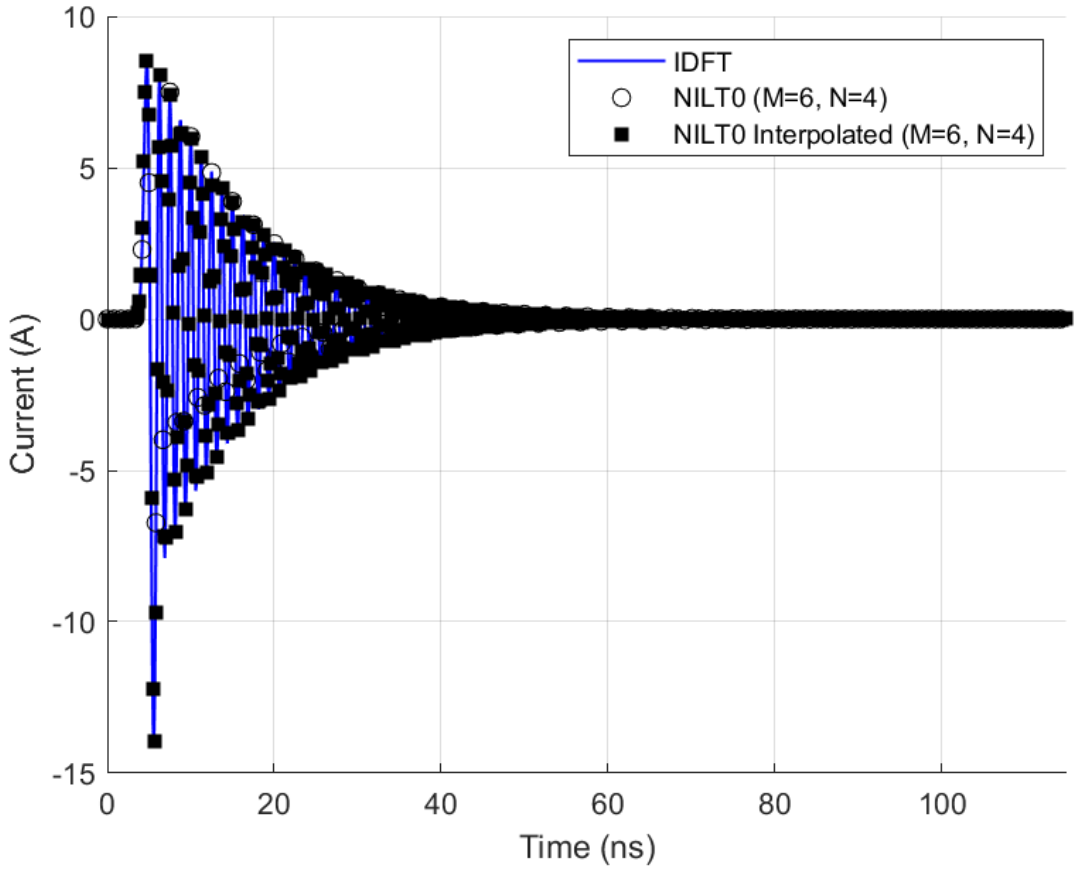

Fig. 5.4-6: The induced current at the feedpoint of the patch antenna when excited by a Gaussian pulse at the feedpoint. The blue line represents the IDFT results. The black circles represent the re-initialized NILT0 results, and the black squares the interpolated re-initialized NILT0 results.

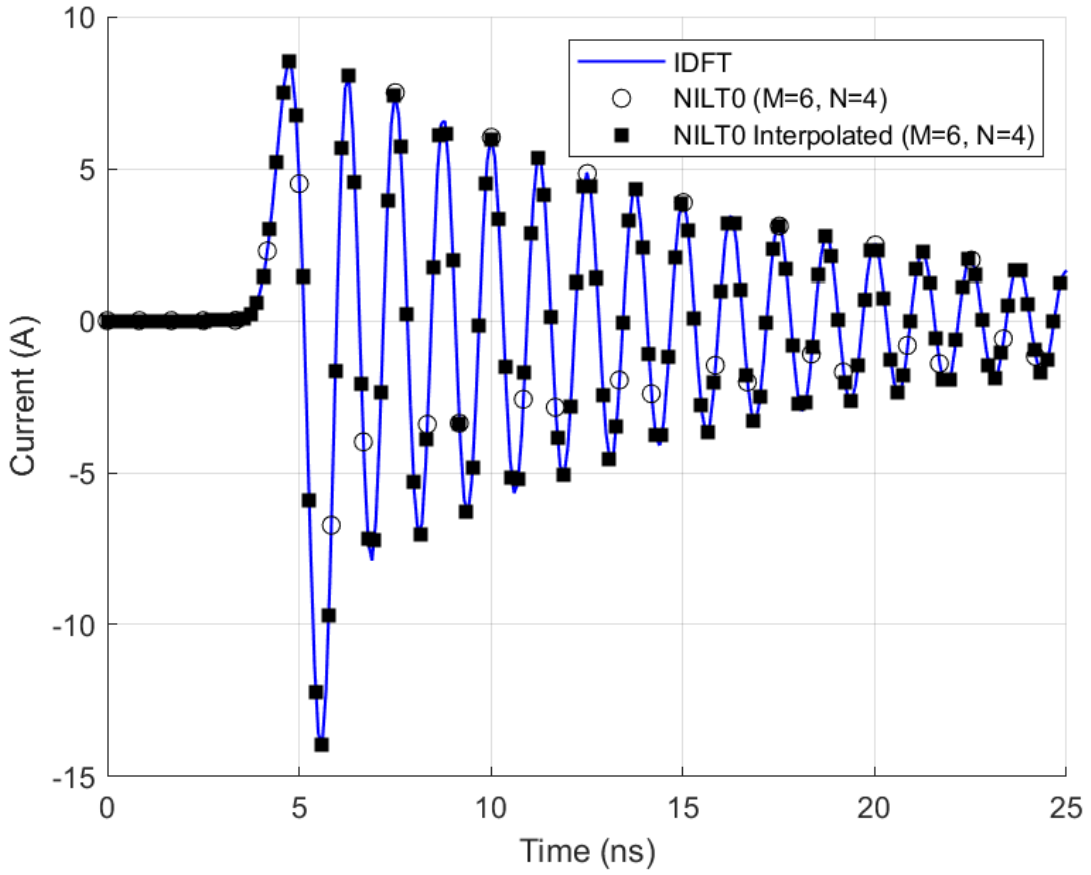

Fig. 5.4-7: The same results as in Fig. 5.4-6, but zoomed in to show the details in the timeframe 0 - 25 ns.

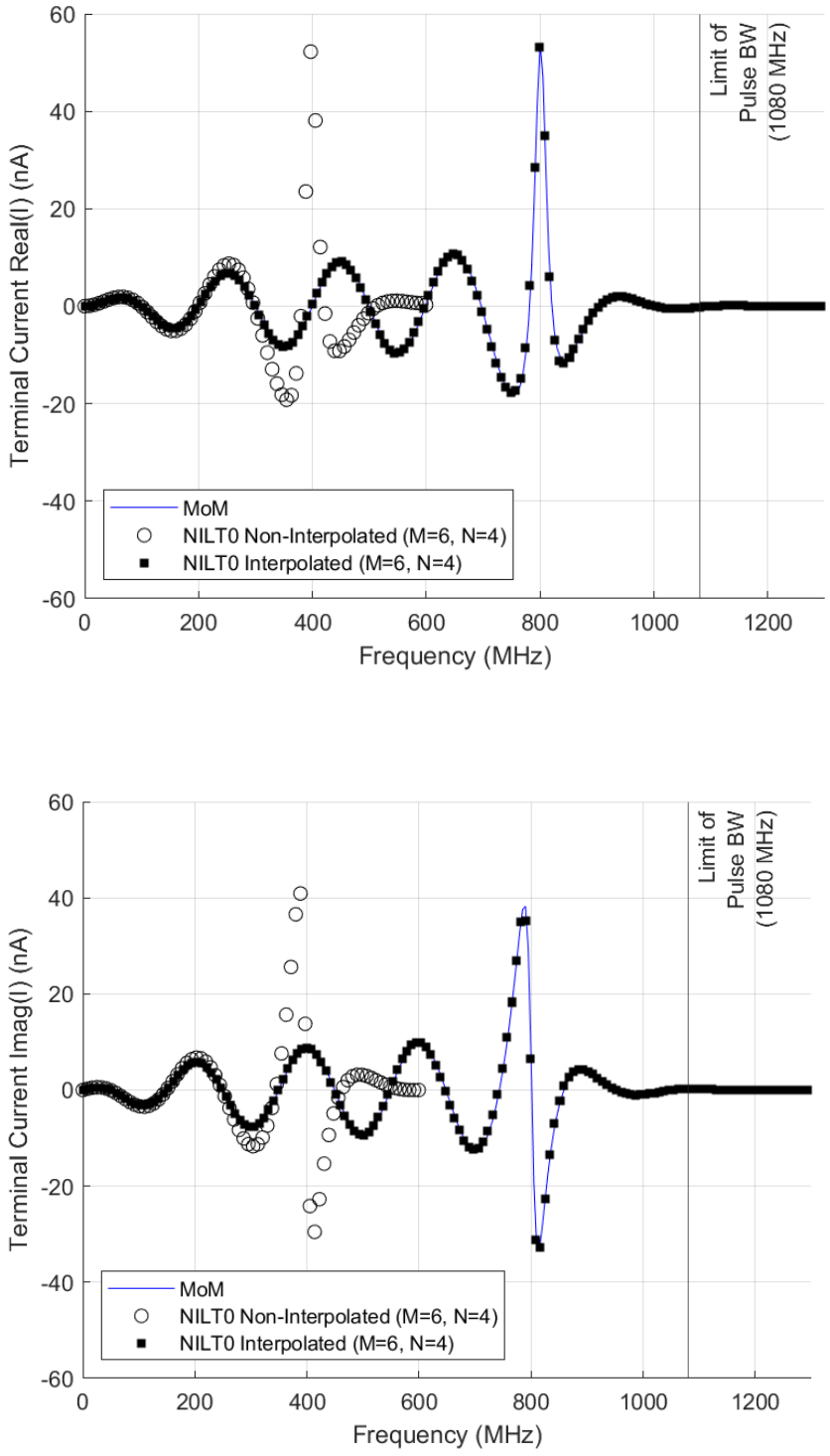

Fig. 5.4-8: The real part (top) and imaginary part (bottom) of the terminal current of the patch antenna. The blue line represents the FD-EFIE results. The black circles represent the FD/non-interpolated re-initialized NILT0 results. The black squares represent FD/interpolated re-initialized NILT0 results.

5.4.5 Remarks on the Complex Frequencies Required for Application of the Re-Initialized NILT*n* Approach

We understood earlier that when using the initial-value form of NILT*n* it is possible to select any set of values of $t_p, p = 1, 2, ...$ at which to determine the current density distribution $\bar{\mathscr{J}}_s(\bar{r}, t)$. These sample times need not be separated by a fixed step size (the initial-value form is not a time-steeping method *per se*). However, for each value of t_p that is indeed chosen, there is a different set of complex frequency values[45]

$$s_i = \frac{(n+1)\, z_i}{t_p} \qquad i = 1, 2, ..., M/2 \tag{5.4-1}$$

at which the matrix equation $[Z(s_i)][I(s_i)] = [V(s_i)]$ has to be solved. This was illustrated in Fig. 3.6-1 and Fig. 4.4-9. With the re-initialized form of NILT*n*, which is a time-stepping method with a step-size that we denoted by h, there is a single set of such complex frequency values

$$s_i = \frac{(n+1)\, z_i}{h} \qquad i = 1, 2, ..., M/2 \tag{5.4-2}$$

that does not change each time we determine $\bar{\mathscr{J}}_s(\bar{r}, t)$ at times $t = h, 2h, 3h, ...$ and thus $[Z(s_i)][I(s_i)] = [V(s_i)]$ need only be solved once. Fig. 5.4-9 shows the distribution of these s_i (just three of them for the $M = 6$ case being used) for the strip dipole geometry, for the re-initialized NILT0, NILT1 and NILT2 approaches. As expected, these are larger for larger n. The value of h depends on the width of the impressed Gaussian pulse; the smaller the value[46] of T_w the smaller the value of step size h required. Hence Fig. 5.4-9 (a), (b) and (c) reveal the proportionate values of the s_i for the strip dipole ($T_w = 10\text{ns}$), bowtie dipole ($T_w = 30\text{ns}$) and patch antenna ($T_w = 2.5\text{ns}$).

[45] With n being "the n in NILTn". The value of integer M is discussed in Section 2.7.
[46] As per Section 2.4.

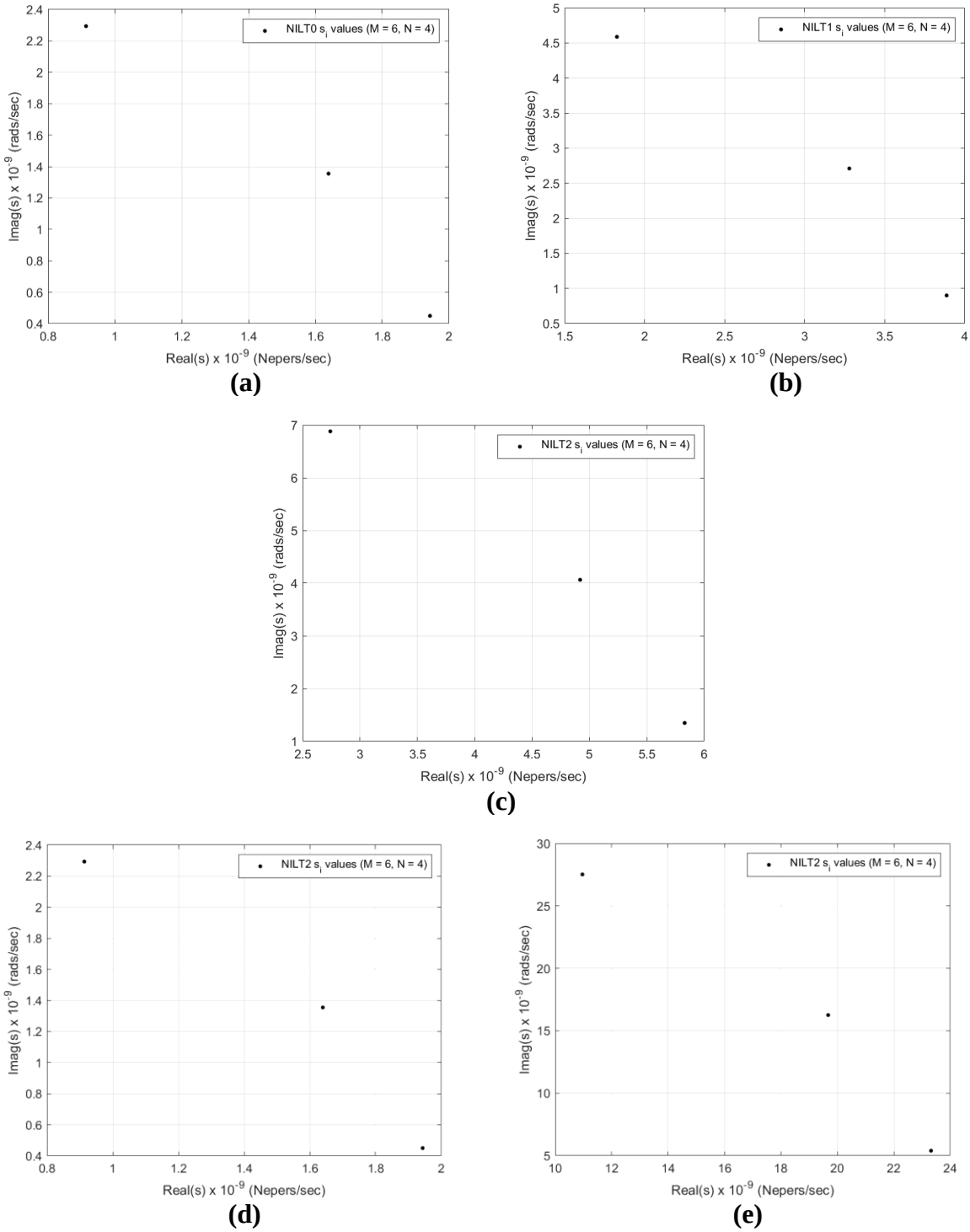

Fig. 5.4-9: Plots (a), (b) and (c) show the values of s_i used for the strip dipole for the NILT0, NILT1 and NILT2 cases, whereas (d) and (e) show these for the NILT2 case for the bowtie dipole and patch antenna, based on the parameters in Tables 4.4-1, 4.4-2 and 4.4-3.

5.5 COMMENTS ON COMPUTATIONAL COMPLEXITY

As seen from (5.2-28), the major computational blocks in the re-initialized NILT, proposed in this work, are:

1) LU factorization of the impedance matrix [$Z(s)$],

2) computation of the right-hand-side vector $[\Xi(s)]$, and

3) forward/backward substitution with that vector, for values of $s = z_i/h$, with $i = 1,...,M/2$.

Due to the use of re-initialization, the first operation needs to be done only once, while the other two operations need to be repeated at each time step. Analysis of the computational complexity will be carried out for the second operations, since this operation is unique to the proposed approach.

From (5.2-27), computing $[\Xi(z_i/h)]$ requires computing four vectors. The complexity of computing the first (antecedent) vector $\left[U\left(z_i/h\right)\right]$, depends, among other things, on the complexity of computing the term $U_{mnpq}^{\kappa_1\kappa_2}\left(z_i/h\right)$ given by (5.2-21), which in turn, is determined by the degree of the interpolating polynomial u as well as the integer $\zeta_{mnpq}^{\kappa_i\kappa_2}$. A closer examination of the three expressions used in (5.2-21) to compute $U_{mnpq}^{\kappa_1\kappa_2}\left(z_i/h\right)$, reveals that the order of arithmetic operations can be expressed as

$$\mathcal{O}\left(\frac{(v+1)(v+2)}{2}\left(\zeta_{mnpq}^{\kappa_1\kappa_2}+1\right)\right) \tag{5.5-1}$$

operations. Defining $\zeta_{\max}$ as

$$\zeta_{\max} \triangleq \max_{m,n,p,q,\kappa_1\kappa_2}\left(\zeta_{mnpq}^{\kappa_1\kappa_2}\right) \tag{5.5-2}$$

one can see that the overall order of computational complexity of the antecedent vector $\left[U\left(z_i/h\right)\right]$ can be expressed as

$$\mathcal{O}\left(\frac{(v+1)(v+2)}{2}\left(\zeta_{\max}+1\right)N_s^2\right) \tag{5.5-3}$$

with $i = 1,...,M/2$.

The computation of the second two vectors on the right-side of (5.2-27), i.e., $\left[i\right]$ and $\left[\dot{i}\right]$ depends only on the degree of the interpolating polynomial u but not on the integer $\zeta_{mnpq}^{\kappa_1\kappa_2}$ or the value of z_i. Therefore, the complexity of their computation is given by

$$\mathcal{O}\left(\frac{(v+1)}{2}N_s^2\right) \tag{5.5-4}$$

The fourth vector, namely the excitation vector $\left[V\left(z_i/h\right)\right]$, depends on the value of z_i, and hence its computation is repeated $M/2$ times. This vector, however, requires only N_s operations to be computed, thus making its complexity on the order of

$$\mathcal{O}\left(\frac{MN_s}{2}\right) \tag{5.5-5}$$

Based on the above analysis, the overall computational cost of the re-initialized NILT is dominated by the cost of computing the vector $\left[U\left(z_i/h\right)\right]$, resulting in a good estimation of the computation complexity at

$$\mathcal{O}\left(\frac{(v+1)(v+2)}{2}\left(\zeta_{\max}+1\right)N_s^2\right) \tag{5.5-6}$$

In most situations, $\zeta_{\max}$ is equal to 0, or occasionally, 1. The reason is that the high-order approximation power of NILT enables the step size h to be larger than, or at least comparable to, the longest of the travel times, $\tau_{mnpq}^{\kappa_1\kappa_2}$ given by (4.2-4) – between any two points on the PEC surface.

5.6 CONCLUDING REMARKS

Chapter 3 formulated, implemented and applied the *initial-value* NILT*n*/MoM approach to find solutions to the TD-EFIE for 2D PEC objects. Chapter 4 extended this work so that 3D PEC objects can be accommodated. Although this appears to be the first time such material for direct solution of the TD-EFIE using NILT*n* has been described anywhere, some might argue that doing things this way was implied in the so-called NILT*n*/PEEC approach[47], even though not actually done or details given. At any rate, what was achieved in the afore-mentioned chapters was in a sense preparation for the major contribution whose discussion has occupied all of Chapter 5, namely the ability to use a *re-initialized* form of the NILT*n*/MoM approach to find solutions to the TD-EFIE of 3D PEC objects. The need to use re-initialization was very clearly borne out by the results in Chapters 3 and 4. The difficulty of effecting such re-initialization in this context became apparent when the work of Chapter 5 was begun. The unavoidable presence of a multiplicity of delay terms was a stumbling block that has been overcome by the research described in the present chapter. This has been formulated, implemented and validated. It has been shown that the new re-initialized form of the NILT*n*/MoM approach for solution of the TD-EFIE is vastly superior to the initial-value form.

[47] Referred to in Section 2.6

CHAPTER 6 - General Conclusions

At the start of this work the NILT*n* method had not yet been applied directly to the solution of the TD-EFIE for scattering from PEC objects. It had certainly not yet been applied to any IE-type electromagnetic field analysis in its re-initialized time-stepping mode of operation. This was due to the considerable difficulty in applying such re-initialization when propagation delay is present. This thesis has overcome the above-mentioned knowledge gap, and so contributed to the subject in the following manner:

■ Chapter 5 formulated and validated a new, heretofore unavailable, re-initialized NILT*n*/MoM method for the solution of the differentiated TD-EFIE for PEC scattering. This is the principal contribution of this thesis to the field of computational electromagnetics. It allows one to obtain accurate and stable time-domain solutions using relatively large time steps, far out in time. In addition, the use of the interpolation allows the formulation to take these large time steps while accurately recreating the waveform between these time steps. Another beneficial use of the re-initialization NILT*n* is solutions of the s-domain MoM matrix equation $[Z(s_i)][I(s_i)]=[V(s_i)]$ is needed at the same complex frequency values s_i at each time point, and so the associated set of matrices $[Z(s_i)]$ need not be re-factored at each time step. Complete details have been provided on the details and formulation of the re-initialized differentiated TD-EFIE NILT*n* method. The validity and usefulness of the derivation done in Chapter 5 was demonstrated by testing three differently-shaped PEC objects and comparing the results to well studied computational electromagnetic formulations (i.e., the typical differentiated EFIE in the frequency-domain).

■ Many details, needed in order to successfully achieve the above contribution, and which were not available in the open literature, have been presented for the first time and thus constitute relevant contributions. Chapter 4 formulated an initial mode NILT*n*/MoM solution for the undifferentiated TD-EFIE for PEC scattering. Importantly, this chapter validated the implementation of the complex frequency domain EFIE, and confirmed that there would be no issue using the RWG expansion and weighting functions. This was confirmed by seeing the results for the initial mode NILT*n* accurately reproducing the known results early on in time. It

also confirmed that there was a need for re-initialization, as unlike the 2D case, the 3D case could not accurately reproduce the waveform for results further along in time.

■ The 2D applications of Chapter 3 were studied chiefly to provide concrete experience before moving to the general 3D cases. Nevertheless, to the best of the author's knowledge, their NILT*n*/MoM formulations are not available elsewhere, and so they represent a useful contribution in their own right. When an intuitive understanding of scattering from complicated objects, or radiation from new antenna ideas, is desired, this is still often done by first understanding and applying it to 2D problems. This was done in Chapter 3, using the initial mode NILT*n*/MoM for the undifferentiated TD-EFIE. The formulation was validated by comparing the results to the well known 2D PEC problems.

There remain some issues whose investigation in the future would prove useful:

■ The immediate investigation should be to see if the NILT*n*/MoM can avoid the internal resonance issue with closed PEC objects. These internal resonances occur in the frequency-domain due to singularities in the $\left[Z(\omega)\right]$ matrix. However, it is theorized that these singularities may not occur in the complex frequency-domain $\left[Z(s)\right]$ matrix. The NILT*n*/MoM formulation, by using the complex-frequency-domain may be well suited to produce FD results including the resonant frequencies.

■ Now that the details have been worked out for the TD-EFIE, it will be possible to apply the same NILT*n*/MoM approach for solution of the TD-MFIE and TD-CFIE of PEC objects, as well as IE formulations for scattering from penetrable objects. Because the discretized forms of the TD-IEs are solved in the Laplace domain, penetrable material with frequency-dependent permittivity and/or permeability could be more easily handled than is possible in MOT-type solutions due to the presence of additional convolution terms in the latter approach.

■ A similar discussion to the above can be had regarding the use oof the NILTn/MoM approach with dispersive materials.

■ Albeit not for PEC scattering problems, for which most of the TD-IE studies have been done, and associated stability and accuracy issues studied, one situation in which time-domain solutions are desirable is for physical problems involving materials that are non-linear[48] or are time-varying in a controlled manner. Non-linear materials cannot be handled using the NILT*n* methods described in this work. However, the use of NILT*n* in the context of lumped circuits containing nonlinear components has recently been described in recent literature, and the approach could be investigated for its potential in computational electromagnetics.

[48] The values of their permittivity and permeability at a point in space are dependent on the magnitude of the fields at that point, or are even known impressed functions of time (e.g. for time-varying material problems).

REFERENCES

[ANTO 23] G.Antonini, A.E.Ruehli, D.Romano and F.Loreto, “The partial elements equivalent circuit method : The state of the art”, IEEE Trans. Electromagnetic Compatibility, Early Access on IEEE Xplore, October 2023.

[AZAR 14] A.Azari, Z.H.Firouzeh and A.Zeidaabadi-Nezhad, “A new efficient technique for transient scattering of conducting cylinders illuminated by a TM-polarized wave”, IEEE Antennas and Wireless Propagation Letters, Vol.13, pp.1421-1424, 2014.

[BAKE 95] G. A. Baker and P.Graves-Morris, “Padé approximates,”, Encyclopedia of Mathematics, G. C. Rota, Ed. New York, NY, USA, Cambridge Univ. Press, 1995

[BARD 22] B.Bandali, E.Gad and M.Nakhla, “Fast and stable transient simulation of nonlinear circuits using the numerical inversion of the Laplace transform”, IEEE Trans. on Components, Packaging and Manufacturing Technology, Vol.12, No.7, pp.1171-1185, July 2022.

[BEGH 13] Y. Beghein, K. Cools, H. Bagci and D. De Zutter, “A Space-Time Mixed Galerkin Marching-on-in-Time Scheme for the Time-Domain Combined Field Integral Equation”, IEEE Transactions on Antennas and Propagation, vol. 61, no. 3, pp. 1228-1238, March 2013,

[BEGH 15] Y. Beghein, K. Cools and F. P. Andriulli, “A DC Stable and Large-Time Step Well-Balanced TD-EFIE Based on Quasi-Helmholtz Projectors” IEEE Transactions on Antennas and Propagation, vol. 63, no. 7, pp. 3087-3097, July 2015

[BENN 70] C.L.Bennett and W.L.Weeks, “Transient scattering from conducting cylinders”, IEEE Trans. Antennas and Propagation, Vol.18, No.5, pp.627-633, Sept.1970.

[BLUC 97] M.J.Bluck and S.P.Walker, “Time-domain BIE analysis of large three-dimensional electromagnetic scattering problems”, IEEE Trans. Antennas and Propagation, vol.45, no.5, pp.894-901, May 1997.

[DÉLY 20] A.Dély, F.Andriulli and K.Cools, “Large time step and DC stable TD-EFIE discretized with implicit Runge-Kutta methods”, IEEE Trans. Antennas & Propagation, Vol.68, No.2, pp.976-985, Feb.2020

[DÉLY 23] A.Dély, A.Merlini, K.Cools and F.Andriulli, “Convolution quadrature time domain integral equation methods for electromagnetic scattering”, Chap. 8 in : Q.Ren, S.Yan & A.Z.Elsherbini (Edits.), *Advances in Time-Domain Computational Electromagnetic Methods* (Wiley, 2023).

[ERDE 54] A.Erdélyi (Edit.), *Table of Integral Transforms* (McGraw-Hill, 1954).

[ERGI 98] A.A.Ergin, B.Shanker and E.Michielssen, “Fast evaluation of three-dimensional transient wave fields using diagonal translation operators”, J. Computational Physics, vol.146, pp.157-180, 1998.

[ERGI 99] A.A.Ergin, B.Shanker, and E.Michielssen, “The plane wave time domain algorithm for the fast analysis of transient wave phenomena”, IEEE Antennas Propagat. Mag., vol. 41, no. 4, pp. 39–52, 1999.

[FURS 00] C.M.Furse, D.H.Roper, D.N.Buechler, D.A.Christensen and C.H.Durney, “The problem and treatment of DC offsets in FDTD simulations”, IEEE Trans. Antennas and Propagation, Vol.48, No.8, pp. 1198-1201, Aug.2000.

[GAD 22] E.Gad, Y.Tao and M.Nakhla, “Fast and stable circuit simulation via interpolation-supported numerical inversion of the Laplace transform”, IEEE Trans. on Components, Packaging and Manufacturing Technology, Vol.12, No.1, pp.121-130, Jan.2022.

[GERA 09] A.Geranmayeh, W.Ackermann and T.Weiland, “Temporal discretization choices for stable boundary element methods in electromagnetic scattering problems”, Applied Numerical Mathematics, Vol.59, pp.2751-2773, 2009.

[GRAG 15] R.D.Graglia and A.F.Peterson, “Higher-Order Techniques in Computational Electromagnetics” (SciTech Publ., 2015)

[HERS 98] N.Herscovici, “A wide-band single-layer patch antenna”, IEEE Trans. Antennas & Propagation, Vol.46, No.4, pp.471-474, April 1998.

[JIN 10] J.Jin, *Theory and Computation of Electromagnetic Fields* (Wiley, 2010).

[JIN 14] J.Jin, *The Finite Element Method in Electromagnetics* (Wiley, 2014).

[JOHN 90] W.A.Johnson, D.R.Wilton and R.M.Sharpe, "Modeling scattering from and radiation by arbitrarily shaped objects with the electric field integral equation triangular surface patch code", *Electromagnetics*, Vol.10, pp.41-63, 1990.

[KHAY 05] M.A.Khayat and D.R.Wilton, “Numerical evaluation of singular and near-singular potential integrals”, IEEE Trans. Antennas Propagat., Vol.53, No.10, pp.3180-3190, Oct.2005.

[KHAY 08] M.A.Khayat, D.R.Wilton and P.W.Fink, “An improved transformation and optimized sampling scheme for the numerical evaluation of singular and near-singular potentials”, IEEE Antennas and Wireless Propagation Letters, Vol.7, pp.377-380, 2008.

[LORE 22] F.Loreto, G.Pettanice, G.Antonini, E.Gad, M.S.Nakhla, Y.Tao and A.Ruehli, "Modified numerical inversion of Laplace transform methods for the time-domain analysis of retarded partial elements equivalent circuit models", IEEE Trans. Electromagnetic Compatibility, Vol.64, No.6, pp.2179-2188, Dec. 2022.

[LORE 23] F.Loreto, D.Romano, G.Pettanice and G.Antonini, "A comparative analysis of numerical inverse Laplace transform methods for electromagnetic transient analysis", IEEE Trans. Microwave Theory & Techniques, Early Access on IEEE Xplore, September 2023.

[LU 00] M.Lu, J.Wang, A.A.Ergin & E.Michielssen, "Fast evaluation of two-dimensional transient wave fields", J. Computational Physics, Vol.158, pp.161-185, 2000.

[MA 96] J.Ma, V.Rokhlin and S.Wandzura, "Generalized Gaussian quadrature rules for systems of arbitrary functions", SIAM Journal on Numerical Analysis, Vol.33, No.3, pp.971-996, June 1996.

[MCCL 16] J.H.McClellan, R.W.Schafer and M.Yoder, *DSP First* (Pearson, 2016) 2nd Edition.

[MCNA 21] D.A.McNamara, *Course Notes for ELG7100 : The Moment Method in Engineering Electromagnetics*, School of Electrical Engineering & Computer Science, University of Ottawa, Canada, 2021.

[MITT 76] R.Mittra, "Integral Equation Methods for Transient Scattering", Chap.2 in : L.B.Felsen (Edit.), *Transient Electromagnetic Fields* (Springer, 1976)

[MORS 53] P.M.Morse & H.Feshbach, *Methods of Theoretical Physics, Part I* (McGraw-Hill, 1953) pp.688 & Section 7.3.

[NEVE 04] R.Nevels and J.Jeong, "The time domain Green's function and propagator for Maxwell's equations", IEEE Trans. Antennas & Propagation, Vol.52, No.11, pp.3012-3018, Nov. 2004.

[PETE 97] A.Peterson, S.Ray and R.Mittra, *Computational Methods for Electromagnetics* (IEEE Press, 1997).

[RAO 82] S.M.Rao, D.R.Wilton and A.W.Glisson, "Electromagnetic scattering by surfaces of arbitrary shape", *IEEE Trans. Antennas Propagat.*, Vol.30, pp.409-418, May 1982.

[RAO 91] S.M.Rao and D.R.Wilton, "Transient scattering by conducting surfaces of arbitrary shape", *IEEE Trans. Antennas & Propagation*, Vol.39, No.1, pp.56-61, Jan.1991.

[RAO 99] S.M.Rao, D.A.Vechinski and T.K.Sarkar, “Infinite Conducting Cylinders : TDIE Solution”, Chap. 3 in : S.M.Rao (Edit.), *Time Domain Electromagnetics* (Academic Press, 1999).

[RAO 20] S.M.Rao, “A straight-forward method of moments procedure to solve the time domain integral equation applicable to PEC bodies via triangular patch modeling”, *ACES Journal*, vol. 35, no. 8, pp.843-854, Aug.2020.

[REN 23] Q.Ren, S.Yan & A.Z.Elsherbini (Edits.), *Advances in Time-Domain Computational Electromagnetic Methods* (Wiley, 2023).

[RYNN 90] B.P.Rynne and P.D.Smith, “Stability of time marching algorithms for the electric field integral equation”, Journal of Electromagnetic Waves and Applications, Vol.12, pp.1181-1205, 1990.

[SHAN 00] B.Shanker, A.A.Ergin, K.Aygün and E.Micheilssen, “Analysis of transient electromagnetic scattering from closed surfaces using a combined field integral equation”, *IEEE Trans. Antennas & Propagation*, Vol.48, No.7, pp.1064-1074, July 2000.

[SHI 11] Y.Shi, M.Xia, R.Chen, E.Michielssen and M.Lu, “Stable electric field TDIE solvers via quasi-exact evaluation of MOT matrix elements”, *IEEE Trans. Antennas & Propagation*, Vol.59, No.2, pp.574-585, Feb.2011.

[SING 75] K.Singhal and J.Vlach, “Computation of time domain response by numerical inversion of the Laplace transform”, J. Franklin Institute, Vol.299, No.2, pp.109-126, Feb.1975.

[SING 93] K.Singhal and J.Vlach, “Computer Methods for Circuit Analysis and Design, 2nd ed”, New York, NY, USA: John Wiley & Sons, inc 1993.

[SMIT 97] G.S.Smith, *An Introduction to Classical Electromagnetic Radiation* (Cambridge University Press, 1997)

[TAGG 19] K.Taggar, E.Gad & D.A.McNamara, “High-order unconditionally stable time-domain finite-element method approach", *IEEE Antennas Wireless Propagat. Letters*, Vol.18, No.9, pp.1775-1779, Sept.2019.

[TAO 21] Y.Tao, E.Gad and M.Nakhla, “Fast and stable time-domain simulation based on modified numerical inversion of the Laplace transform”, IEEE Trans. on Components, Packaging and Manufacturing Technology, Vol.11, No.5, pp.848-858, May 2021.

[VOLA 12] J.L.Volakis and K.Sertel, *Integral Equation Methods for Electromagnetics* (SciTech Publishing, 2012).

[VLAC 83] J.Vlach and K.Singhal, *Computer Methods for Circuit Analysis and Design* (Van Nostrand Reinhold Co., 1983).

[WANG 11] X.Wang and D.S.Weile, “Implicit Runge-Kutta methods for the discretization of time domain integral equations”, IEEE Transactions on Antennas & Propagation, Vol.59, No.12, pp.4651-4663, Dec.2011.

[WANG 21] X.Wang, Y.Shi, B.Shanker, E.Michielssen and H.Bagcı, “Stable and accurate marching-on-in-time solvers of time domain EFIE, MFIE, and CFIE based on quasi-exact integration technique”, IEEE Transactions on Antennas & Propagation, Vol.69, No.4, pp.2218-2229, April 2021.

[WEID 94] J.A.C.Weideman, “Computation of the complex error function”, SIAM Journal on Numerical Analysis, Vol. 31, No. 5, pp. 1497-1518, Oct.1994.

[WYLI 66] C.R. Wylie, *Advanced Engineering Mathematics* (McGraw-Hill, 1966). Chap.7

APPENDIX I - Some Useful Mathematical Facts

I.1 Laplace Transforms

According to [WYLI 63],

$$\mathcal{L}\{f'(t)\} = s\mathcal{L}\{f(t)\} - f(0^+) \tag{I-1}$$

$$\mathcal{L}\{f''(t)\} = s^2\mathcal{L}\{f(t)\} - sf(0^+) - f'(0^+) \tag{I-2}$$

$$\mathcal{L}\left\{\int_a^t f(t)dt\right\} = \frac{1}{s}\mathcal{L}\{f(t)\} + \frac{1}{s}\int_a^0 f(t)dt \tag{I-3}$$

$$\mathcal{L}\left\{\int_{-\infty}^{\infty} f(t')\,\delta(t-t'-a)\,dt'\right\} = \mathcal{L}\left\{f(t-a)\right\} = e^{-sa}\mathcal{L}\left\{f(t)\right\} \tag{I-4}$$

$$\mathcal{L}\{f(t)e^{at}\} = F(s-a) \quad \text{where} \quad F(s) = \mathcal{L}\{f(t)\} \tag{I-5}$$

I.2 Bessel Functions

The derivative of the modified Bessel function is

$$\frac{d}{dx}\left\{K_\nu(x)\right\} = \frac{\nu}{x}K_\nu(x) - K_{\nu+1}(x) \tag{I-6}$$

APPENDIX II - Notation and Expressions for the Terms in the Interaction Matrix and Excitation Vector in the MoM Formulation for the s-Domain EFIE

This appendix has been included to provide some straightforward but distracting details related to the description of the MoM solution of the s-domain EFIE in Section 4.2. Once the spatial expansion and testing functions have been chosen, in particular identical sets of these because we use a Galerkin MoM approach, we must numerically evaluate the individual terms $Z_{mn}(s)$ in the interaction matrices $[Z(s)]$. The expressions for each $Z_{mn}(s)$ contain a double-integral with respect to the primed spatial variable (over triangle-pair T_n) lying within a double-integral with respect to the unprimed spatial variable (over triangle-pair T_m). The integrals take the form

$$\iint_{T_m}\left\{\iint_{T_n}\frac{\mu}{4\pi}s\,e^{-\frac{s}{c}|\bar{r}-\bar{r}'|}\,\frac{\bar{j}_m(\bar{r})\cdot\bar{j}_n(\bar{r}')}{|\bar{r}-\bar{r}'|}+\frac{1}{4\pi\varepsilon_0}\frac{1}{s}e^{-\frac{s}{c}|\bar{r}-\bar{r}'|}\,\frac{\left(\nabla\cdot\bar{j}_m(\bar{r})\right)\left(\nabla'\cdot\bar{j}_n(\bar{r}')\right)}{|\bar{r}-\bar{r}'|}dS'\right\}dS \qquad \text{(II-1)}$$

Writing the integrands simply as $f(\bar{r},\bar{r}')$ and $g(\bar{r})$ for purposes of illustration, we have

$$\begin{aligned}\iint_{T_m} g(\bar{r})\left\{\iint_{T_n} f(\bar{r},\bar{r}')\,dS'\right\}dS &= \iint_{T_m^+} g(\bar{r})\left\{\iint_{T_n^+} f(\bar{r},\bar{r}')\,dS'\right\}dS+\iint_{T_m^-} g(\bar{r})\left\{\iint_{T_n^+} f(\bar{r},\bar{r}')\,dS'\right\}dS\\ &\quad+\iint_{T_m^+} g(\bar{r})\left\{\iint_{T_n^-} f(\bar{r},\bar{r}')\,dS'\right\}dS+\iint_{T_m^-} g(\bar{r})\left\{\iint_{T_n^-} f(\bar{r},\bar{r}')\,dS'\right\}dS\end{aligned} \qquad \text{(II-2)}$$

Each of the four integrals on the right-hand side of (II-1) are evaluated using a quadrature formula as

$$\iint_{T_m} g(\bar{r}) \left\{ \iint_{T_n} f(\bar{r}, \bar{r}') \, dS' \right\} dS$$

$$\approx \sum_p w_p \, g(\bar{r}_{pm}^{+}) \left\{ \sum_q w_q \, f(\bar{r}_{pm}^{+}, \bar{r}_{qn}^{+}) \right\} + \sum_p w_p \, g(\bar{r}_{pm}^{-}) \left\{ \sum_q w_q \, f(\bar{r}_{pm}^{-}, \bar{r}_{qn}^{+}) \right\}$$

$$+ \sum_p w_p \, g(\bar{r}_{pm}^{+}) \left\{ \sum_q w_q \, f(\bar{r}_{pm}^{+}, \bar{r}_{qn}^{-}) \right\} + \sum_p w_p \, g(\bar{r}_{pm}^{-}) \left\{ \sum_q w_q \, f(\bar{r}_{pm}^{-}, \bar{r}_{qn}^{-}) \right\} \tag{II-3}$$

where the w_p, w_q, $\bar{r}_{pm}^{\kappa_1}$ and $\bar{r}_{qn}^{\kappa_2}$ are the weights and sampling points[49] (on the respective triangles), respectively, for the particular quadrature rule used[50]. Dummy symbols κ_i represent either a plus or a minus sign. We can rewrite (II-2) as

$$\iint_{T_m} g(\bar{r}) \left\{ \iint_{T_n} f(\bar{r}, \bar{r}') \, dS' \right\} dS$$

$$\approx \sum_p \sum_q w_p \, w_q \, g(\bar{r}_{pm}^{+}) \, f(\bar{r}_{pm}^{+}, \bar{r}_{qn}^{+}) + \sum_p \sum_q w_p \, w_q \, g(\bar{r}_{pm}^{-}) \, f(\bar{r}_{pm}^{-}, \bar{r}_{qn}^{+})$$

$$+ \sum_p \sum_q w_p \, w_q \, g(\bar{r}_{pm}^{+}) \, f(\bar{r}_{pm}^{+}, \bar{r}_{qn}^{-}) + \sum_p \sum_q w_p \, w_q \, g(\bar{r}_{pm}^{-}) \, f(\bar{r}_{pm}^{-}, \bar{r}_{qn}^{-}) \tag{II-4}$$

In order to write down expressions that appear less cumbersome, we will write (II-3) as

$$\iint_{T_m} g(\bar{r}) \left\{ \iint_{T_n} f(\bar{r}, \bar{r}') \, dS' \right\} dS \approx \sum_{p=1}^{N_g} \sum_{q=1}^{N_g} \sum_{(\kappa_1, \kappa_2)} \underbrace{g(\bar{r}_{pm}^{\kappa_1}) \, f(\bar{r}_{pm}^{\kappa_1}, \bar{r}_{qn}^{\kappa_2})}_{L_{mn}^{\kappa_1 \kappa_2} \text{ or } C_{mn}^{\kappa_1 \kappa_2}} \tag{II-5}$$

Dummy symbols κ_i of course continue to represent either a plus or a minus sign, and the symbol $\Sigma_{(\kappa 1, \kappa 2)}$ denotes the summation of four terms, one for each possible combination of (κ_1, κ_2). The reference to $L_{mn}^{\kappa_1 \kappa_2}$ or $C_{mn}^{\kappa_1 \kappa_2}$ will be clear from Section 4.2. Hence, we arrive at expression (II-6).

[49] We will assume an N_g-point quadrature rule.

[50] Singularities or near-singularities that occur for diagonal and other terms are properly taken care of [KHAY 05][KHAY 08].

$$\frac{\mu}{4\pi}\sum_{n=1}^{N_s}\sum_{p=1}^{N_g}\sum_{q=1}^{N_g}\sum_{(\kappa_1,\kappa_2)} w_p w_q\, I_n(s)\, s\, e^{-s\tau_{mnpq}^{\kappa_1\kappa_2}} L_{mnpq}^{\kappa_1\kappa_2}$$

$$+\frac{1}{4\pi\varepsilon_0}\sum_{n=1}^{N_s}\sum_{p=1}^{N_g}\sum_{q=1}^{N_g}\sum_{(\kappa_1,\kappa_2)} w_p w_q\, I_n(s)\frac{e^{-s\tau_{mnpq}^{\kappa_1\kappa_2}}}{s} C_{mnpq}^{\kappa_1\kappa_2}$$

$$=\sum_{q=1}^{N_g}\sum_{(\kappa_1,\kappa_2)} w_p \bar{j}_m\left(\bar{r}_{pm}^{\kappa_1}\right)\cdot\bar{E}^{inc}\left(\bar{r}_{pm}^{\kappa_2}, s\right) \tag{II-6}$$

where

$$\tau_{mnpq}^{\kappa_1\kappa_2} = \frac{\left|\bar{r}_{pm}^{\kappa_1\kappa_2} - \bar{r}'^{\kappa_1\kappa_2}_{qn}\right|}{c} \tag{II-7}$$

$$L_{mnpq}^{\kappa_1\kappa_2} = \frac{\bar{j}_m\left(\bar{r}_{pm}^{\kappa_1\kappa_2}\right)\cdot\bar{j}_n\left(\bar{r}'^{\kappa_1\kappa_2}_{qn}\right)}{\left|\bar{r}_{pm}^{\kappa_1\kappa_2} - \bar{r}'^{\kappa_1\kappa_2}_{qn}\right|} \tag{II-8}$$

and

$$C_{mnpq}^{\kappa_1\kappa_2} = \frac{\left(\nabla\cdot\bar{j}_m\left(\bar{r}_{pm}^{\kappa_1\kappa_2}\right)\right)\left(\nabla'\cdot\bar{j}_n\left(\bar{r}'^{\kappa_1\kappa_2}_{qn}\right)\right)}{\left|\bar{r}_{pm}^{\kappa_1\kappa_2} - \bar{r}'^{\kappa_1\kappa_2}_{qn}\right|} \tag{II-9}$$

APPENDIX III - Laplace Transforms of Backward-Shifted Functions

It was important to remind ourselves in Section 3.7 if we can analytically determine $F(s) = \mathcal{L}\{f(t)\}$, then the Laplace transform of the forward-shifted function $f(t-h)$, $h \geq 0$ is easily found from a well-known identity as $\mathcal{L}\{f(t-h)\} = e^{-sh}F(s)$, but that there is no similar straightforward identity for finding the Laplace transform $\mathcal{L}\{f(t+h)\})$ of a backward-shifted function $f(t+h)$, $h \geq 0$ in general. We said that in some specific cases, in other words when $f(t)$ is some specific function with some known useful properties, one might be "lucky" and be able to manipulate matters to find $\mathcal{L}\{f(t+h)\})$. We give two examples here, the first because it explicitly demonstrates what we mean, and the second that is found using a more circuitous route but is actually used in Chapter 5.

Example#1

If $f(t) = \sin(t)$, and we are looking to implement re-initialization on it, firstly the change of variable results in

$$f(\hat{t} + rh) = \sin(\hat{t} + rh) \tag{III-1}$$

since we are looking to perform the Laplace transform with respect to $\hat{t}$, we need to find a way to remove the rh term from the sin function. Fortunately, there is a trigonometric identity

$$\sin(A+B) = \sin(A)\cos(B) + \cos(A)\sin(B) \tag{III-2}$$

applying (III-2) to (III-1) results in

$$f(\hat{t} + rh) = \sin(\hat{t})\cos(rh) + \cos(\hat{t})\sin(rh) \tag{III-3}$$

at this point in (III-3) the Laplace transform can be found with respect to $\hat{t}$, multiplied by a constant. Re-initialization can be applied on both terms in (III-3).

Example#2

If $f(t)=e^{-(t-t_o)^2/\tau_w^2}$, then first, applying the change of variable $t=\hat{t}+rh$

$$f(\hat{t}+rh)=e^{-(\hat{t}+rh-t_o)^2/\tau_w^2} \tag{III-4}$$

next, using the definition of the Laplace transform

$$\mathcal{L}\left\{f(\hat{t}+rh)\right\}=\int_0^\infty e^{-(\hat{t}+rh-t_o)^2/\tau_w^2}d\hat{t} \tag{III-5}$$

it can be shown by completing the square and through a change of variables, that the above integral can be written as

$$\mathcal{L}\{f(t+h)\}=\frac{\tau_w\sqrt{\pi}}{2}e^{\frac{2rht_o-t_o^2-rh^2}{\tau_w^2}}erfcx\left(\frac{s\tau_w}{2}+\frac{rh-t_o}{\tau_w}\right) \tag{III-6}$$

where $erfcx(..)$ is the so-called scaled complex complementary error function defined by

$$erfcx(x)=e^{-x^2}\int_x^\infty e^{-p^2}\,dp \tag{III-7}$$

APPENDIX IV – Discussion of the Selection of the Mesh Density

Although not explicitly stated in the main body of the thesis in Chapter 4.4 and Chapter 5.4, there is a methodology used to select the mesh density of the various antenna tested in the aforementioned chapters. It is important to select a mesh density such that the ratio between the smallest wavelength of s_i, (λ_i)[51] and the average edge length of the mesh is $10 = \lambda_i / l_{edge}^{avg}$.

Firstly, the range of desired frequencies was selected. Then we can determine the correct Gaussian pulse width using (2.4-4) such that the excitation term has enough spectral power in the desired range of frequencies. It is repeated below for convenience.

$$f_u = \frac{6\sqrt{2}}{\pi T_{\mathrm{w}}} \tag{IV-1}$$

Afterwards, it is necessary to select a correct step size for either the initial NILT or the re-initialized NILT such that enough time samples lie upon the Gaussian pulse in the time-domain. This is to assure that both the initial mode NILT and the re-initialized NILT can accurately capture the Gaussian pulse. Based on experimental results, a good rule of thumb is $h = T_w/3$.

Once the time-step h is selected, you can determine the appropriate value for λ_i depending on the *M/N* padé approximation used for NILT, and therefore select the appropriate mesh density such that $10 = \lambda_i / l_{edge}^{avg}$.

Note that we have found from numerical experiments that if the NILT0 is satisfied with $10 = \lambda_i / l_{edge}^{avg}$, the same mesh density can be used for NILT1 and NILT2 despite the fact that the s_i increases based on the NILT*n* used $s_i = (n+1) z_i / h$.

---

[51] $\lambda_i = \frac{c}{f_i}$, where f_i comes from the imaginary component of s_i, ($s_i = (n+1) z_i / h = \sigma_i + j(2\pi f_i)$). Note the expression is for the re-initialized NILT. Thus, for the initial NILT, simply switch h for the current time step t

APPENDIX V – Discussion on the use of the Differentiated TD-EFIE for Re-Initialization vs Undifferentiated TD-EFIE

The reader may be interested in the justification for using the differentiated TD-EFIE in Chapter 5 for the re-initialized NILT*n* compared to the undifferentiated TD-EFIE in Chapters 3 and 4 for the initial mode NILT*n*. Firstly, examining the undifferentiated TD-EFIE as shown in (2.3-4) (repeated here for convenience),

$$\frac{\mu}{4\pi}\hat{n}(\bar{r})\times\frac{\partial}{\partial t}\left(\int_{-\infty}^{\infty}\left\{\iint_{S}\bar{\mathscr{J}}_s(\bar{r}',t')\,\frac{\delta(t-t'-|\bar{r}-\bar{r}'|/c)}{|\bar{r}-\bar{r}'|}dS'\right\}dt'\right)$$
$$-\frac{1}{4\pi\varepsilon_o}\hat{n}(\bar{r})\times\nabla\int_{0}^{t}\left(\int_{-\infty}^{\infty}\left\{\iint_{S_c}\nabla'\cdot\bar{\mathscr{J}}_s(\bar{r}',t')\,\frac{\delta(\gamma-t'-|\bar{r}-\bar{r}'|/c)}{|\bar{r}-\bar{r}'|}dS'\right\}dt'\right)d\gamma=\hat{n}(\bar{r})\times\bar{\mathscr{E}}^{inc}(\bar{r},t)\qquad \bar{r}\in S$$

(V-1)

we can see the second term in the left-hand side of (V-1) has an integral ranging from 0 to *t*. When apply the required change of variable for re-initialization, this integral causes a problem, as one must find a way to isolate the $\hat{t}$ term from the *rh* term. This would require extensive mathematical manipulation. Instead, it is much easier to eliminate this integral by using the differentiated TD-EFIE. As stated in Section 2.3.3, we can obtain the differentiated TD-EFIE by taking the time-domain derivative with respect to *t* in (IV-1).

$$\frac{\mu}{4\pi}\hat{n}(\bar{r})\times\frac{\partial^2}{\partial t^2}\left(\int_{-\infty}^{\infty}\left\{\iint_{S}\bar{\mathscr{J}}_s(\bar{r}',t')\,\frac{\delta(t-t'-|\bar{r}-\bar{r}'|/c)}{|\bar{r}-\bar{r}'|}dS'\right\}dt'\right)$$
$$-\frac{1}{4\pi\varepsilon_o}\hat{n}(\bar{r})\times\nabla\left(\int_{-\infty}^{\infty}\left\{\iint_{S_c}\nabla'\cdot\bar{\mathscr{J}}_s(\bar{r}',t')\,\frac{\delta(t-t'-|\bar{r}-\bar{r}'|/c)}{|\bar{r}-\bar{r}'|}dS'\right\}dt'\right)=\hat{n}(\bar{r})\times\frac{\partial}{\partial t}\bar{\mathscr{E}}^{inc}(\bar{r},t)\qquad \bar{r}\in S$$

(V-2)

(V-2) has no time-domain integral. Thus, it is "easier" for the re-initialization to handle, as no mathematical "tricks" are required to separate an integral ranging from 0 to *t* (it no longer exists). It is important to note that using the differentiated form of the TD-EFIE has no inherent drawbacks, thus one can feel comfortable using it.

APPENDIX VI - Details of Steps Leading from Expression (5.2-7) to (5.2-8)

We begin with the integral in expression (5.2-7), which is[52]

$$\int_0^{\infty} i_n\left(\hat{t} + rh - \tau_{mnpq}^{\kappa_1\kappa_2}\right) e^{-s\hat{t}}\, d\hat{t} \tag{VI-1}$$

The first step is to define a variable $\gamma = \hat{t} - \tau_{mnpq}^{\kappa_1\kappa_2}$, so that $\hat{t} = \gamma + \tau_{mnpq}^{\kappa_1\kappa_2}$. When $\hat{t} = 0$ we have $\gamma = -\tau_{mnpq}^{\kappa_1\kappa_2}$. Also, since $\tau_{mnpq}^{\kappa_1\kappa_2}$ is a constant, $d\gamma = d\hat{t}$. Thus we can rewrite (VI-1) as

$$\int_0^{\infty} i_n\left(\hat{t} + rh - \tau_{mnpq}^{\kappa_1\kappa_2}\right) e^{-s\hat{t}}\, d\hat{t} = \int_{-\tau_{mnpq}^{\kappa_1\kappa_2}}^{\infty} i_n(\gamma + rh) e^{-s\gamma} e^{-s\tau_{mnpq}^{\kappa_1\kappa_2}}\, d\gamma = e^{-s\tau_{mnpq}^{\kappa_1\kappa_2}} \int_{-\tau_{mnpq}^{\kappa_1\kappa_2}}^{\infty} i_n(\gamma + rh) e^{-s\gamma}\, d\gamma \tag{VI-2}$$

The expression on the far-right of (VI-2) can be expressed as the sum of two integrals as

$$e^{-s\tau_{mnpq}^{\kappa_1\kappa_2}} \int_{-\tau_{mnpq}^{\kappa_1\kappa_2}}^{\infty} i_n(\gamma + rh) e^{-s\gamma}\, d\gamma = e^{-s\tau_{mnpq}^{\kappa_1\kappa_2}} \int_0^{\infty} i_n(\gamma + rh) e^{-s\gamma}\, d\gamma + e^{-s\tau_{mnpq}^{\kappa_1\kappa_2}} \int_{-\tau_{mnpq}^{\kappa_1\kappa_2}}^{0} i_n(\gamma + rh) e^{-s\gamma}\, d\gamma \tag{VI-3}$$

Since γ is just a dummy variable as far as the two integrals on the right of (VI-3) are concerned, we can replace it by any symbol, and so we simply set $\gamma \to \hat{t}$, to get

$$\int_0^{\infty} i_n\left(\hat{t} + rh - \tau_{mnpq}^{\kappa_1\kappa_2}\right) e^{-s\hat{t}}\, d\hat{t} = e^{-s\tau_{mnpq}^{\kappa_1\kappa_2}} \int_0^{\infty} i_n(\hat{t} + rh) e^{-s\hat{t}}\, d\hat{t} + e^{-s\tau_{mnpq}^{\kappa_1\kappa_2}} \int_{-\tau_{mnpq}^{\kappa_1\kappa_2}}^{0} i_n(\hat{t} + rh) e^{-s\hat{t}}\, d\hat{t} \tag{VI-4}$$

which (VI-4) is expression (5.2-8).

[52] Renumbered here for convenience.

APPENDIX VII - Additional Results Related to Section 5.4

A. ADDITIONAL RESULTS RELATED TO THOSE OF THE STRIP DIPOLE GEOMETRY IN SECTION 5.4.2

■ ***Re-initialized NILT1 : Strip Dipole***

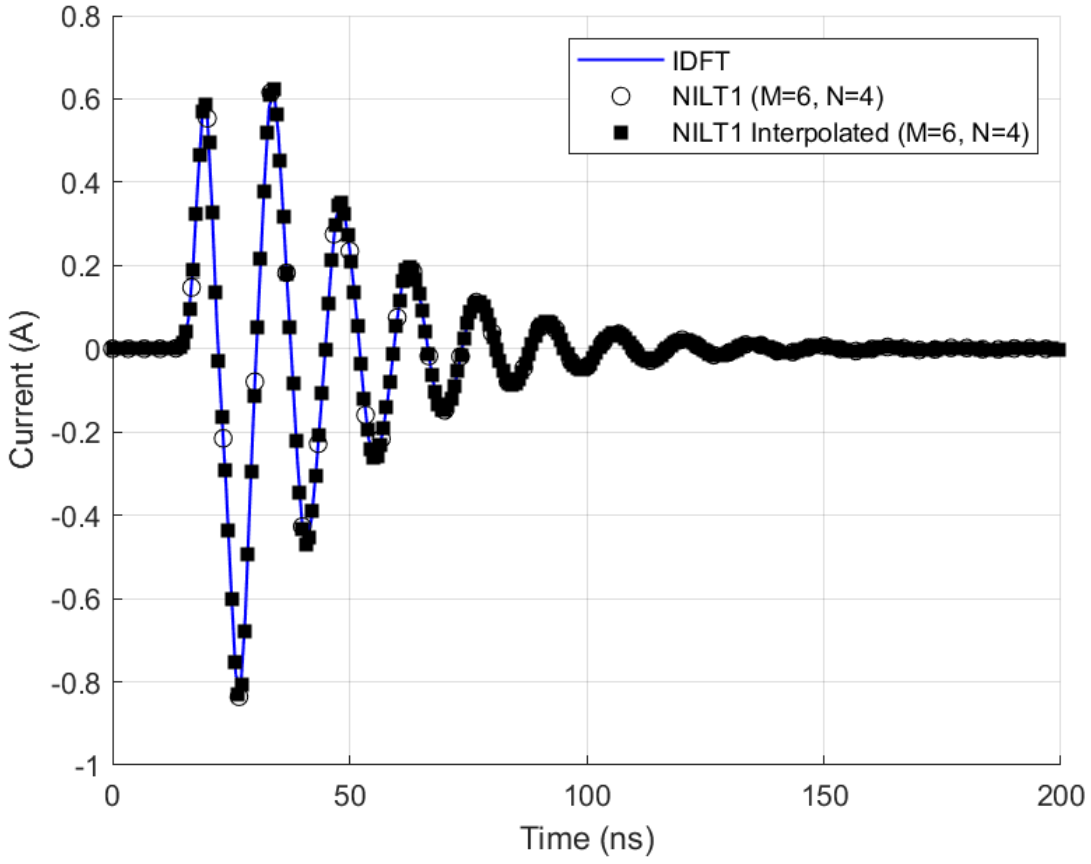

Fig. VII-1: The induced current at the feedpoint of the strip dipole antenna when excited by a Gaussian pulse at the feedpoint. The blue line represents the IDFT results. The black circles represent the re-initialized NILT1 results, and the black squares the interpolated re-initialized NILT1 results.

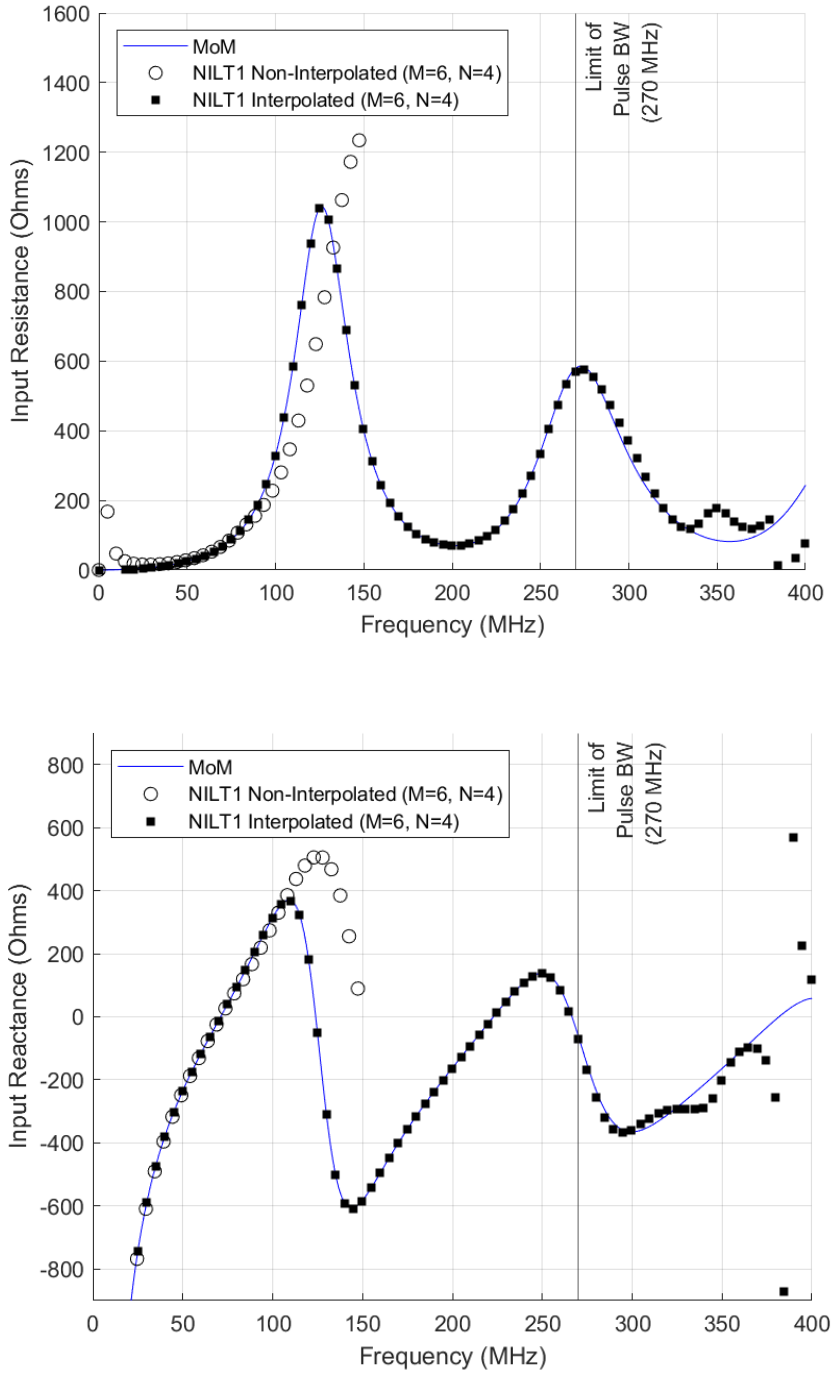

Fig. VII-2: The input resistance (top) and input reactance (bottom) of the strip dipole. The blue line represents the FD-EFIE results. The black circles represent the FD/non-interpolated re-initialized NILT1 results. The black squares represent FD/interpolated re-initialized NILT1 results.

■ ***Re-initialized NILT2 : Strip Dipole***

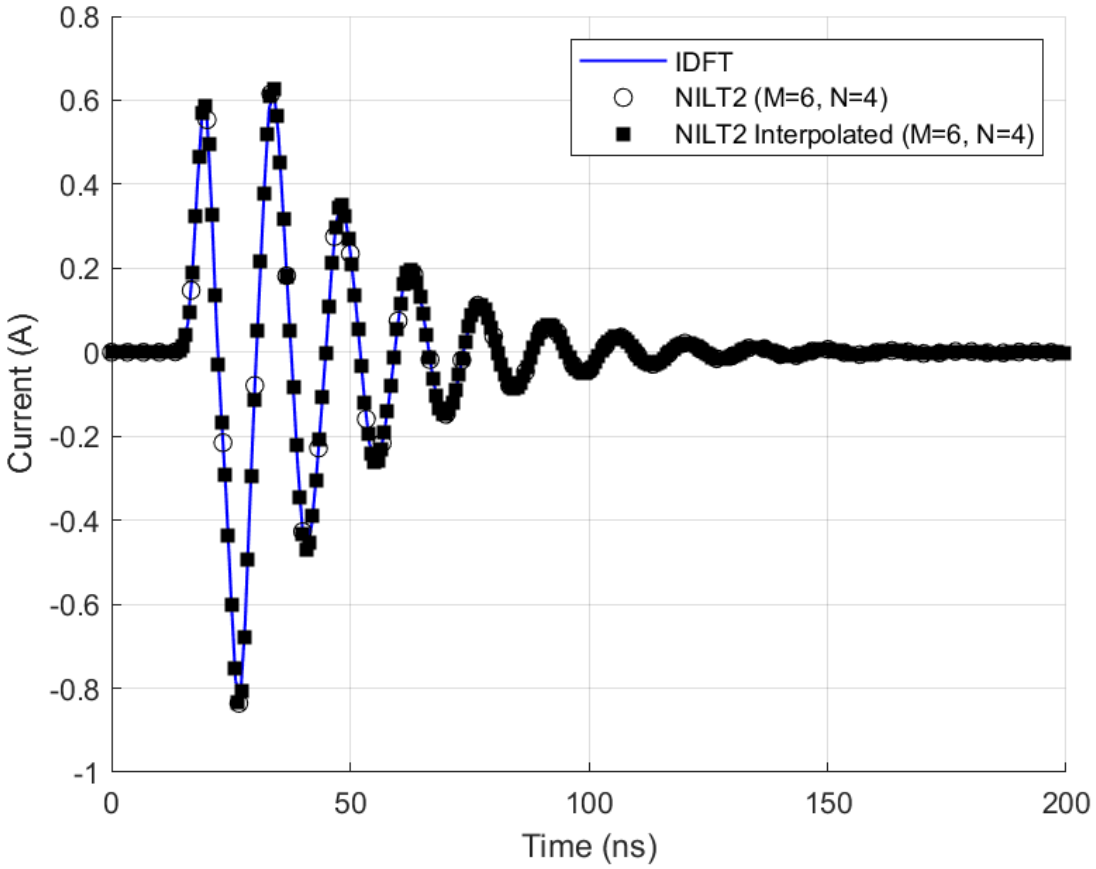

Fig. VII-3: The induced current at the feedpoint of the strip dipole antenna when excited by a Gaussian pulse at the feedpoint. The blue line represents the IDFT results. The black circles represent the re-initialized NILT2 results, and the black squares the interpolated re-initialized NILT2 results.

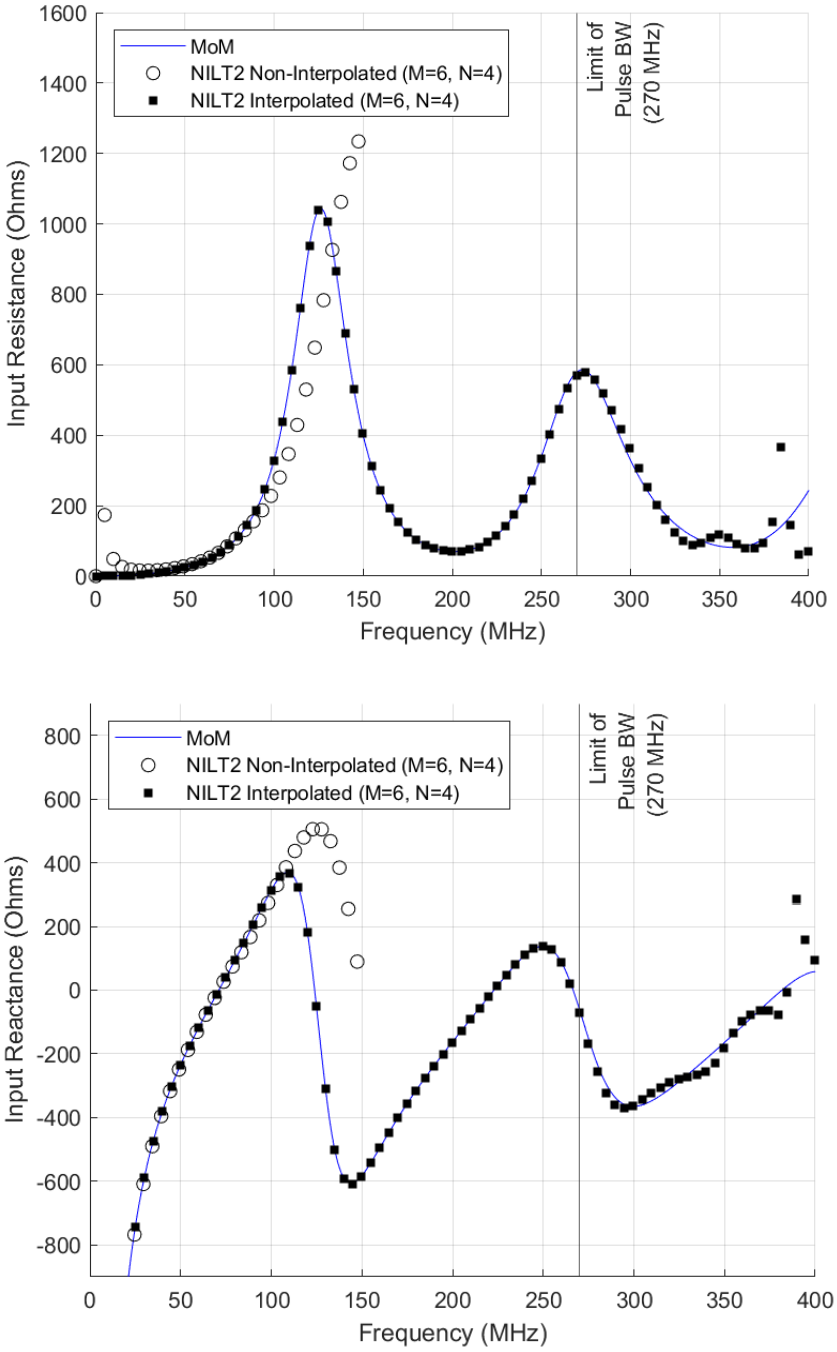

Fig. VII-4 The input resistance (top) and input reactance (bottom) of the strip dipole. The blue line represents the FD-EFIE results. The black circles represent the FD/non-interpolated re-initialized NILT2 results. The black squares represent FD/interpolated re-initialized NILT2 results.

B. ADDITIONAL RESULTS RELATED TO THOSE OF THE BOWTIE DIPOLE GEOMETRY IN SECTION 5.4.3

■ ***Re-initialized NILT1 : Bowtie Dipole***

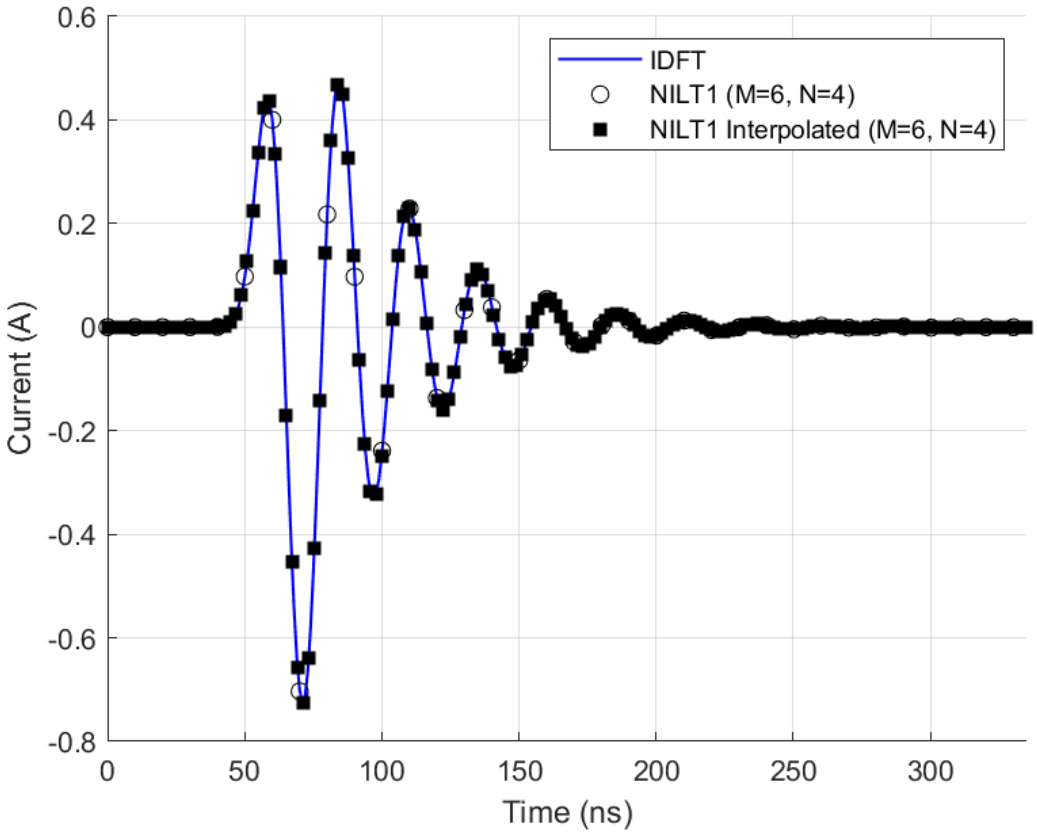

Fig. VII-5: The induced current at the feedpoint of the bowtie dipole antenna when excited by a Gaussian pulse at the feedpoint. The blue line represents the IDFT results. The black circles represent the re-initialized NILT1 results, and the black squares the interpolated re-initialized NILT1 results.

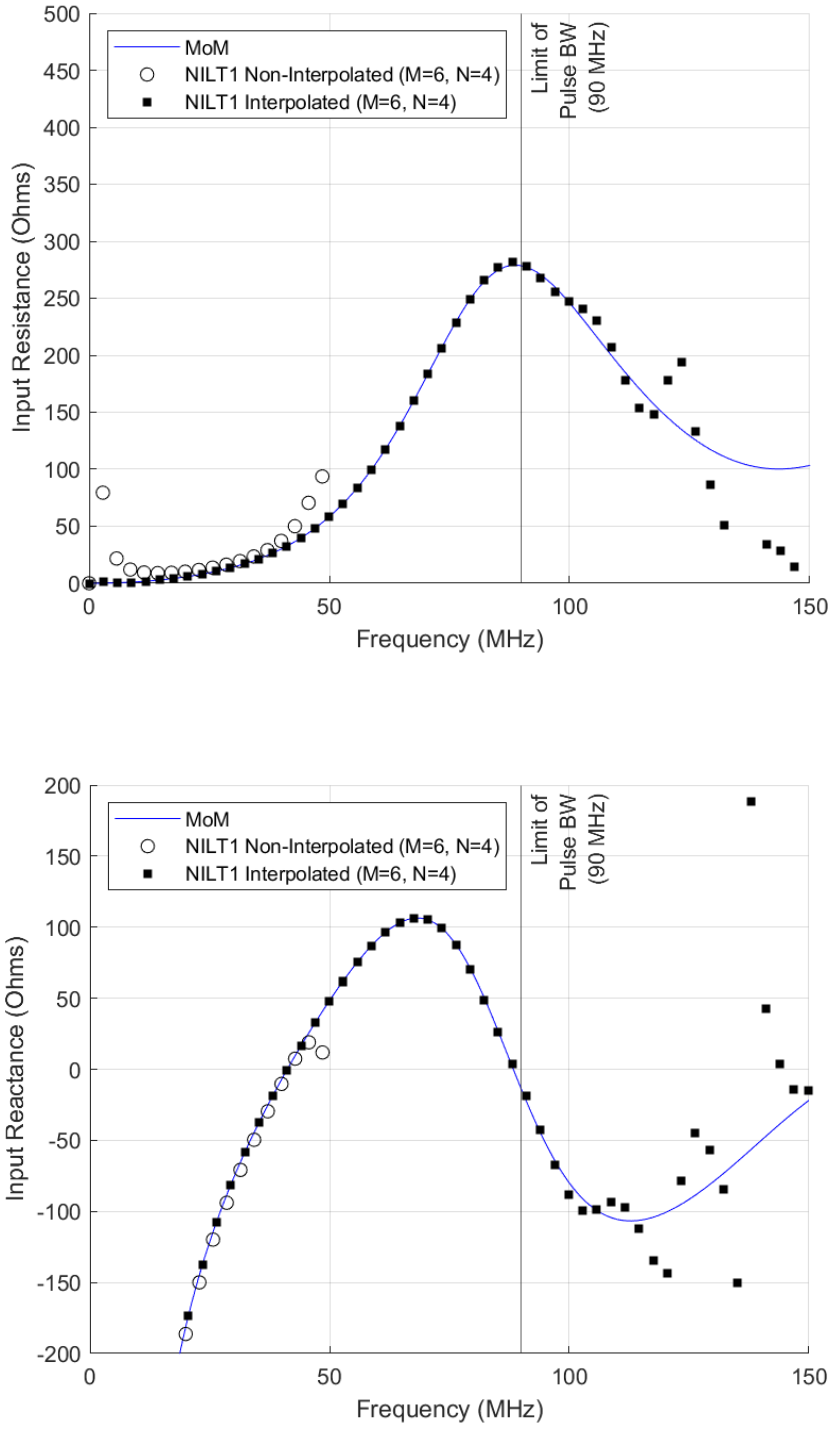

Fig. VII-6: The input resistance (top) and input reactance (bottom) of the bowtie dipole. The blue line represents the FD-EFIE results. The black circles represent the FD/non-interpolated re-initialized NILT1 results. The black squares represent FD/interpolated re-initialized NILT1 results.

■ ***Re-initialized NILT2 : Bowtie Dipole***

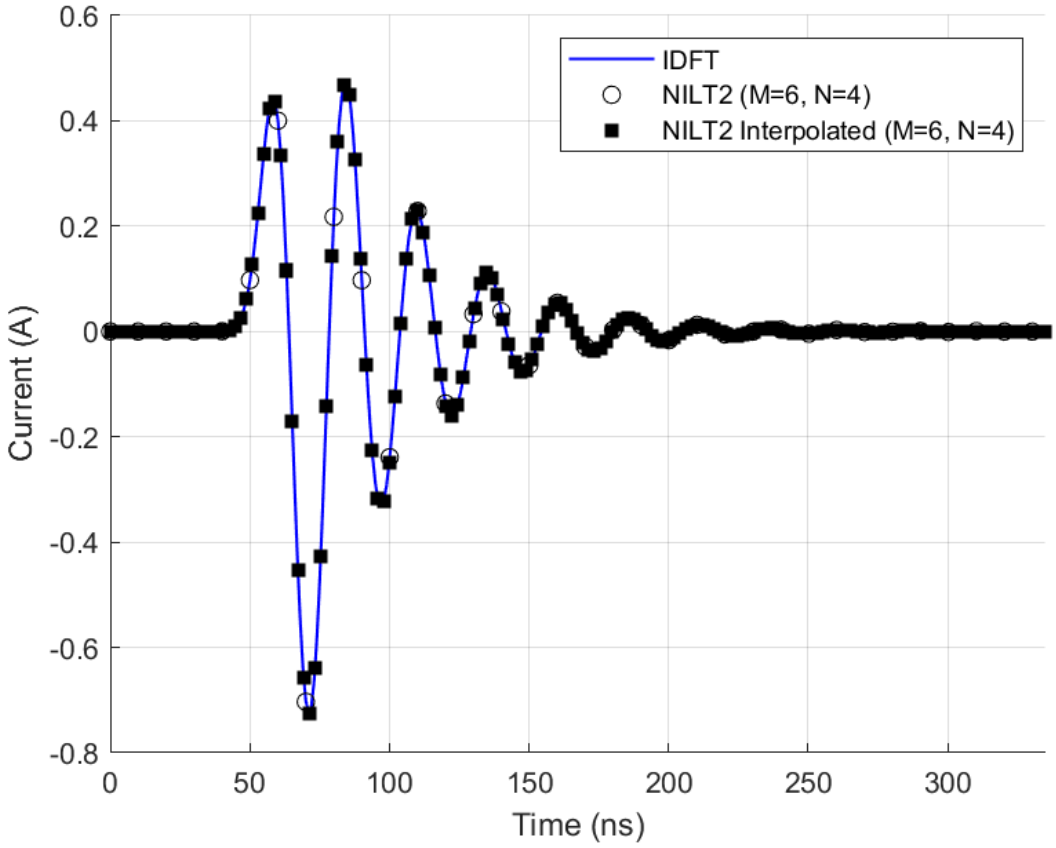

Fig. VII-7: The induced current at the feedpoint of the bowtie dipole antenna when excited by a Gaussian pulse at the feedpoint. The blue line represents the IDFT results. The black circles represent the re-initialized NILT2 results, and the black squares the interpolated re-initialized NILT2 results.

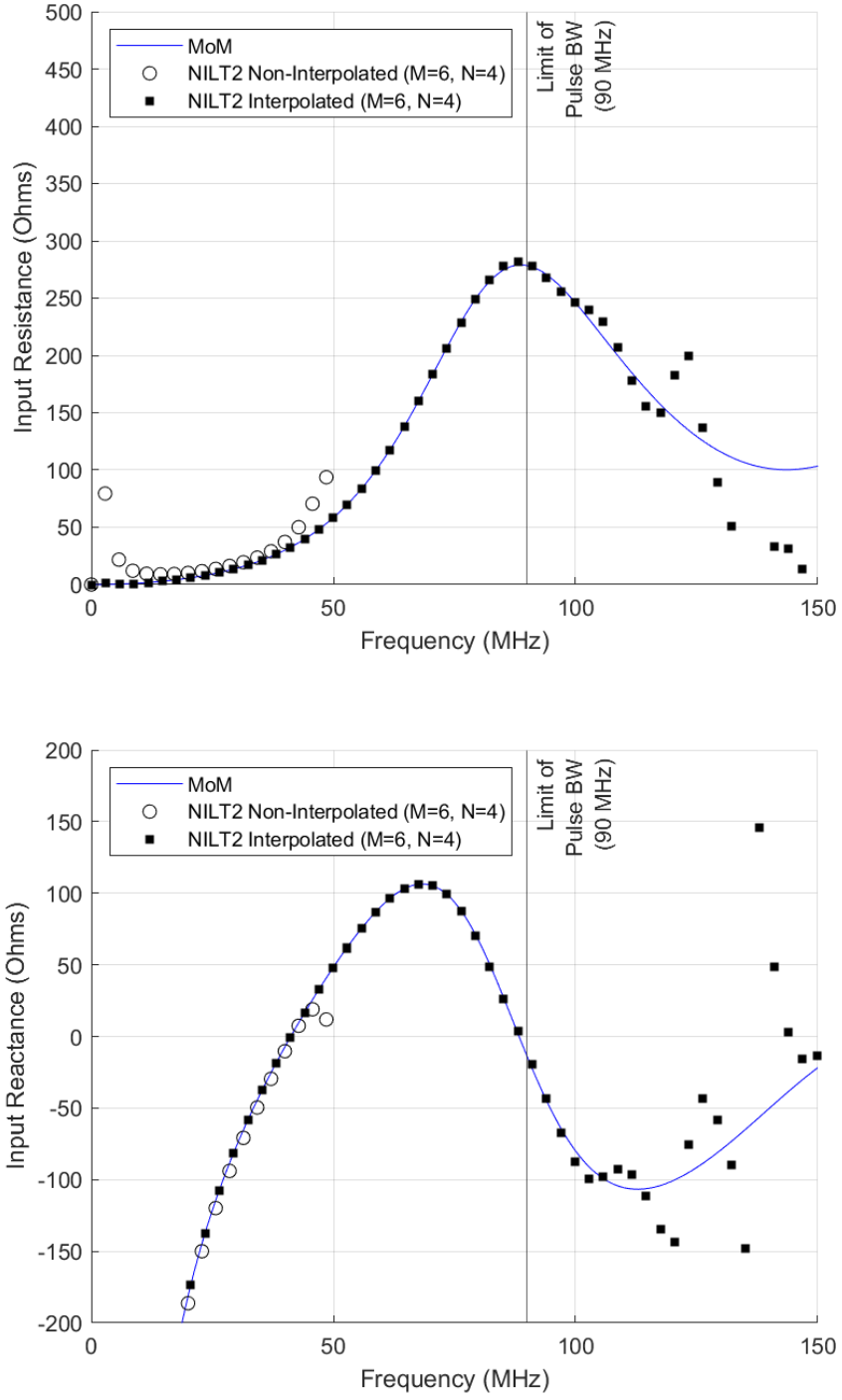

Fig. VII-8: The input resistance (top) and input reactance (bottom) of the bowtie dipole. The blue line represents the FD-EFIE results. The black circles represent the FD/non-interpolated re-initialized NILT2 results. The black squares represent FD/interpolated re-initialized NILT2 results.

C. ADDITIONAL RESULTS RELATED TO THOSE OF THE PATCH ANTENNA GEOMETRY IN SECTION 5.4.4

■ ***Re-initialized NILT1 : Patch Antenna***

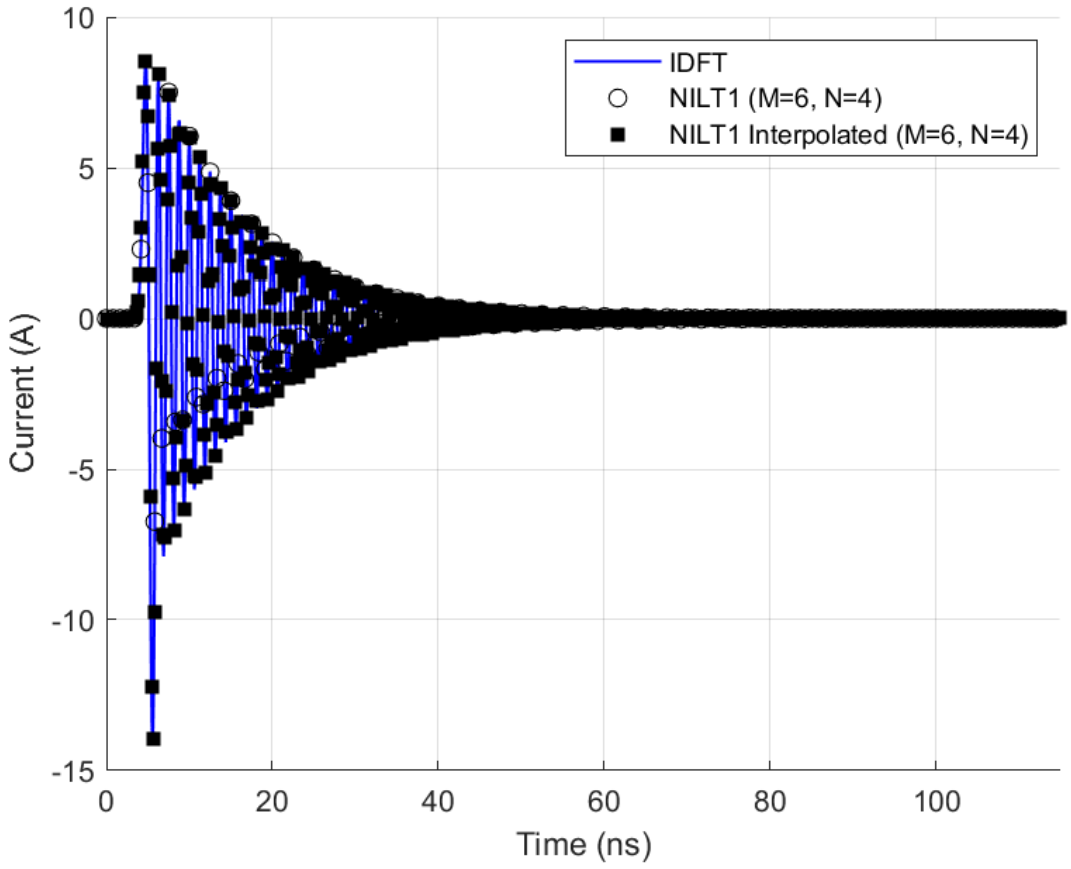

Fig. VII-9: The induced current at the feedpoint of the patch antenna when excited by a Gaussian pulse at the feedpoint. The blue line represents the IDFT results. The black circles represent the re-initialized NILT1 results, and the black squares the interpolated re-initialized NILT1 results.

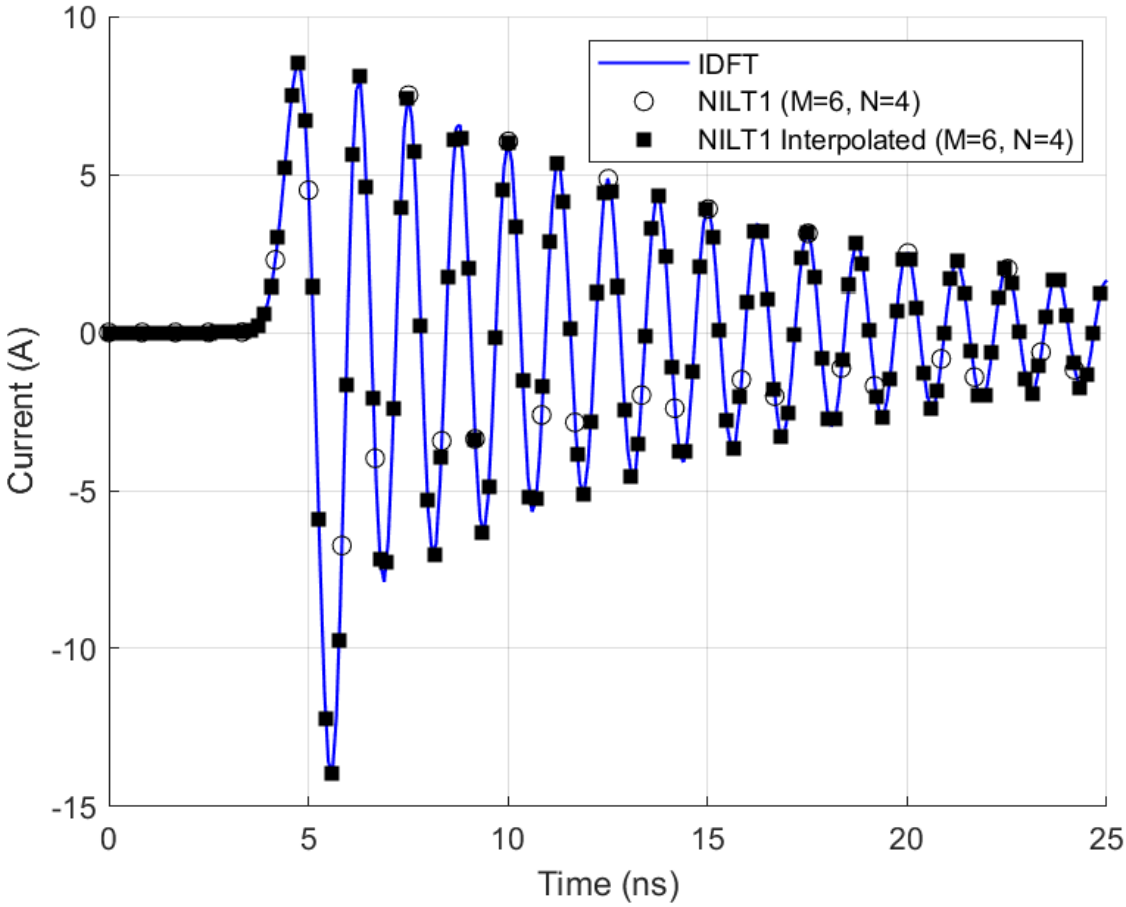

Fig. VII-10 : The same sets of results as in Fig. VII-9, but focused on a shorter time-frame to reveal details more closely.

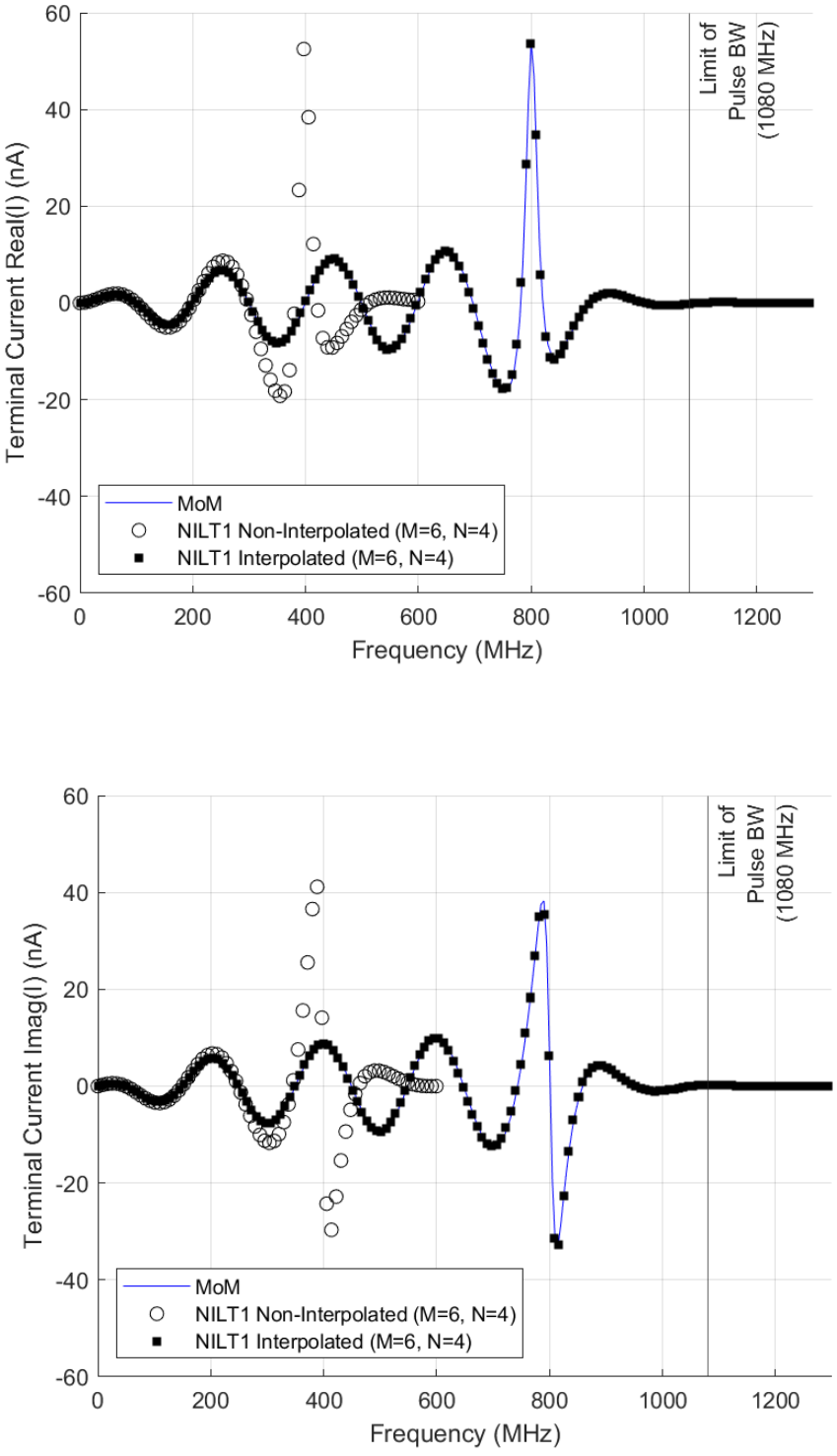

Fig. VII-11: The real part (top) and imaginary part (bottom) of the terminal current of the patch antenna. The blue line represents the FD-EFIE results. The black circles represent the FD/non-interpolated re-initialized NILT1 results. The black squares represent FD/interpolated re-initialized NILT1 results.

■ ***Re-initialized NILT2 : Patch Antenna***

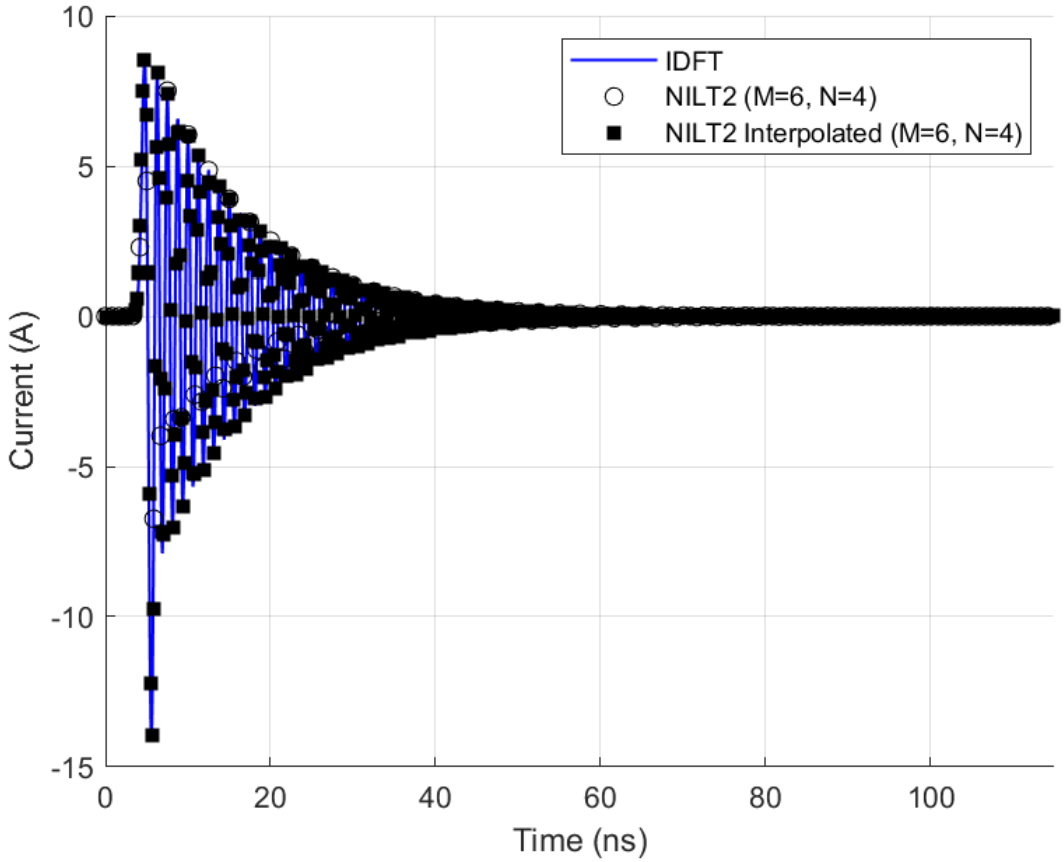

Fig. VII-12: The induced current at the feedpoint of the patch antenna when excited by a Gaussian pulse at the feedpoint. The blue line represents the IDFT results. The black circles represent the re-initialized NILT2 results, and the black squares the interpolated re-initialized NILT2 results.

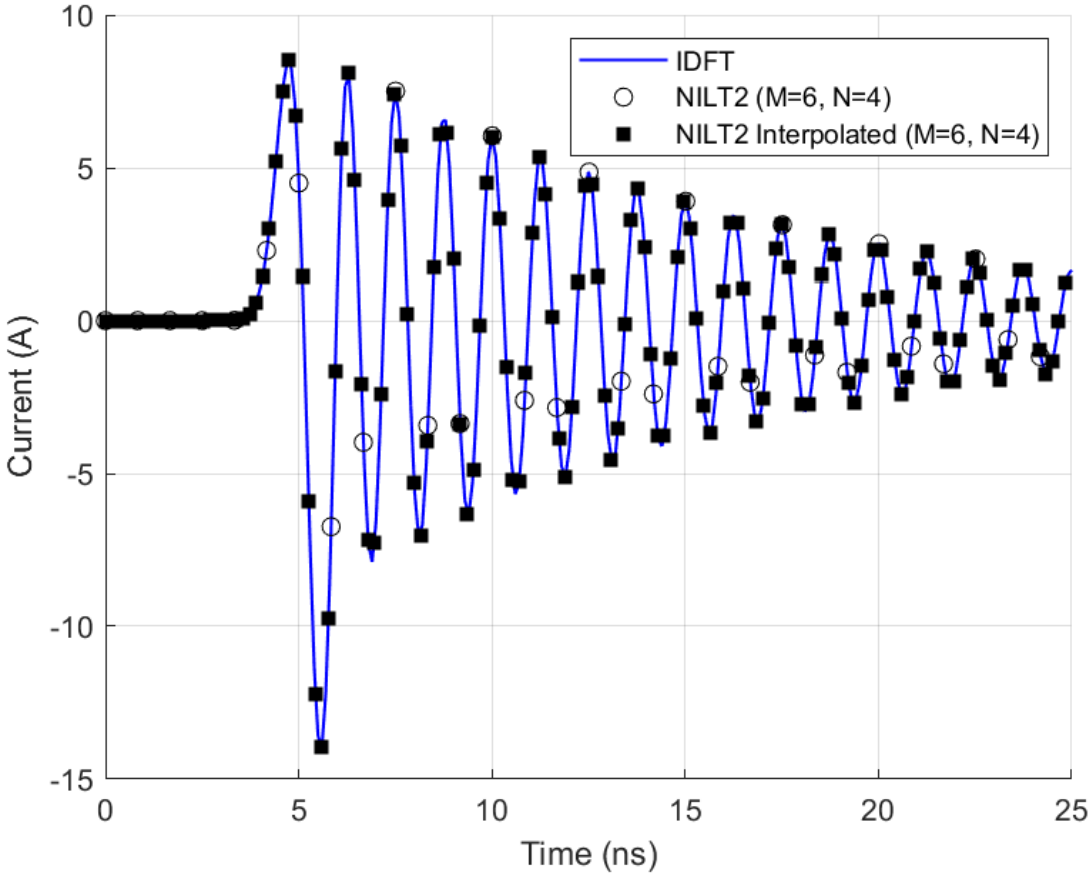

Fig. VII-13: The same plot as the Fig. VII-12, however zoomed in at the initial timeframe for 0-25 ns.

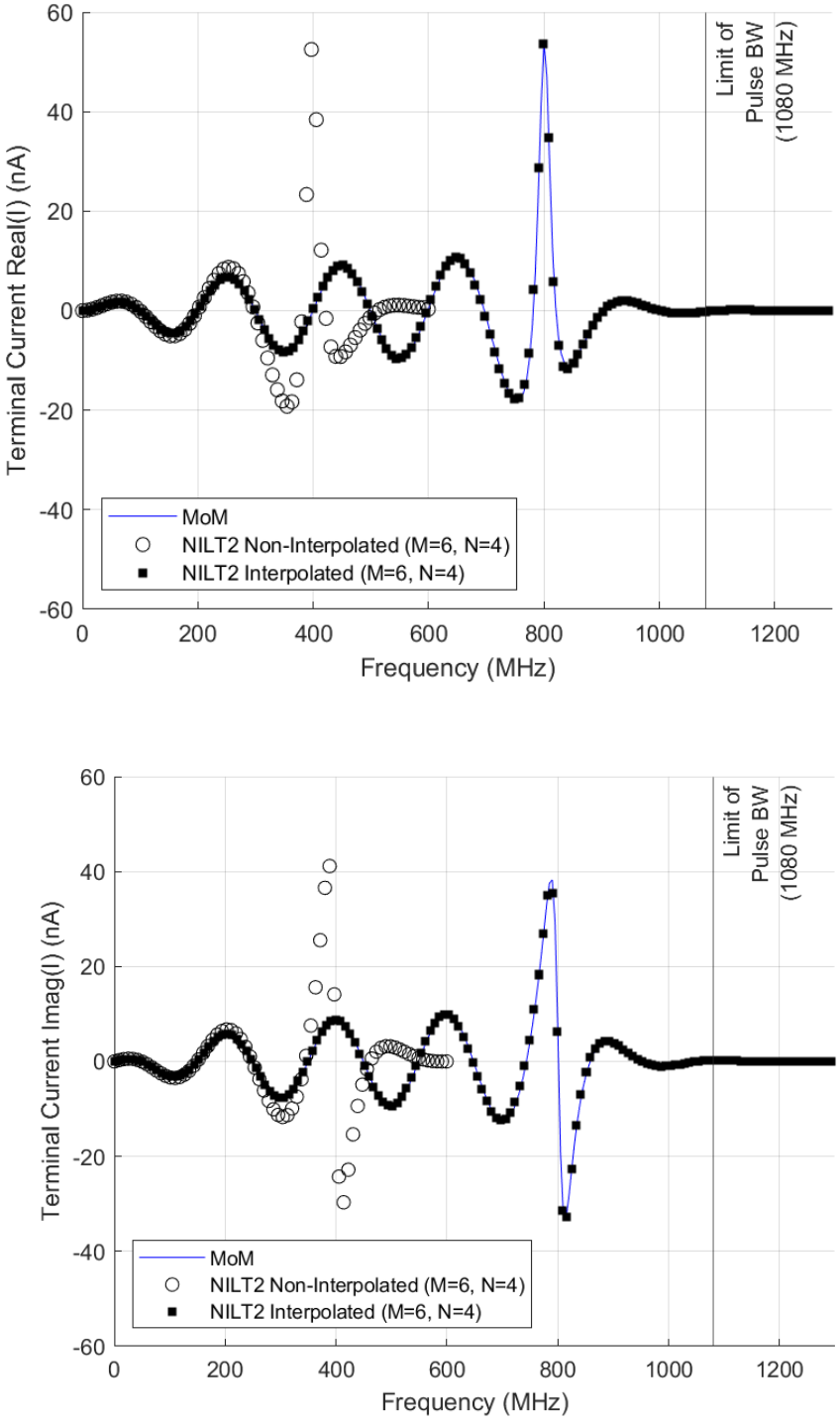

Fig. VII-14: The real part (top) and imaginary part (bottom) of the terminal current of the patch antenna. The blue line represents the FD-EFIE results. The black circles represent the FD/non-interpolated re-initialized NILT2 results. The black squares represent FD/interpolated re-initialized NILT2 results.